STATISTICAL MECHANICS OF JAMMED PACKINGS OF SPHERES

by

Yuliang Jin

A dissertation submitted to the Graduate Faculty in Physics in partial fulfillment of the requirements for the degree of Doctor of Philosophy, The City University of New York

2012

This manuscript has been read and accepted for the Graduate Faculty in Physics in satisfaction of the dissertation requirement for the degree of Doctor of Philosophy.

Prof. Hernan A. Makse

Date Chair of Examining Committee

Prof. Igor L. Kuskovsky

Date Executive Officer

Prof. Hernan A. Makse, Levich Institute and Physics Department, CCNY
Prof. Mark D. Shattuck, Levich Institute and Physics Department, CCNY
Prof. Joel I. Gersten, Physics Department, CCNY
Prof. Jeff Morris, Levich Institute and Department of Chemical Engineering, CCNY
Prof. Corey S. O'Hern, Department of Mechanical Engineering and Physics, Yale University
Supervisory Committee

THE CITY UNIVERSITY OF NEW YORK

Abstract

STATISTICAL MECHANICS OF JAMMED PACKINGS OF SPHERES

by

Yuliang Jin

Adviser: Professor Hernán A. Makse

The problem of finding the most efficient way to pack spheres has an illustrious history, dating back to the crystalline arrays conjectured by Kepler and the random geometries explored by Bernal in the 60's. There are presently numerous experiments showing that randomly packing spheres of equal size into a container consistently results in a static configuration with a density of ∼64%. The ubiquity of random close packing (RCP) rather than the equilibrium crystalline array at 74% begs a new statistical framework. Here we introduce a general volume ensemble statistical approach for jammed packings of spheres. This approach provides a thermodynamic definition of RCP: RCP can be interpreted as a manifestation of a thermodynamic singularity, which defines it as the "freezing point" in a first-order phase transition between ordered and disordered packing phases. We generalize the theory to jammed packings of high dimensional and different size spheres. The asymptotic high-dimensional scaling of the RCP density is consistent with that of other approaches, such as replica theory and density functional theory. The theory predicts the density of random close packing and random loose packing (RLP) of polydisperse systems for a given distribution of sphere size. The present mean-field approach may help to treat packing problems of non-spherical particles, and could serve as a starting point to understand the higher-order correlations present in jammed packings.

Acknowledgements

I am deeply grateful for my supervisor, Professor Hernán A. Makse, Physics Department and Levich Institute, City College of New York, for initiating this work and providing continual support of my research.

I am also grateful for my collaborators Professor Patrick Charbonneau, Department of Chemistry and Department of Physics, Duke University, and Professor Francesco Zamponi, Laboratoire de Physique Théorique, Ecole Normale Supérieure.

In addition, I am grateful for useful discussions with Professor Mark D. Shattuck, Dr. Chaoming Song, Dr. Ping Wang, Dr. Shomeek Mukhopadhyay, Dr. Diego Rybski, Dr. Hernan Rozenfeld, Dr. Lazaros Gallos, Dr. Kun Wang, Maximilien Danisch, Lin Bo and Yanqing Hu.

Lastly, I would like to thank my parents, without whom none of this could be possible.

Contents

List of Tables

List of Figures

Chapter 1

Introduction

Filling containers with balls is one of the oldest mathematical puzzles known to scientists. The study of disordered sphere packings raises an interesting problem: How efficient and uniform will spheres pack if assembled randomly? This problem has an important application in the jamming phenomenon, which takes place in particulate systems where all particles are in close contact with one another. The study of jammed granular media offers unexpected challenges in physics since the equilibrium statistical mechanics fail for these out-of-equilibrium systems. The goal of the present study is to develop an ensemble theory of volume fluctuations to describe the statistical mechanics of jammed matter with the aim of shedding light to the long-standing problem of characterizing random sphere packings. The theory is then generalized to describe the jammed packings of high-dimensional and polydisperse spheres.

1.1 Sphere packing problem

The study of the sphere packing problem started four centuries ago when Johannes Kepler conjectured that the most efficient arrangement of spheres is the FCC lattice (an important part of the 18th problem proposed by Hilbert in 1900). Even though this is a tool used for centuries in fruit markets around the globe, nearly 400 years passed before this conjecture was considered a mathematical proof, which has been developed only recently by Hales [4] in a series of articles covering 250 pages supplemented by 3Gb of computer code to determine the best ordered packing through linear programming. The difficulty arises since in 3d it is not enough to look at the packing of one cell, but it is necessary to consider several Voronoi cells at once. That is, the packing that minimizes the volume locally (the dodecahedron) does not tile the system globally. Such a situation does not arise in 2d, where the hexagonal packing minimizes the volume locally and globally; the equivalent of the Kepler conjecture in 2d, which is also known as Thue's theorem, was proved long ago [5,6].

The analogous problem for disordered packings has also a illustrious but unfinished history. This problem was initiated by the pioneering work of Bernal in the 1960's [7–9] (although earlier attempts can be found). The traditional view states that [10] "packings of spherical particles have been shaken, settled in different fluids and kneaded inside rubber balloons and all with no better results than a maximum density of 63%". This is the so-called random close packing RCP limit [7–14]. On the other hand, other experiments have shown that densities as low as 55% can be obtained in random loose packings, RLP [11,14,15]. While the two limits seem reproducible in various experiments and computer simulations, a mathematically-rigorous definition is still unavailable. Indeed it was conjectured [16] that the RCP conception is mathematically ill-defined and should be replaced by the maximally random jammed (MRJ) conception in terms of an ensemble of order parameters. The competition between the highest densities of the amorphous and the lattice packings raises an intriguing question. Indeed, it has been proposed that the ground state in high dimensions may be amorphous [17]. Furthermore, the sphere packing problem in large spatial dimension d is related to several important mathematical problems in the context of signal digitalization and of error correcting codes, in particular [18, 19].

To this date there is no well-accepted physical explanation of this phenomenon, no well-accepted theoretical prediction of such density values and heated debates are still found in the literature regarding the existence of rigorous definitions of the RCP and RLP, the uniqueness of the RCP state and the nature of their state of randomness.

1.2 Jammed matter

One of the most important physical applications of the sphere packing problem is to understand the intrinsic geometrical structures of jammed systems. The jammed systems are ubiquitous and fundamental in physics, from both practical and theoretical viewpoints. The phenomenon of jamming takes place in particulate systems when the density of particles is increased to a point where all particles are in close contact with one another [20, 21]. "Jammed matter" may refer to a large class of physical systems, such as granular materials, glasses, emulsion droplets, colloidal suspensions, and powders [22]. Theoretically, sphere packings of simple interactions (such as the hard-sphere interaction), have been proposed as fundamental models for jammed mater. A great deal of research has been devoted by physicists to the properties of packings of granular materials and other jammed systems such as compressed emulsions, dense colloids and glasses [23, 24], due to their "out-of-equilibrium" nature.

1.3 Theoretical approaches

Generally speaking, there are four interrelated approaches to understand the nature of the packing problem and the jammed state of matter:

(a) Statistical mechanics of jammed matter: The jammed phase is described with the ensemble of volume and force fluctuations proposed by Edwards [24–32]. Ideas from the physics of glasses provide interesting cross-fertilization between the jamming transition and the glass transition [33–36].

(b) Critical phenomena of deformable particle: jamming is seen as a critical point at which observables such as pressure, coordination number and elastic moduli behave as power-law near the critical volume fraction, ϕ_c, [20–22, 37–42]. The jammed state is modelled as granular media composed of soft particles, typically Hertz-Mindlin [38,43,44] grains under external pressure and emulsions compressed under osmotic pressure [45], as they approach the jamming transition from the solid phase above the critical density: $\phi \to \phi_c^+$.

(c) Hard-sphere glasses: In parallel to studies in the field of jamming there exists a community attempting to understand the packing problem approaching jamming

from the liquid phase [3, 46, 47], that is, $\phi \to \phi_c^-$. Here, amorphous jammed packings are seen as infinite pressure glassy states [3,48]. Therefore, the properties of the jamming transition are intimately related to those of the glass transition [3].
(d) Geometric-structure approach: This approach emphasizes quantitative characterization and classification of all single-packing configurations, without regard to their occurrence frequency in the ensemble [16,49].

A great deal of effort has been devoted to the study of the packing problem and the jamming phenomenon by applying these approaches. A large body of experiments and simulations have fully characterized the jammed state in the critical phenomena framework of soft-particles. The hard-sphere field studies frictionless amorphous packings interacting with hard-core normal forces only. Their results are a particular case of the more general problem of jammed matter composed of frictional and frictionless hard spheres.

1.4 Outline

This dissertation is organized as follows. In Chapter 2, we introduce a volume ensemble statistical approach of jammed matter. Based on this theoretical framework, in Chapter 3 we study the phase transition between the disordered and ordered packings, which provides a thermodynamic definition of the random close packing. This theory is then applied to jammed packings in high dimensions (Chapter 4) and jammed packings of different size spheres (Chapter 5). Finally, we make conclusions and give an outlook for future research in Chapter 6.

The results presented here have been appeared in the following publications:

- Chapter 2: P. Wang, C. Song, Y. Jin, and H. A. Makse, Physica A **390**, 427 (2011); C. Song, P. Wang, Y.Jin, and H. A. Makse, Physica A **389**, 4497 (2010).
- Chapter 3: Y. Jin and H. A. Makse, Physica A **389**, 5362 (2010).
- Chapter 4: Y. Jin, P. Charbonneau, S. Meyer, C. Song, and F. Zamponi, Phys. Rev. E **82**, 051126 (2010).
- Chapter 5: M. Danish, Y. Jin, and H. A. Makse, Phys. Rev. E **81**, 051303 (2010).

Chapter 2

Edwards' statistical mechanics of jammed packings: a volume ensemble approach

Statistical mechanics studies of jammed matter were initiated in 1989 with the work of Sir Sam Edwards. It was first recognized that the main theoretical difficulty to develop a statistical formulation results from the lack of well-defined conservation laws on which an ensemble description of jammed matter could be based. Unlike equilibrium statistical mechanics where energy conservation holds, granular matter dissipates energy through frictional inter-particle forces. Therefore, it is doubtful that energy in granular matter could describe the microstates of the system and a new ensemble needs to be considered.

Stemming from the fact that it is possible to explore different jammed configuration at a given volume in systematic experiments [30–32, 50], Edwards proposed the volume ensemble (V-ensemble) as a replacement of the energy ensemble in equilibrium systems. A simple experiment is merely pouring grains in a fixed volume and applying perturbations, sound waves or gentle tapping, to explore the configurational changes. Concomitant with a given network geometry there is a distribution of contact forces or stresses in the particulate medium. This means that the V-ensemble must be supplemented by the force or stress ensemble (F-ensemble) determined by the contact forces [26, 51, 52] for a full characterization of jammed matter.

Following this theoretical framework, a large body of experiments, theory and simulations [24–32, 45, 53–55] have focused on the study of volume fluctuations in granular media. Statistical studies have been concerned with testing for the existence of thermodynamics quantities such as effective temperatures and compactivity [35] as well as challenging the foundations based on the ergodic hypothesis or equal probability of the jammed states [56, 57]. It is recognized that thermodynamic analogies may illuminate methods for attempting to solve certain granular problems, but will inevitably fail at some point in their application. The mode of this failure is an interesting phenomenon, as the range of phenomena for which ergodicity of some kind or other will apply or not is an interesting question. This has been illustrated by the compaction experiments of the groups of Chicago, Texas, Rennes and Schlumberger [30–32, 50]. They have shown that reversible states exist along a branch of compaction curve where statistical mechanics is more likely to work. Conversely, experiments also showed a branch of irreversibility where the statistical framework is not expected to work. Poorly consolidated formations, such as a sandpile, are irreversible and a new "out-of-equilibrium" theory is required to describe them.

In this section we will describe the reversible states which are amenable to the ergodic hypothesis. Unfortunately, there is no first principle derivation of the granular statistical mechanics analogous to the Liouville theorem for equilibrium systems [58]. Therefore, advancing the statistical mechanics of granular matter requires well-defined theoretical predictions that can be tested experimentally or numerically. While the possibility of a thermodynamic principle describing jammed matter is recognized as a sensible line of research, the problem with the statistical approach is that after almost 20 years there are no practical applications yet. We require predictions of practical importance such as equations of state relating the observables: pressure, volume, coordination number, entropy, etc, that may lead to new phenomena to be discovered and tested experimentally that will allow for a concrete exploitation of the thermodynamic framework.

2.1 Partition function

Conventional statistical mechanics uses the ergodic hypothesis to derive the microcanonical and canonical ensembles, based on the quantities conserved, typically the energy E [58]. Thus the entropy in the microcanonical ensemble is $S(E) = k_B \log \int \delta(E - \mathcal{H}(p,q)) dpdq$, where $\mathcal{H}(p,q)$ is the Hamiltonian. This becomes the canonical ensemble with $\exp[-\mathcal{H}(\partial S/\partial E)]$.

The analogous development of a statistical mechanics of granular and other jammed materials presents many difficulties. Firstly, the macroscopic size of the constitutive particles forbids the equilibrium thermalization of the system. Secondly, the fact that energy is constantly dissipated via frictional interparticle forces further renders the problem outside the realm of equilibrium statistical mechanics due to the lack of energy conservation. In the absence of energy conservation laws, a new ensemble is needed in order to describe the system properties.

Following this theoretical perspective, Edwards proposed the statistical mechanics of jammed matter and interest in the problem of volume fluctuations has flourished [25]. The central concept is that of a volume function W replacing the role of the Hamiltonian in describing the microstates of the system in the V-ensemble and the stress boundary

$$\Pi_{ij} = \int \sigma_{ij} dV$$

with the stress $\sigma_{ij} = 1/(2V) \sum_c f_i^c r_j^c$ describing the F-ensemble [26, 51, 52], where f_i^c, r_i^c are the force and position at contact c. For simplicity only the isotropic case is described. Thus, only the pressure $\sigma = \sigma_{ii}/3$ is necessary to describe force fluctuations.

If we partition the space associating each particle with its surrounding volume, W_i (for instance with a Voronoi tessellation as it will be done bellow), then the total volume, W, of a system of N particles is given by:

$$W = \sum_{i=1}^{N} W_i. \tag{2.1}$$

The ensemble average of the volume function W provides the volume of the system, $V = \langle W \rangle$, in an analogous way to the average of the Hamiltonian is the energy in the canonical ensemble of equilibrium statistical mechanics.

The full canonical partition function in the V-F ensemble is the starting point of the statistical analysis [26]:

$$Z(X, A) = \int g(W, \Pi)\ \exp\left[-\frac{\Pi}{A} - \frac{W}{X}\right]\ \Theta_{\rm jam}\ dW\ d\Pi, \qquad (2.2)$$

where $g(W, \Pi)$ is the density of states for a given volume and boundary stress. Here $\Theta_{\rm jam}$ formally imposes the jamming restriction and therefore defines the ensemble of jammed matter. This crucial function will be discussed at length below. As a minimum requirement it should ensure touching grains, and obedience to Newton's force laws.

Just as $\partial E/\partial S = T$ is the temperature in equilibrium systems, the temperature-like variables in granular systems are the compactivity [25]:

$$X = \frac{\partial V}{\partial S}, \qquad (2.3)$$

and the angoricity (from the Greek "$\acute{\alpha}\gamma\chi o\zeta$" (ankhos) = stress) [26] [1]:

$$A = \frac{\partial \Pi}{\partial S}. \qquad (2.4)$$

The compactivity measures the power to compactify while the angoricity measures the power to stress. These quantities have remained quite abstract so far, perhaps, this fact being the primary reason for the great deal of controversy surrounding the statistical mechanics of jammed matter. In the present work we attempt to provide a meaning and interpretation for the compactivity (the angoricity will be treated

---

[1] Note that in [25], the angoricity is denoted Z. Here we use A for the isotropic angoricity since Z is used to denote the mechanical coordination number. In general the angoricity is a tensor, $A_{ij} = \frac{\partial \Pi_{ij}}{\partial S}$, here we simplify to the isotropic case.

in subsequent papers) by developing equations of states as well interpretations in terms of a "compactimeter" to measure the "temperature" of jammed matter. In Eq. (2.2), the analogue of the Boltzmann constant are set to unity for simplicity, implying that the compactivity is measured in units of volume and the angoricity in units of boundary stress (stress times volume).

In the limit of vanishing angoricity, $A \to 0$, the system is described by the V-ensemble alone. This is the hard sphere limit which will be the focus of the present work where the following partition function describes the statistics:

$$Z_{\rm sph}^{\rm hard}(X) = \int g(W)\ e^{-W/X}\ \Theta_{\rm jam}\ dW, \tag{2.5}$$

where $g(W)$ is the density of states for a given volume W.

2.2 Volume Function

While it is always possible to measure the total volume of the system, it is unclear how to partition the space to associate a volume to each grain. Thus, the first step to study the V-ensemble is to find the volume function W_i associated to each particle that successfully tiles the system. This is analogous to the additive property of energy in equilibrium statistical mechanics. This derivation is explained in Refs. [1, 59] and is the main theoretical result that leads to the solution of the partition function for granular matter. We refer to these papers for details and Sec. 4.2.1 for a simple derivation. Here we just state the main two results, Eqs. (2.6) and (2.7), and explain their significance for the solution of the statistical problem.

Initial attempts at modelling W included, (a) a model volume function under mean-field approximation [25], (b) the work of Ball, Blumenfeld and Edwards in 2d [27,60] and in 3d [61], and (c) simpler versions in terms of the first coordination shell by Edwards [55]. These definitions are problematic: (a) is not given in terms of the contact network, (c) is not additive, (b) and (c) are proportional to the coordination number of the balls contrary to expectation (see below). In Refs. [1, 59] we have found an analytical form of the volume function in any dimensions and demonstrated that it is the Voronoi volume of the particle.

The definition of a Voronoi cell is a convex polygon whose interior consists of all points closer to a given particle than to any other (see Fig. 2.1). Its formula in terms of particle positions for monodisperse spherical packings in 3d is [59]:

$$W_i^{\mathrm{vor}} = \frac{1}{3} \left\langle \left(\frac{1}{2R} \min_j \frac{r_{ij}}{\cos\theta_{ij}} \right)^3 \right\rangle_s \equiv \langle W_i^s \rangle_s, \tag{2.6}$$

where $\vec{r}_{ij}$ is the vector from the position of particle i to that of particle j, the average is over all the directions $\hat{s}$ forming an angle θ_{ij} with $\vec{r}_{ij}$ as in Fig. 2.1, and R is the radius of the grain. W_i^s defines the orientational Voronoi volume which is obtained without the integration over $\hat{s}$. This formula has a simple interpretation depicted in Fig. 2.1.

The Voronoi construction is additive and successfully tiles the total volume. Prior to Eq. (2.6), there was no analytical formula to calculate the Voronoi volume in terms of the contact network r_{ij}. Equation (2.6) provides such a formula which allows theoretical analysis in the V-ensemble. However this microscopic version is difficult to incorporate into the partition function since it would necessitate a field theory. The next step is to develop a theory of volume fluctuations to coarse grain

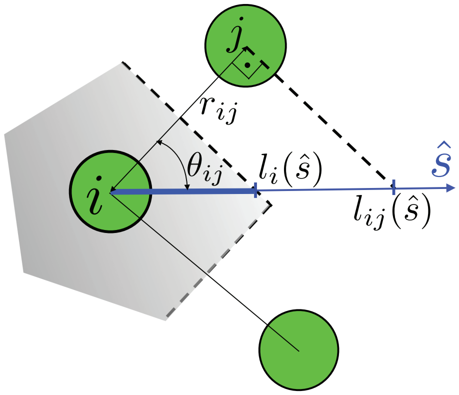

Figure 2.1: The Voronoi volume is the light grey area (shown in 2d for simplicity). The limit of the Voronoi cell of particle i in the direction $\hat{s}$ is $l_i(\hat{s}) = r_{ij}/2\cos\theta_{ij}$. Then the Voronoi volume is proportional to the integration of $l_i(\hat{s})^3$ over $\hat{s}$ as in Eq. (2.6).

W_i^{vor} over a mesoscopic length scale and calculate an average volume function. The coarsening reduces the degrees of freedom to one variable, the coordination number of each grain, and defines a mesoscopic volume function which is more amenable to statistical calculations than Eq. (2.6). We find a (reduced) free volume function [59]:

$$w(z) \equiv \frac{\langle W_i^s \rangle_i - V_g}{V_g} \approx \frac{2\sqrt{3}}{z}, \tag{2.7}$$

approximately valid for monodisperse hard spheres with volume V_g, where z is the geometrical coordination number (which is different from the mechanical coordination number, Z, see below). The average is over all the balls.

The inverse relation with z in Eq. (2.7) is in general agreement with experiments [53]. Many experiments have focused on the analysis of the system volume and single particle volume fluctuations in granular media [30, 32, 53, 54]. Of particular importance to the present theory are the recent advances in X-ray tomography [53] and confocal microscopy [45,62] which have revealed the detailed internal structure of jammed matter allowing for the study of the free volume per particle. By partitioning the space with Voronoi diagrams, these studies show that W_i^{vor} is distributed with wide tails [45, 53–55]. More importantly, the X-ray tomography experiments with 300,000 monodisperse hard spheres performed by the Aste group [53] find that the Voronoi volumes are inversely proportional, on average, to the coordination number of the particle, z, in reasonable agreement with the prediction of the volume function Eq. (2.7). Such data is displayed in Fig. 6 in [53] where the local volume fraction defined as $\phi_i^{-1} - 1 = W_i^{vor}/V_g$ is plotted against the coordination number. From Eq. (2.7) we find:

$$\phi_i = \frac{1}{w+1} = \frac{z}{z + 2\sqrt{3}}, \tag{2.8}$$

which agrees relatively well with the shape of the curves displayed in Fig. 6 of [53] for different packing preparations. It should be noted that for a more precise comparison a coarse grained volume fraction and geometrical coordination number should be considered in Eq. (2.8).

The free volume function decreases with z as expected since the more contacts per grain, the more jammed the particle is and the smaller the free volume associated with the grain. The coordination number z in Eq. (2.7) can be considered as a coarse-grained average associated with "quasiparticles" with mesoscopic free volume w. The quasiparticles can be considered as particles in a self-consistent field of surrounding jammed matter. In the presence of this field, the volume of the quasiparticles depends on the surrounding particles as expressed in Eq. (2.6). The assembly of quasiparticles can be regarded as a set of non-interacting particles and a single particle approximation can be used to solve the partition function as we will formulate in Sec. 2.4.

While Eq. (2.6) is difficult to treat analytically, the advantage of the mesoscopic Eq. (2.7) is that the partition function can be solved analytically since w depends on z only, instead of r_{ij}. The key result is the relation between the Voronoi volume and the coordination number which allow us to incorporate the volume function into a statistical mechanics approach of jammed hard spheres, by using the constraint of mechanical stability as we show below.

2.3 Definition of jamming: isostatic conjecture

The definition of the constraint function Θ_{jam} in the partition function Eq. (2.5) is intimately related to the proper definition of a jammed state and should contain the minimum requirement of mechanical equilibrium.

Distinguishing between metastable and mechanically stable packings that define the jammed state through the Θ_{jam} function remains a problem under debate, related to the more fundamental question of whether or not a jammed packing is well-defined [16]. In practice, it is widely believed that the isostatic condition is necessary for a jammed disordered packing following the Alexander conjecture [63–65] which was tested in several works [20, 37, 39, 41].

It is well known that mechanical equilibrium imposes an average coordination number larger or equal than a minimum coordination where the number of force variables equals the number of force and torque balance equations [63–65]. The so-called isostatic condition.

In the case of frictionless spherical particles the isostatic condition is $Z = 2d =$

6 (in 3d), while the coordination in the case of infinitely rough particles (with interparticle friction coefficient $\mu \to \infty$) is $Z = d+1 = 4$, where d is the dimension of the system. Numerical simulations and theoretical work suggest that at the jamming transition the system becomes exactly isostatic [20, 21, 37, 41, 42, 64, 65]. But no rigorous proof of this statement exists. In the following, we will use this isostatic conjecture to define the ensemble of jammed matter.

While isostaticity holds for perfectly smooth and infinitely rough grains, the main problem is to extend it to finite frictional systems. For finite friction, the Coulomb condition takes the form of an inequality between the normal interparticle contact force F_n and the tangential one F_t: $F_t \leq \mu F_n$ and therefore no trivial solution to the minimum number of contacts can be obtained.

It is worth noting that other attempts to define the jammed state have been developed. A rigorous attempt is that of Torquato *et al.* who propose three categories of jamming [66]: locally jammed, collectively jammed and strictly jammed based on geometrical constraints. However, the definition of [66] is based purely on geometrical considerations and therefore only valid for frictionless particles. Thus it is not suitable for granular materials with inter-particle frictional tangential forces; their configurational space is influenced by the mechanics of normal and shear forces. Other approaches to define a jammed state based on the potential energy landscape [37] fail for granular materials too since such a potential does not exist for frictional grains due to their inherent path-dependency. Thus, the definition of jammed state for granular materials must consider interparticle normal and tangential contact forces beyond geometry [67].

2.4 Phase diagram

According to the statistical mechanics of jammed matter, the volume partition function $\mathcal{Z}$ is defined by Eq. (2.5). In the quasiparticle approximation we can write:

$$\mathcal{Z}_{\rm sph}^{\rm hard}(X) = \int \dots \int g\Big(\sum w(z_i)\Big)\ e^{-\sum w(z_i)/X}\Theta_{\rm jam} \prod_i^N dw(z_i). \tag{2.9}$$

Considering N non-interacting quasiparticles with free volume $w(z)$, the partition function can be written as:

$$\mathcal{Z}_{\rm sph}^{\rm hard} = \Big(\int g(w)\ e^{-w/X}\ \Theta_{\rm jam}\ dw\Big)^N. \tag{2.10}$$

Here, $g(w)$ is the density of states for a given quasiparticle free volume.

Since the mesoscopic w is directly related to z through Eq. (2.7), we change variables to the geometrical coordination number in the partition function. The density of states for a single quasiparticle, $g(w)$, is:

$$g(w) = \int_Z^6 P(w|z) g(z) dz, \tag{2.11}$$

where $P(w|z)$ is the conditional probability of a free volume w for a given z, and $g(z)$ is the density of states for a given z. Here, we have used the bounds

$$Z(\mu) \le z \le 2d = 6, \tag{2.12}$$

where the geometrical coordination number z in Eq. (2.7) counts both zero and non-zero forces, the mechanical coordination number Z counts only the contacts with non-zero forces, and the upper bound of z is given by the isostatic condition [68].

The density of states $g(z)$ is assumed to have an exponential form due to the z average position constrains for each particle:

$$g(z) = (h_z)^z. \tag{2.13}$$

We neglect the fluctuations in the coordination number due to the coarse graining procedure. Therefore the conditional probability $P(w|z)$ becomes a delta function due to the one-to-one correspondence in Eq. (2.7):

$$P(w|z) = \delta(w - 2\sqrt{3}/z). \tag{2.14}$$

Substituting Eq. (2.14) and Eq. (2.13) into Eq. (2.10), we find the isostatic partition function which is used in the remaining of this study:

$$\mathcal{Z}_{\text{iso}}(X, Z) = \int_Z^6 (h_z)^z \exp\left(-\frac{2\sqrt{3}}{zX}\right) dz. \tag{2.15}$$

Next, we obtain the equations of state to define the phase diagram of jammed matter by solving the partition function. From Eq. (2.15), we calculate the ensemble average volume fraction $\phi = (w+1)^{-1} = z/(z+2\sqrt{3})$ as:

$$\phi(X, Z) = \frac{1}{\mathcal{Z}_{\text{iso}}(X, Z)} \int_Z^6 \frac{z}{z+2\sqrt{3}} \exp\left(-\frac{2\sqrt{3}}{zX} + z\ln h_z\right) dz. \tag{2.16}$$

We start by investigating the limiting cases of zero and infinite compactivity.

(a) In the limit of vanishing compactivity ($X \to 0$), only the minimum volume or ground state at $z = 6$ contributes to the partition function. Then we obtain the ground state of jammed matter with a density:

$$\phi_{\rm RCP} = \phi(X = 0, Z) = \frac{6}{6 + 2\sqrt{3}} \approx 0.634, \quad Z(\mu) \in [4, 6]. \tag{2.17}$$

The meaning of the subscript RCP in (2.17) will become clear below.

(b) In the limit of infinite compactivity ($X \to \infty$), the Boltzmann factor $\exp[-2\sqrt{3}/(zX)] \to 1$, and the average in (2.16) is taken over all the states with equal probability. We obtain:

$$\phi_{\rm RLP}(Z) = \phi(X \to \infty, Z) = \frac{1}{\mathcal{Z}_{\rm iso}(\infty, Z)} \int_Z^6 \frac{z}{z + 2\sqrt{3}} \exp\left(z \ln h_z\right) dz. \tag{2.18}$$

The constant h_z determines the minimum volume in the phase space. We expect $h_z \ll 1$, such that the exponential in Eq. (2.18) decays rapidly. Then the leading contribution to Eq. (2.18) is from the highest volume at $z = Z$ and therefore:

$$\phi_{\rm RLP}(Z) \approx \frac{Z}{Z + 2\sqrt{3}}, \quad Z(\mu) \in [4, 6]. \tag{2.19}$$

This dependence of the volume fraction on Z suggests using the (ϕ, Z) plane to define the phase diagram of jammed matter as plotted in Fig. 2.2. The equations of state (2.17) and (2.19) are plotted in the (ϕ, Z) plane in Fig. 2.2 providing two limits of the phase diagram. Since the mechanical coordination number is limited by $4 \le Z \le 6$ we have two more horizontal limits: The phase space is delimited from below by the minimum coordination $Z = 4$ for infinitely rough grains, denoted the granular-line or G-line in Fig. 2.2.

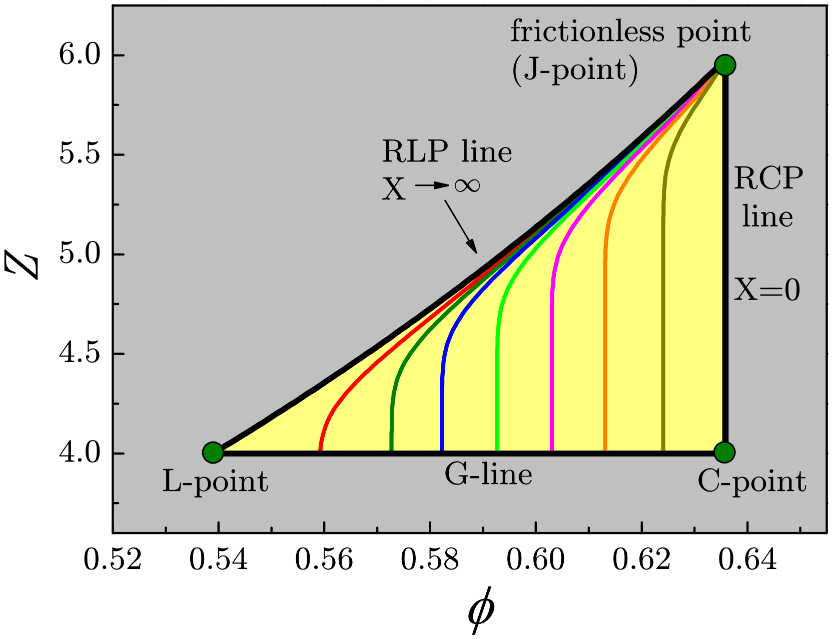

Figure 2.2: Phase diagram of jammed matter. All disordered packings lie within the yellow triangle demarcated by the RCP line, RLP line and G line. Lines of finite isocompactivity are in color. The grey area is the forbidden zone where no jammed random packings can exist.

All mechanically stable disordered jammed packings lie within the confining limits of the phase diagram (indicated by the yellow zone in Fig. 2.2), while the grey shaded area in Fig. 2.2 indicates the forbidden zone for disordered packings. For example, a packing of frictional hard spheres with $Z = 5$ cannot be equilibrated at volume fractions below $\phi < \phi_{\rm RLP}(Z = 5) = 5/(5 + 2\sqrt{3}) = 0.591$ or above $\phi > \phi_{\rm RCP} = 0.634$. It is worth noting that particular packings can exist in the forbidden zone. Our contention is that they are either disordered packing with zero measure or packings with some kind of order. This will be discussed in detail in Chapters 3, where we extend the phase diagram from pure disordered states to ordered states.

These results provide a statistical interpretation of the RLP and RCP limits:

(i) The RCP limit–Stemming from the statistical mechanics approach, the RCP limit arises as the result of the relation (2.17), which gives the maximum volume fraction of disordered packings under the mesoscopic framework. To the right of the RCP-line, packings exist only with some degree of order (for instance with crystalline regions). The prediction,

$$\phi_{\mathrm{RCP}} = \frac{6}{6+2\sqrt{3}} \approx 0.634, \tag{2.20}$$

is valid for all friction coefficients and approximates the experimental and numerical estimations [10–14] which find a close packing limit independent of friction in a narrow range around 0.64.

Beyond the fact that 63-64% is commonly quoted as RCP for monodisperse hard spheres, we present a physical interpretation of that value as the ground state of frictional hard spheres characterized by a given interparticle friction coefficient. In this representation, as μ varies from 0 to ∞ and Z decreases from 6 to 4, the state of RCP changes accordingly while its volume fraction remains the same, given by Eq. (2.20). The present approach has led to an unexpected number of states that all lie in the RCP line from $Z = 6$ to $Z = 4$ as depicted in Fig. 2.2, suggesting that RCP is not a unique point in the phase diagram.

(ii) The RLP limit–Equation of state (2.19) provides the lowest volume fraction for a given Z and represents a statistical interpretation of the RLP limit depicted by the RLP-line in Fig. 2.2. We predict that to the left of this line, packings are not mechanically stable or they are experimentally irreversible as discussed in [30–32]

A review of the literature indicates that there is no general consensus on the value of RLP as different estimations have been reported ranging from 0.55 to 0.60 [11, 12, 14, 15], proposing that there is no clear definition of RLP limit. The phase diagram proposes a solution to this problem. Following the infinite compactivity RLP line, the volume fraction of the RLP decreases with increasing friction from the frictionless point $(\phi, Z) = (0.634, 6)$, towards the limit of infinitely rough hard spheres, $Z \to 4$. Indeed, experiments [11, 12] indicate that lower volume fractions are achieved for larger coefficient of friction. We predict the lowest volume fraction in the limit: $\mu \to \infty$, $X \to \infty$ and $Z \to 4$ (and $h_z \to 0$) at

$$\phi_{\rm RLP}^{\rm min} = \frac{4}{4 + 2\sqrt{3}} \approx 0.536. \tag{2.21}$$

Even though this is a theoretical limit, our results indicate that for $\mu > 1$ this limit can be approximately achieved.

The finding of a random loose packing bound is an interesting prediction of the present theory. The RLP limit has not been well investigated experimentally, and so far it was not certain whether this limit can or cannot be reached in real systems. The lowest stable volume fraction ever reported, 0.550 ± 0.006, obtained by Onoda and and Liniger [15] as the limit of vanishing gravity for spherical glass beads, is not far from the present prediction.

The intersections of the RCP, RLP and the G-line identify three interesting points in the $(\phi, Z(\mu))$ plane.

(a) The frictionless point $\mu = 0$, denoted J-point in [37], at

$$J \equiv (\phi_{\rm RCP}, Z(0)) = (0.634, 6),$$

corresponds to a system of compressed emulsions in the limit of small osmotic pressure as measured by J. Brujić [69].

(b) The lowest coordination number $Z = 4$ plotted as the G-line defines two associated points from the lowest volume fraction of loose packings at infinite compactivity, L-point,

$$L \equiv (\phi_{\rm RLP}^{\rm min}, Z(\infty)) = (0.536, 4),$$

to the zero compactivity state of close packing, C-point,

$$C \equiv (\phi_{\rm RCP}, Z(\infty)) = (0.634, 4).$$

The full JCL triangle defines the isostatic plane where the frictional hard sphere packings reside.

(iii) Intermediate isocompactivity states–For finite X, Eq. (2.16) can be solved numerically. For each X, the function $\phi(X, Z)$ can be obtained and is plotted as each isocompactivity color line in Fig. 2.2. Between the two limits Eqs. (2.17) and (2.19), there are packings inside the yellow zone in Fig. 2.2 with finite compactivity, $0 < X < \infty$. Since X controls the probability of each state, like in condensed matter through a Boltzmann-like factor in Eq. (2.5), it characterizes the number of possible ways to rearrange a packing having a given volume and entropy, S. Thus, the limit of the most compact and least compact stable arrangements correspond to $X \to 0$ and $X \to \infty$, respectively. Between these limits, the compactivity determines the volume fraction from RCP to RLP.

Chapter 3

A thermodynamic definition of the random close packing

Since the time of Kepler it is thought that the most efficient packing of monodisperse spherical grains is the face centered cubic arrangement with a density of 74 % [70]. Thus, we might expect that spherical particles will tend to optimize the space they occupy by crystallizing up to this limiting density. Instead, granular systems of spheres arrest in a random close packing, which is not optimal but occupies $\sim$64% of space [7, 10, 14]. In Chapter 2 we have derived a geometric statistical model [1] to map the microscopic origin of the much debated 64% density of RCP [3, 7, 10, 14, 16, 20, 37, 71–73]. However, the physical laws that govern its creation and render it the most favorable state for randomly packed particles remains a salient question in understanding jammed matter. For instance, while it is known that systems in equilibrium follow energy minimization and entropy maximization to reach a steady state, the mechanism by which RCP is achieved is much sought after.

Here we propose a thermodynamic view in the light of Edwards framework [25] of the sphere packing problem where the experimentally observed RCP is a manifestation of a singularity in a first-order phase transition. Despite the inherent out-of-equilibrium nature of granular matter, the formation of a jammed crystal can be mapped to a thermodynamic process that occurs at a precise compactivity where the volume and entropy are discontinuous. Thus our numerical results suggest that RCP is well defined in a thermodynamic framework. Our results apply to frictional and frictionless monodisperse spheres in 3d. The relation to other systems, such as systems in 2d where crystallization is highly possible, polydisperse systems in 3d and systems in higher dimensions where crystallization is highly suppressed, is discussed. We also discuss the relation between the present thermodynamic viewpoint and other views of the RCP problem, like the replica approach [3].

3.1 Algorithm

We use computer simulations to obtain jammed packings containing $N = 10,000$ mono-disperse spheres of radius $R = 100\mu$m with periodic boundary conditions. We first apply a modified Lubachevsky-Stillinger (LS) algorithm [46, 47] to generate packings of volume densities up to ~ 0.72. In the algorithm, a set of random distributed points grow into nonoverlaping spheres at a fixed expansion rate γ. The spheres are considered perfectly elastic and frictionless, and evolve in time according to Newtonian dynamics. The configurations eventually arrive at out-of-equilibrium states with a diverging collision rate and a volume fraction ϕ_i. Practically, we set the reduced kinetic pressure of the fluid defined as $p = PV/Nk_BT$ to be 10^{12} [47] as a criteria of the diverging collision rate. The final packing configurations depend on the expansion rate γ: large values of expansion rate result in random packings with very low packing densities, while small values of expansion rate result in packings with higher densities.

The hard-sphere packings obtained from the modified LS algorithm are not always mechanically stable and do not necessarily satisfy the isostatic condition. For example, the hard-sphere packings generated by LS algorithm with volume fraction below 64% (when the compression rate is large) are usually hypostatic [74] and unstable under perturbation. We define mechanically stable packings, which satisfy the isostatic condition, as the jammed states in our simulations. For deformable granular particles, the jammed states are characterized by a jamming transition [20], which occurs at the hard sphere limit. In order to study mechanically stable packings, we model the microscopic interaction between deformable grains by the nonlinear Hertz normal forces F_n, the Mindlin tangential forces F_t, and the Coulomb condition ($F_t \leq \mu_f F_n$ with μ_f the interparticle friction coefficient) [1, 20]. We use configurations from the modified LS as the starting point, ϕ_i, and apply molecular dynamics to simulate Newton equations for the evolution of the particles following algorithms in [1, 20].

The aim of this part of the protocol is to generate mechanically stable jammed packings at the jamming transition ϕ_j [1]. For the packings obtained by the LS

---

[1] In this chapter, we use ϕ_j for the volume fraction of jammed packings of soft spheres at the hard sphere limit (zero pressure), and use ϕ for the volume fraction of packings at non-zero pressure. In other chpaters, when there is no confusion, we use ϕ for the volume fraction of jammed packings of hard spheres. This also applies to other parameters such as Z, σ, etc.

algorithm, we first reset the velocities of the particles to zero. At this point the system stress σ and mechanical coordination number Z_j are zero since there is no deformation or overlapping between the particles. We notice that the stress σ is not the kinetic pressure, p, measured in the LS packings which diverges at the end of the LS protocol. Here σ refers to the mechanical pressure related to the trace of the stress tensor σ_{ij} via $\sigma = \sigma_{ii}/3$, where

$$\sigma_{ij} = \frac{R}{2V} \sum_{\text{contacts}} f_i^c n_j^c + f_j^c n_i^c, \tag{3.1}$$

where the sum is over all the contact forces, f_i^c denotes the i-th component of the contact force, $\hat{\mathbf{n}}^c$ is the unit vector joining the center of two spheres of radius R in contact and V is the system volume.

To generate force-equilibrated packings, we apply the split algorithm (SA) of Ref. [1]. The system is compressed isotropically by a constant compression rate until a given nonzero stress σ is reached. Next, we turn off the compression and allow the system to relax with constant volume. If the system eventually reaches a jammed state with a fixed nonzero σ and coordination number, the system pressure will remain unchanged over a large period of time (usually $\sim 10^7$ MD steps); otherwise, if the system is not stable, the pressure will relax to zero very fast [1]. Friction is particularly important to generate force-equilibrated configurations below RCP. While frictionless packings with $\mu_f = 0$ cannot exist below RCP, infinitely rough particles with $\mu_f \to \infty$ can have packing fraction ranging from the lower limit $\sim 55\%$ (random loose packing, RLP) to the higher limit 74% (FCC).

Previous studies [20] show that there exists a jamming transition for granular matter as

$$\sigma(\phi) - \sigma_j \sim (\phi - \phi_j)^\alpha, \tag{3.2}$$

and

$$Z(\phi) - Z_j \sim (\phi - \phi_j)^\beta. \tag{3.3}$$

Here, σ_j is zero for frictionless packings. However, it could has nonzero value for frictional packings, in general. The exponent $\alpha = 3/2$ is trivially related to the Hertz-law of interparticle contact force and $\beta = 1/2$ seems to be universal over different force laws.

For deformable Hertz-Mindlin particles, it is difficult to reach a jammed packing exactly at the transition point ϕ_j while it is much easier to get a stable packing with slightly higher pressure. In order to approach the transition point, a jammed packing at higher pressure than σ_j in Eq. (3.2) obtained using the above protocol is decompressed with a negative compression rate until certain lower pressure is reached. Then the system is allowed to relax again to check for mechanical stability. If it is stable, then the system is decompressed further to an even lower pressure, and we check its stability again. By this process (called the split algorithm in [1]) we are able to approach the density ϕ_j at the jamming transition point as close as possible within the system error. The pressure of the packings at the jamming point studied in this paper is 100 ± 8 KPa. The difference between the volume fraction ϕ of these packings and the critical volume fraction ϕ_j from power-law fitting in Eq. (3.2) is about 10^{-3}.

The same preparation protocol is repeated by using the force-biased algorithm (FBA) of [75] as initial protocol. The force-biased algorithm is a variant of the original method of Jodrey and Tory [76]. We also generate packings following the split algorithm of [1] starting with low initial volume fractions at $\phi_i = 0.3$ below RLP.

3.2 A phase diagram of the RCP transition

We investigate mechanically stable packings generated by above algorithms, ranging from the lowest possible volume fraction of RLP [15] to FCC. The mechanical coordination number averaged over all the particles in a packing, Z_j, characterizes different states of granular matter [1, 53]. Therefore, our study begins by plotting Z_j versus ϕ_j for all generated packings. Figure 3.1 suggests the existence of a transition occurring at RCP evidenced by the abrupt plateau in Z_j. This transition could be thought of as an analogue to the classical hard sphere liquid-solid phase transition in thermal equilibrium [77,78]. Such an analogy becomes apparent if one identifies Z_j of the jammed packing with the kinematic pressure of the equilibrium hard sphere system [3].

Figure 3.1 identifies two branches and a coexistence region: (i) An ordered branch of crystallized states with ϕ_j ranging from 0.68 to a FCC lattice at 0.74. (ii) A disordered branch within $0.55 \sim 0.64$ which can be fitted with the statistical theory of [1]: $\phi_j = Z_j/(Z_j+2\sqrt{3})$ as shown in the figure. (iii) A coexistence region between 0.64 to 0.68 displaying a plateau at the isostatic coordination number, $Z_{\rm iso} = 6$ [64]. The intersection between the disordered branch and the coexistence line identifies the "freezing point" of the transition providing a definition of RCP. Using the theoretical results of [1], freezing occurs at $Z_{\rm iso} = 6$ and $\phi_{\rm rcp} = 6/(6+2\sqrt{3}) \approx 0.634$.

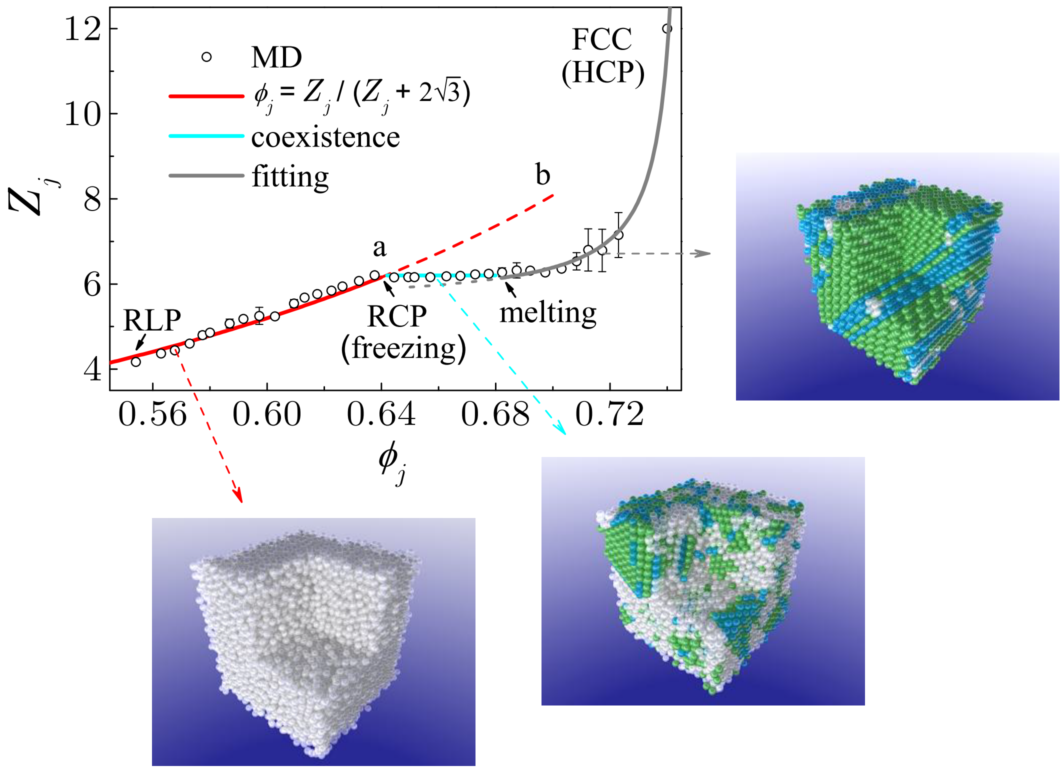

Figure 3.1: The RCP transition. We plot the mechanical coordination number Z_j versus the volume fraction ϕ_j for each packing. We identify: (i) a disordered branch which can be fitted with the statistical model of [1] as shown, (ii) a coexistence region, and (iii) an ordered branch. Error bars are calculated over 523 packings obtained from initial LS configurations. The 3d plots visualize how the transition occurs in terms of arrangements of contacting particles. White particles are random clusters, light blue are HCP and green are FCC clusters. The dash line from $a \to b$ denotes the metastable states.

The corresponding "melting point" appears at the other end of the coexistence at $\phi_{\rm melt} \approx 0.68$, signaling the beginning of the ordered branch. The analysis of finite size effects and algorithm dependence is shown in Fig. 3.2. While Fig. 3.1 shows the average of Z_j over the LS packings, Fig. 3.2 shows each point representing a single packing obtained with the indicated algorithms for different system sizes. The results for 500 and 10,000 spheres are consistent with each other, and the transition seems to be independent of the protocols used here: the LS and FBA algorithms as well as a direct MD simulation using SA produce the same results as shown in Fig. 3.2.

3.3 Descriptive viewpoint of the RCP transition

To reveal the nature of the newly found phases we start with a descriptive viewpoint of the transition.

3.3.1 Local Voronoi volume distribution

We first plot the probability distribution $P(\phi_{\rm vor})$ of local volume fractions of the Voronoi volumes [1, 53] of each particle, see Fig. 3.3. The definition of a Voronoi cell is a convex polygon whose interior consists of all points closer to a given particle than to any other. For every packing, each particle in the packing is associated with its local Voronoi volume fraction $\phi_{\rm vor} = V_g/V_{\rm vor}$, where V_g is the particle volume and $V_{\rm vor}$ is the Voronoi volume of each particle. The probability distribution function $P(\phi_{\rm vor})$ is calculated for every packing with global volume fraction ϕ_j. Microscopically, the existence of two pure phases is starkly represented by the two

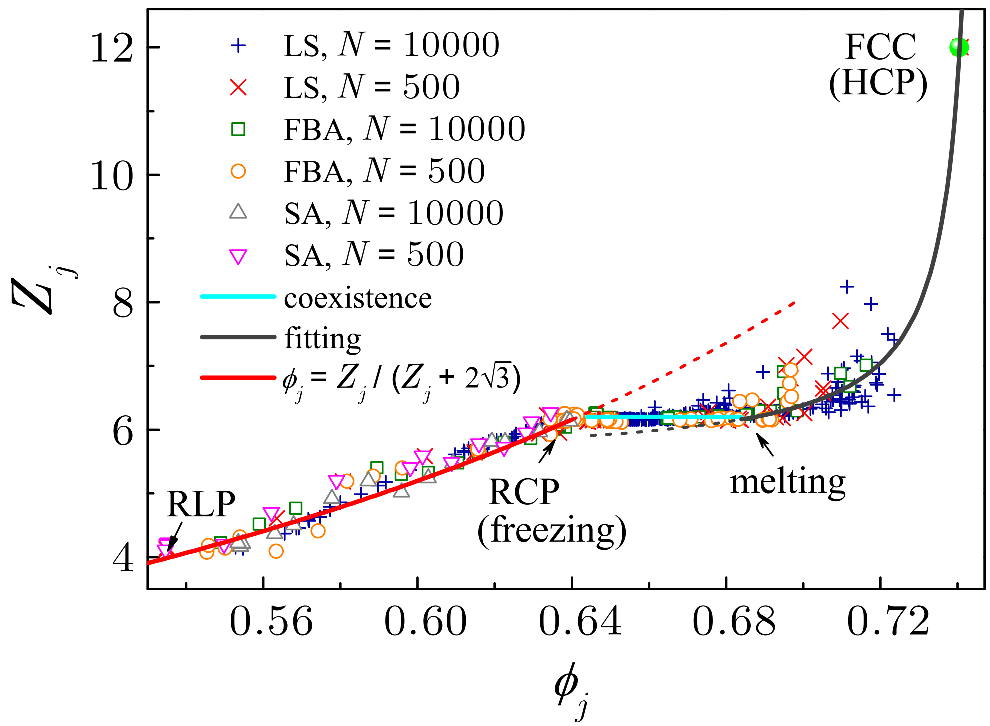

Figure 3.2: The mechanical coordination number Z_j versus the volume fraction ϕ_j with different system sizes (500 and 10,000 particles) and algorithms (Lubachevsky-Stillinger LS, force-biased FBA, and split SA algorithms). The total number of packings is 720. The results show that the transition does not depend on the system size and the algorithm used.

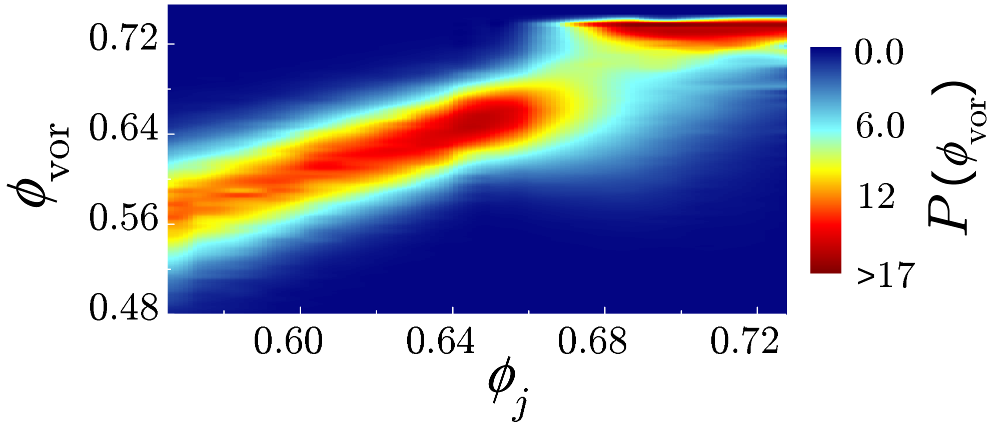

Figure 3.3: Probability distribution of local volume fractions of the Voronoi volumes of each particle, $P(\phi_{\rm vor})$ versus $\phi_{\rm vor}$ (vertical axis) for different ϕ_j (horizontal axis). The plot indicates a clear discontinuity between both branches, which is evidence for a first-order phase transition. Color bar indicates the values of $P(\phi_{\rm vor})$ which are plotted up to the indicated value.

separated distributions of local Voronoi volume fractions $P(\phi_{\rm vor})$. The existence of two phases is further supported by the local analysis of order parameters in the following subsections.

3.3.2 Orientational order parameter

In order to investigate if the concept of phase transition applies to the trend observed in Z_j, one commonly looks at the global (Q_l, W_l), and local (q_6) orientational order parameters for a signature of varying amounts of crystallization present in the packings as defined in [2].

The orientational order is measured by associating a set of spherical harmonics with every bond joining a sphere and its neighbors [2]:

$$Q_{lm}\left(\vec{r}\right) = Y_{lm}\left(\theta\left(\vec{r}\right), \phi\left(\vec{r}\right)\right), \tag{3.4}$$

where $\vec{r}$ refers to the midpoint of a bond, $\theta(\vec{r})$ and $\phi(\vec{r})$ are the polar angles of the bond, and the $\{Y_{lm}(\theta,\phi)\}$ are spherical harmonics. The local orientational order parameter q_l for a particle i is given by rotationally invariant combinations of Q_{lm},

$$q_l = \left[\frac{4\pi}{2l+1}\sum_{m=-l}^{l}\left|\overline{Q}_{lm,i}\right|^2\right]^{1/2}, \tag{3.5}$$

where $\overline{Q}_{lm,i}$ is averaged over N_i neighbors of this particle,

$$\overline{Q}_{lm,i} = \frac{1}{N_i}\sum_{j=1}^{N_i} Q_{lm}\left(\vec{r}_{ij}\right). \tag{3.6}$$

We also consider the global orientational order Q_l, as well as the third-order invariants W_l, which are

$$Q_l = \left[\frac{4\pi}{2l+1}\sum_{m=-l}^{l}\left|\overline{Q}_{lm}\right|^2\right]^{1/2}, \tag{3.7}$$

where the average is taken over all the N_b bonds in the packing,

$$\overline{Q}_{lm} = \frac{1}{N_b}\sum_{bonds} Q_{lm}\left(\vec{r}\right), \tag{3.8}$$

and

$$W_l = \sum_{\substack{m_1,m_2,m_3 \\ m_1+m_2+m_3=0}} \begin{bmatrix} l & l & l \\ m_1 & m_2 & m_3 \end{bmatrix} \times \overline{Q}_{lm_1}\overline{Q}_{lm_2}\overline{Q}_{lm_3}, \tag{3.9}$$

where the coefficients $\begin{bmatrix} l & l & l \\ m_1 & m_2 & m_3 \end{bmatrix}$ are the Wigner $3j$ symbols.

We use a definition of bond as in [2] where all spheres within $r_c = 2.4R$ of a given sphere are near neighbors, where R is the sphere radius. We note that $r_c = 2.4R$

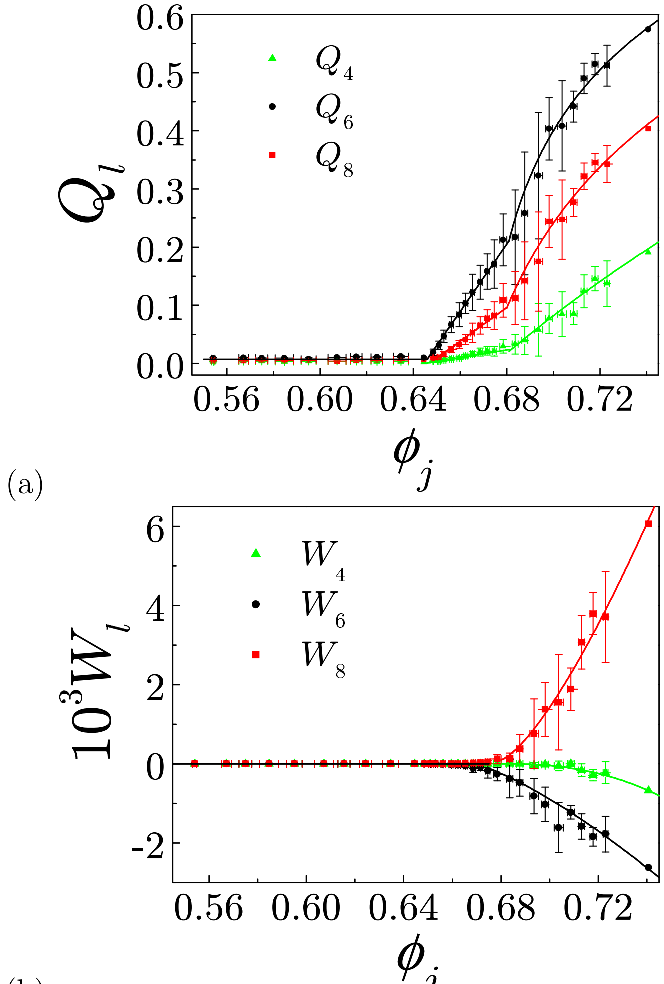

Figure 3.4: (a) Global orientational order parameters Q_l versus ϕ_j for different packings signaling the freezing point at ϕ_{rcp}. A linear fit is possible in the coexistence region. (b) Global third-order invariants W_l versus ϕ_j signaling the melting point at ϕ_{melt}.

is the midpoint between the first peak (centered at $r = 2R$) and the second peak (centered at $r = 2.8R$) in the radial distribution function $g(r)$ of a perfect FCC lattice. Thus, this criteria is also consistent with the definition used in [79], where r_c is the first minimum in $g(r)$. The neighbors can also be defined as those who have mechanical contacts with the given sphere, Z_j. The basic results do not change by changing the definition of nearest neighbors.

The results of the global orientational order Q_l and W_l are shown in Fig. 3.4a and Fig. 3.4b. The salient feature of Q_l is that its zero value means disorder and non-zero value means crystallization. Therefore, the presence in Fig. 3.4a of an increase in Q_l from zero at $\phi_{\rm rcp}$ defines the beginning of the coexistence region. Typically, a first-order transition is marked by a nonzero third-order invariant W_l [2,80] which we find appears at the melting point $\phi_{\rm melt}$ signaling the onset of the ordered branch (Fig. 3.4b).

To investigate the structures of the phases, Fig. 3.5 plots the probability distribution $P(q_6)$ of the local orientational order parameter q_6. Interestingly, the ordered phase has two significant peaks in the probability distribution $P(q_6)$ of the local order parameter of each particle, q_6 (Fig. 3.5). The peaks correspond to FCC and HCP [2] signaling that both crystalline configurations are present in the ordered structure. From the available data we cannot rule out the possibility of another transition from HCP to FCC before $\phi_j \sim 0.74$. The Gaussian distributions $P(q_6)$ obtained for ϕ_j within $0.55 \sim 0.64$ show no preferred lattice structure in the random branch. While the relative peak positions in $P(q_6)$ do not change, the percentage of crystal and random phase found in the packing progresses from one to the other in the coexistence region.

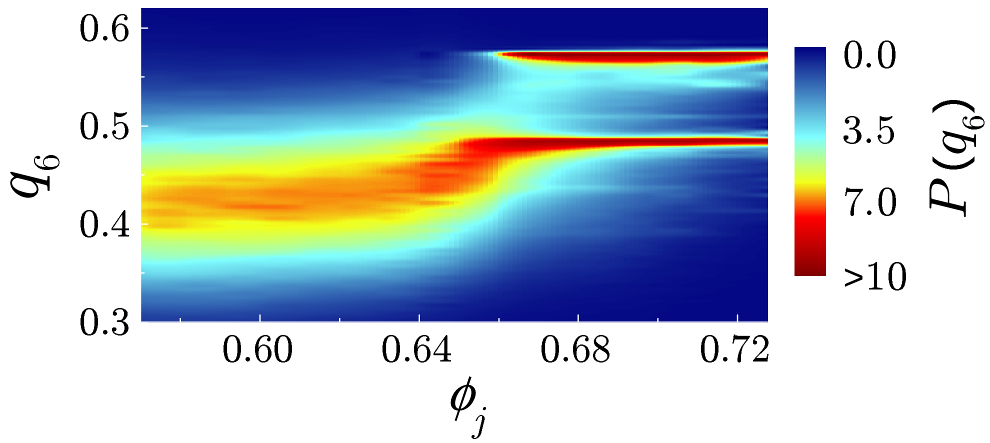

Figure 3.5: Probability distribution of local orientational order parameter $P(q_6)$ versus q_6 (vertical axis) for packings with ϕ_j (horizontal axis). For packings with ϕ_j within $0.68 \sim 0.72$, the distributions have two significant peaks centered at $q_6^{\mathrm{fcc}} = 0.57$ and $q_6^{\mathrm{hcp}} = 0.48$, which correspond to FCC and HCP arrangements, respectively [2]. Color bar indicates the values of $P(q_6)$. Since the peaks are very pronounced, we plot $P(q_6)$ up to the indicated value.

3.3.3 Orientational correlation function

The bond-angle correlation functions (Fig. 3.6) can be obtained via [2]:

$$G_l\left(r\right) = \frac{4\pi}{2l+1} \sum_{m=-l}^{l} \langle Q_{lm}\left(\vec{r}\right) Q_{lm}(\vec{0}) \rangle, \tag{3.10}$$

where the angular bracket indicates an average over all particles separated by $\vec{r}$. A non-zero asymptotic value of $G_6\left(r\right)$ implies a long-range correlation in the orientational order. From Fig. 3.6, it is clear that the crystal phase has long-range orientational order, while no order can be found in the random phase.

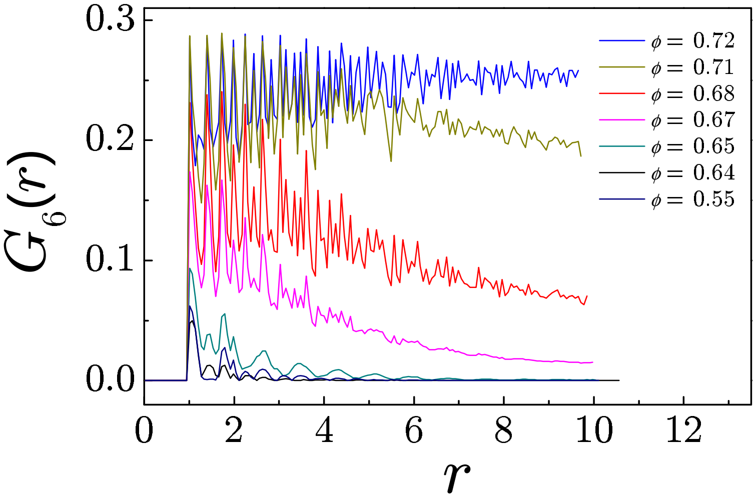

Figure 3.6: The orientational correlation function Eq. (3.10) for different packings with ϕ_j. $G_6(r)$ vanishes at large r below $\phi_j = 0.64$, while it approaches a nonzero constant when $\phi_j > 0.64$. The nonzero asymptote of $G_6(r)$ is a signature of long-range correlation of orientational order. RCP is a well defined singularity at $\phi_j = 0.64$ where the orientational symmetry breaking occurs.

3.3.4 Local orientational disorder

We have established that crystalline structures appear in the coexistence region and solid-like branch. The remaining question is what kind of lattice structure dominates in the crystallized packings. Since the differences of the orientational order parameters, especially Q_6, are not significant between different perfect lattice clusters (such as the icosahedral, FCC, HCP, BCC, and SC clusters, see [2], Fig. 2) we apply another measure, the local orientational disorder, to identify the crystalline nuclei as defined in [81].

For a given sphere i, let θ_{ijk} be the angle between the jth and kth neighbors. Furthermore let θ_{jk}^{fcc}, θ_{jk}^{hcp}, $\theta_{jk}^{\text{icos}}$ be similarly calculated angles for the perfect 13-sphere fragments of FCC, HCP and icosahedral packings, θ_{jk}^{bcc} be the angles for the 8-sphere fragment of a perfect BCC packing, and θ_{jk}^{sc} be the angles for the 6-sphere fragment of a perfect SC packing. The local disorders are defined as following:

$$\theta_i^{\mathrm{fcc}} = \sqrt{\frac{1}{66}\sum_{j=1}^{11}\sum_{k=j+1}^{12}\left(\theta_{ijk} - \theta_{jk}^{\mathrm{fcc}}\right)^2}, \tag{3.11}$$

$$\theta_i^{\mathrm{hcp}} = \sqrt{\frac{1}{66}\sum_{j=1}^{11}\sum_{k=j+1}^{12}\left(\theta_{ijk} - \theta_{jk}^{\mathrm{hcp}}\right)^2}, \tag{3.12}$$

$$\theta_i^{\mathrm{icos}} = \sqrt{\frac{1}{66}\sum_{j=1}^{11}\sum_{k=j+1}^{12}\left(\theta_{ijk} - \theta_{jk}^{\mathrm{icos}}\right)^2}, \tag{3.13}$$

$$\theta_i^{\mathrm{bcc}} = \sqrt{\frac{1}{28}\sum_{j=1}^{7}\sum_{k=j+1}^{8}\left(\theta_{ijk} - \theta_{jk}^{\mathrm{bcc}}\right)^2}, \tag{3.14}$$

$$\theta_i^{\mathrm{sc}} = \sqrt{\frac{1}{15}\sum_{j=1}^{5}\sum_{k=j+1}^{6}\left(\theta_{ijk} - \theta_{jk}^{\mathrm{sc}}\right)^2}. \tag{3.15}$$

Note that to calculate the values properly, we first need to sort the angles θ_{ijk}, $\theta_{jk}^{\mathrm{fcc}}$, $\theta_{jk}^{\mathrm{hcp}}$, $\theta_{jk}^{\mathrm{icos}}$, $\theta_{jk}^{\mathrm{bcc}}$ and $\theta_{jk}^{\mathrm{sc}}$, and then compare them one by one. Also note that the BCC and SC clusters have fewer neighbors than FCC, HCP and icosahedral clusters.

Since the θ_i's measure the local disorder in the packings compared to a particular lattice structure, a perfect lattice cluster would have a zero value of θ. Any packing with significant amount of certain lattice clusters would indicate a peak centered around the origin in the distribution function of the local disorder θ_i corresponding to that particular lattice.

The distribution of FCC clusters $P(\theta_i^{\mathrm{fcc}})$ for packings with different ϕ_j is shown in

Fig. 3.7a. We find that FCC and HCP dominate in the crystalline packings for $\phi_j \geq \phi_{\rm melt}$. Indeed we observe two prominent peaks in the distribution, one at FCC $\theta_i^{\rm fcc} = 0$ and the other at HCP $\theta_i^{\rm fcc} = 0.16$, while BCC, SC and icosahedral ordering are negligible. The FCC peak dominance indicates that the majority of the clusters are FCC with a small proportion of HCP clusters. Similar to the distributions of local orientational orders shown in Fig. 3.5, we find no crystalline clusters in the random packings as evidenced by the Gaussian distributions of $P(\theta_i^{\rm fcc})$ for $\phi_j \leq \phi_{\rm rcp}$ as seen in Fig. 3.7a. In the coexistence region, the distributions are formed by a linear combination of different phases at melting and freezing. The distribution of HCP clusters $P(\theta_i^{\rm hcp})$ has similar behavior as $P(\theta_i^{\rm fcc})$, as showed in Fig. 3.7b. We also calculate $P(\theta_i^{\rm icos})$, $P(\theta_i^{\rm bcc})$, and $P(\theta_i^{\rm sc})$, and do not find any icosahedral, BCC or SC orders.

3.3.5 Cluster analysis of crystalline regions and correlation length

We are able to define crystalline or nearly crystalline clusters in a packing based on the local orientational disorder and mechanical contacts, and visualize them in a 3d plot. The clusters are defined as follows: First, each node in the clusters is a sphere with $\theta_i^{\rm fcc} < \theta_c^{\rm fcc}$ or $\theta_i^{\rm hcp} < \theta_c^{\rm hcp}$, where $\theta_c^{\rm fcc} = 0.1$ and $\theta_c^{\rm hcp} = 0.075$, as determined in Fig. 3.7. The definition ensures that the first peak in $P(\theta_i^{\rm fcc})$ at zero in the distribution function of Fig. 3.7a is included in this consideration (as well as the analogous analysis for HCP). Next, if any two nodes are in mechanical contact, we build a link between the two nodes. Then the crystalline clusters are those nodes that are linked together. The clusters are visualized in Fig. 3.1.

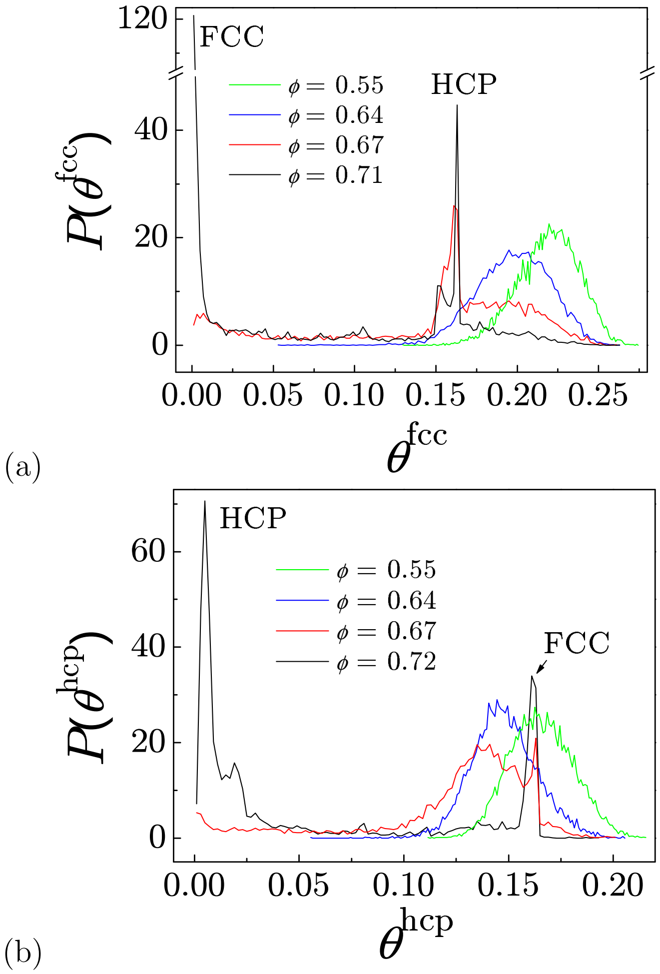

Figure 3.7: (a) Distributions of local disorder $\theta_i^{\rm fcc}$ defined in Eq. (3.11) for packings with different ϕ_j as indicated. The distribution functions below $\phi_j = 0.64$ are Gaussian, the center of the peak moves to $\theta_i^{\rm fcc} = 0.2$ as the volume fraction ϕ_j approaches 0.64. This disordered peak decreases above $\phi_j = 0.64$ and seems to disappear above $\phi_j = 0.68$. Two ordered peaks appear after RCP, the one at $\theta_i^{\rm fcc} = 0$ corresponds to FCC structure, while the other one at $\theta_i^{\rm fcc} = 0.16$ corresponds to HCP. The peak at zero eventually evolves to a delta function as the packing structure approaches a perfect FCC. We use the midpoint between the FCC peak and the disordered peak at $\phi_j = 0.64$ as a cutoff to identify local FCC structure, ie., particles with $\theta_i^{\rm fcc} < \theta_c^{\rm fcc}$ are defined as FCC crystalline nuclei, where $\theta_c^{\rm fcc} = 0.1$. (b) Distributions of local disorder $\theta_i^{\rm hcp}$ defined in Eq. (3.12) for packings with different ϕ_j as indicated. The distribution functions have similar behavior as those of $\theta_i^{\rm fcc}$. The cutoff $\theta_c^{\rm hcp} = 0.075$ is used to identify HCP crystalline nuclei.

Based on the definition of the crystalline clusters, the size of the largest cluster in the system and the correlation length of the clusters, ξ, are measured near the melting point. To calculate the correlation length, we first introduce the radius of gyration, $R_g\left(s\right)$, of a cluster consisting of s particles:

$$R_g^2\left(s\right) = \frac{1}{2s^2}\sum_{i,j}\left(\vec{r_i} - \vec{r_j}\right)^2, \tag{3.16}$$

then the correlation length is given by

$$\xi^2 = \frac{2\sum\limits_s R_g^2\left(s\right)s^2 n_s}{\sum\limits_s s^2 n_s}, \tag{3.17}$$

where n_s is the number of clusters of size s in the packing.

The correlation length ξ of the crystalline clusters is measured near the melting point. Figure 3.8 confirms the linear increase of the size of crystals along the coexistence region from the freezing point where $\xi = 0$ to the melting point. When the system melts at ϕ_{melt}, ξ reaches a plateau consistent with the system size.

3.3.6 Radial distribution function

The radial distribution function $g(r)$ of the packing with volume fraction 0.72 in Fig. 3.9 shows all the peaks in FCC and HCP packings, which are indications of long range spatial order. On the other hand, the radial distribution functions of random packings only have two or three peaks (the second peak splits at $\phi_j = 0.64$), corresponding to short range order. In the coexistence region, $g(r)$ has more peaks than those of random packings, but the magnitude of the peaks decays very fast

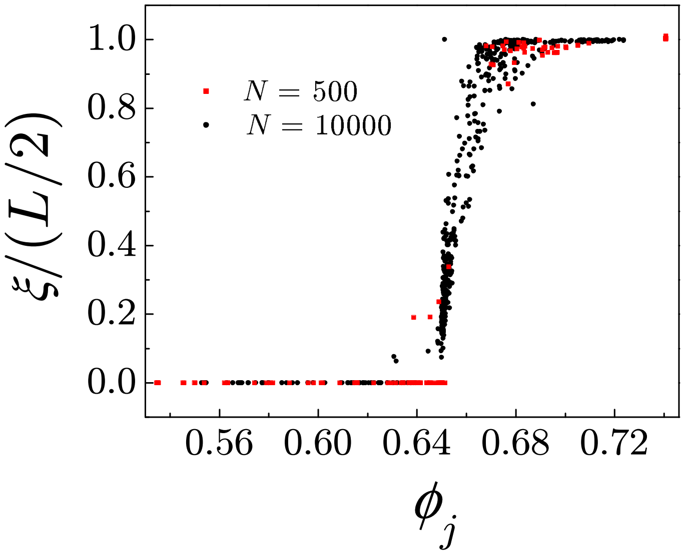

Figure 3.8: Correlation length ξ of crystalline clusters. To calculate the correlation length, we first introduce the radius of gyration, $R_g(s)$, of a cluster consisting of s particles. The correlation length of a perfect FCC lattice with periodic boundary condition is $L/2$, where L is the system size, so the correlation length is scaled by $L/2$ in the figure. The crystalline clusters start to percolate at $\phi_j = 0.68$ as $\xi/(L/2)$ reaches a plateau with value 1. The results also show that the percolation at ϕ_{melt} does not depend on the system size.

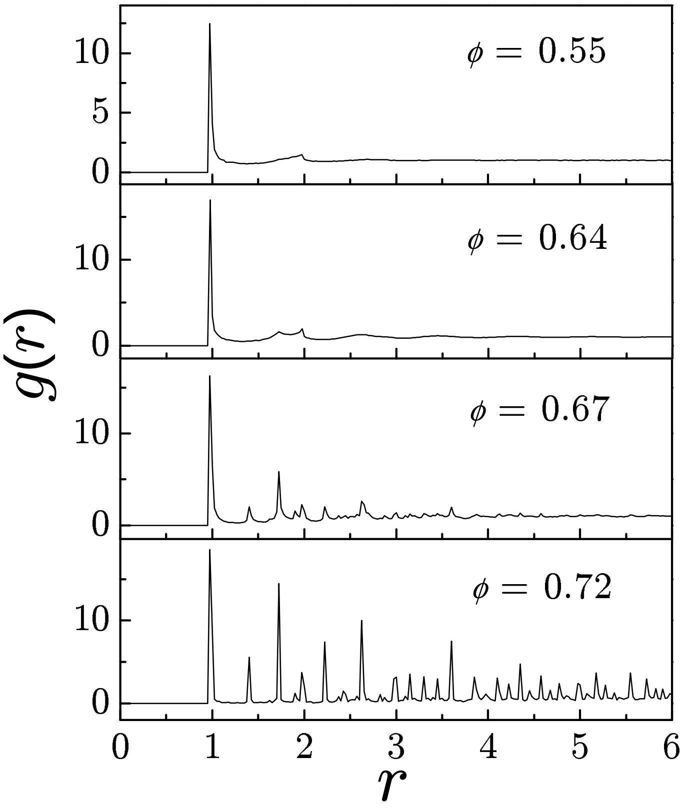

Figure 3.9: Radial distribution functions $g(r)$ with different volume fractions ϕ_j. The figure clearly show the increasing of long range spatial order above $\phi_j = 0.64$.

as the distance r becomes larger. The long-range order increases with the volume fraction in the coexistence region.

3.3.7 Isostatic and geometrical coordination numbers

While the isostatic coordination number has been well documented at RCP [64], the possibility of states with $Z_j = 6$ along the coexistence region with $\phi_{\rm rcp} < \phi_j < \phi_{\rm melt}$ requires more elaboration, particularly in light of the results of replica theory [3]. We recall, however that the limiting condition $Z_{\rm iso} = 6$ is necessary, but not sufficient, for a rigid isostatic aggregate: a kinematic condition for rigidity

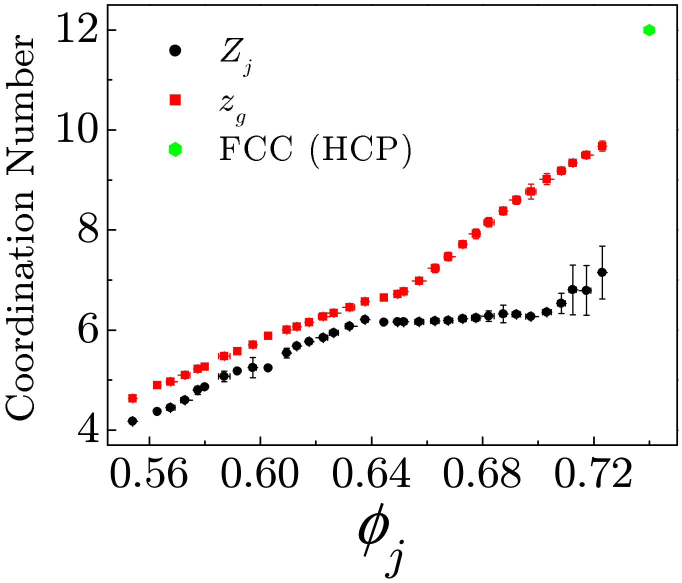

Figure 3.10: Comparison between geometrical coordination number z_g and mechanical coordination number Z_j. Along the disordered branch, z_g closely follows the mechanical coordination number Z_j. We expect that in the thermodynamical limit the gap between both coordinations may diminish. z_g and Z_j start to diverge at RCP, which is an indication of increasing geometric degeneracies in the contact network at the onset of crystallization.

must hold [64] where the functions that describe the connections between the centers of contacting particles are independent. The presence of crystal-like regions indicates that this condition is not satisfied. Thus, the packings with $Z_j = 6$ in the coexistence region are not necessarily isostatic, except exactly at the freezing point.

It is interesting to understand the geometrical rearrangements occurring during the RCP transition in light of the fact that the packings enter the coexistence region from RCP by keeping $Z_j = 6$ constant. The particles modify the positions of the 6 contacts in average at RCP to create crystal-like regions without creating new contacts or destroying old ones. This implies that the arrangements of particles are such that particles in the second coordination shell come closer to the central particle and contribute to the first coordination shell, yet without producing a new contacting force since Z_j is kept at 6 in the entire coexistence region. The new particles moving into the first coordination shell can be considered in geometrical contact but carrying no force. Thus following [1] we introduce the idea of geometrical contact, z_g, as those particles in the first coordination shell that do not provide any force but still are close enough to the central particle to contribute to the geometrical contact network. The geometrical coordination number z_g is different from the mechanical coordination number Z_j which only counts those contacts with nonzero forces. By definition $z_g \geq Z_j$.

While Z_j is easy to measure in computer simulations of soft particles as the number of contacts between overlapping particles, the geometrical coordination number, z_g, can be measured by slightly inflating the spheres up to 4% of their diameters and counting the resulting contact particles, as discussed in [1]. In practice, the geometrical coordination number measures the particles surrounding a central one with a gap between them from zero or negative (giving Z_j) up to $\delta = 0.08R$ as discussed in [1]. We notice that $\delta = 0.08R$ is much smaller than the location of the second peak in the radial distribution function which occurs around $\delta \sim 2R$. The value $\delta = 0.08R$ is specific for a system of N=10,000, and it is expected to go to zero as $N \to \infty$.

Figure 3.10 plots the geometrical and mechanical coordination z_g and Z_j as a function of ϕ_j for the same packings as in Fig. 3.1. We find that along the disordered branch, $z_g \approx Z_j$ as expected [1]. However, in the coexistence region, $Z_j = 6$ stays constant while z_g keeps growing with ϕ_j. The separation between z_g and Z_j is a signature of the onset of ordering at the freezing point. As explained above, the system starts to crystallize by allowing particles in the second coordination shell to come closer to the central particle and moving the Z_j contacting particles towards a FCC arrangement. At the melting point, the condition $Z_j = 6$ cannot hold any longer and the system transitions to the other branch with an increase of Z_j up to 12. We expect (although we require further study) that the difference between mechanical and geometrical coordination number may remain in the thermodynamic limit representing a signature of the symmetry breaking occurring at RCP.

The distinction between z_g and Z_j is not only important for a characterization of the transition. It is also important to interpret the experimental results. Due to the uncertainty in detecting the exact position of the particles in any experiment and the fact that forces are difficult to measure directly, the exact mechanical coordination might be very difficult to obtain. Thus, a small uncertainty in the determination of the contacting particles $\delta = 0.08R$ will produce z_g as shown in Fig.

3.10. One way to obtain the actual mechanical coordination from experimental data is to use the experimentally obtained coordinates of the particles as initial positions of a MD simulation using Hertz-Mindlin forces to relax the experimental packing configurations and find the exact force balance network of the packing.

3.4 Thermodynamic viewpoint of the RCP transition

Having identified the structure of the phases we now develop a thermodynamic viewpoint of the RCP transition to rationalize the obtained results.

3.4.1 Free energy

Transitions in equilibrium physical systems are driven by a competition of energy and entropy. Instead, a transition in athermal jammed matter is driven by the minimization of the system's volume W(usually called the volume function) [25] by compactification and entropy maximization of jammed configurations [25, 29]. In accordance with the second law of thermodynamics, the granular system tends to minimize its Gibbs-Helmholtz "free energy".

$$F = W - XS \tag{3.18}$$

rather than W alone. The compactivity of the system

$$X = dW/dS \tag{3.19}$$

is a measure of how much further compaction a packing can undergo; the lower the volume the lower the compactivity [25]. Thus, we map the packing problem to an Edwards thermodynamic problem where the volume W replaces the energy and X takes the role of temperature. The principle of free energy minimization can thus be applied.

Other thermodynamic potentials, such as enthalpy H and Gibbs free energy G, are related to the volume function W and compactivity X as

$$H = W, \tag{3.20}$$

$$G = F = W - XS, \tag{3.21}$$

Since thermodynamic pressure is not considered in our case, the volume W and enthalpy H are identical. The Helmholtz free energy F and Gibbs free energy G are also identical, so that we refer to them only as the free energy. The differentials of the thermodynamic potentials are

$$dW = XdS + \mu dN, \tag{3.22}$$

$$dF = -SdX + \mu dN, \tag{3.23}$$

where μ is the chemical potential and N is the number of particles.

The free energy F, or Gibbs free energy G is equal to the product of N and μ,

$$F = G = N\mu. \tag{3.24}$$

The free energy and chemical potential are continuous in the first order phase transition. On the other hand, the derivative of the chemical potential, $s = -\frac{\partial \mu}{\partial X}$, is discontinuous in a first order phase transition.

The compactivity X, as well as the entropy density $s = S/N$, can be calculated from the fluctuations of the Voronoi volumes, which is an analogy of the Edwards theory to the standard Boltzmann statistical mechanics. To calculate the equations of state, $\phi_j(X)$ and $S(\phi_j)$, we first calculate the fluctuations of the Voronoi volumes in the disordered and ordered phases [69, 82], $\sigma_1(\phi_j)$ and $\sigma_2(\phi_j)$ respectively. We define

$$\sigma_i^2 \equiv \langle w_{\mathrm{vor}}^2 \rangle - \langle w_{\mathrm{vor}} \rangle^2, \quad i = 1, 2. \tag{3.25}$$

Here

$$\omega_{\mathrm{vor}} = 1/\phi_{\mathrm{vor}} = V_{\mathrm{vor}}/V_g \tag{3.26}$$

is the reduced Voronoi volume, and the average is done over all the particles in a packing. The volume fluctuations are plotted in Fig. 3.11, which shows clearly the existence of the two pure phases and a discontinuity between both branches. From this plot, $\sigma_1(\phi_j)$ and $\sigma_2(\phi_j)$ are fitted with functions as indicated. The fittings are then used to calculate X and S as follows.

We obtain the compactivity using the Einstein fluctuation theorem for jammed matter which is obtained from the similar relation in equilibrium systems by replacing the energy by the volume fluctuations [30–32, 50, 82]:

$$\langle (\delta W)^2 \rangle = k_B X^2 \frac{\partial W}{\partial X}. \tag{3.27}$$

Here we assume that k_B plays the role of the Boltzmann constant in thermodynamics. Its value could be set to unity without changing the obtained results since

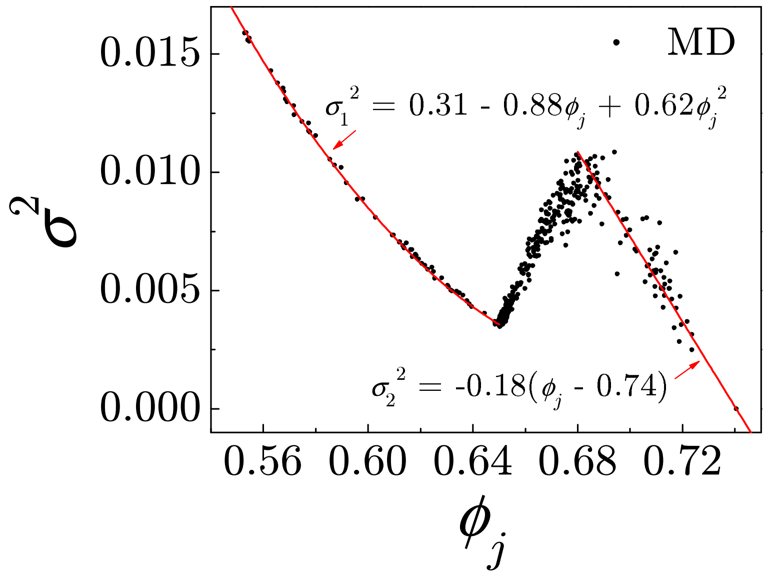

Figure 3.11: Volume fluctuations of the Voronoi cell of a particle as a function of ϕ_j. The data indicates a discontinuity between the ordered and disordered branches which are fitted by functions as indicated. These fittings are used in the integrations of Eq. (3.29). The larger fluctuations in volume observed in the order state compared to the disorder state at similar ϕ_j, which may seem anti-intuitive, are due to the fact that the system packs better in the former and thus displays larger fluctuations when the system volume is the same.

in this context it just defines the units of entropy. This means that we measure the compactivity in units of volume V_g and that the entropy, which has units of k_B, is dimensionless (in the following, we set $k_B = 1$ for simplicity). In terms of the Voronoi fluctuation σ and volume fraction ϕ_j, Eq. (3.27) reads:

$$\sigma_i^2 = -\frac{1}{V_g}\Big(\frac{X}{\phi_j}\Big)^2 \frac{\partial \phi_j}{\partial X}, \quad i = 1, 2. \tag{3.28}$$

Equation (3.28) applies to the disordered and ordered branches, σ_1 and σ_2, separately. It does not apply to the coexistence region, since it requires the pure phases to calculate the fluctuations.

Using Eq. (3.28) we can calculate the thermodynamic quantities by integration. We first obtain the compactivity from:

$$\frac{1}{X(\phi_j)} = \frac{1}{V_g}\int_{\phi_{\rm rlp}}^{\phi_j} \frac{d\phi}{\phi^2\sigma_1^2(\phi)} + \frac{1}{X_{\rm rlp}}, \qquad \phi_{\rm rlp} \le \phi_j \le \phi_{\rm rcp}, \tag{3.29a}$$

$$\frac{1}{X(\phi_j)} = \frac{1}{V_g}\int_{\phi_{\rm melt}}^{\phi_j} \frac{d\phi}{\phi^2\sigma_2^2(\phi)} + \frac{1}{X_{\rm melt}}, \qquad \phi_{\rm melt} \le \phi_j \le \phi_{\rm fcc}, \tag{3.29b}$$

where $X_{\rm melt} = X(\phi_{\rm melt})$ is the compactivity of the packing at the melting point and $X_{\rm rlp} = X(\phi_{\rm rlp})$ at RLP.

The entropy density is then obtained by a second integration using the definition Eq. (3.19) which reads:

$$\frac{1}{X} = -\frac{\phi_j^2}{V_g}\frac{\partial s}{\partial \phi_j}. \tag{3.30}$$

We integrate Eq. (3.30) for each branch to obtain:

$$s(\phi_j) = s_{\rm rcp} + V_g \int_{\phi_j}^{\phi_{\rm rcp}} \frac{d\phi}{X(\phi)\phi^2}, \qquad \phi_{\rm rlp} \le \phi_j \le \phi_{\rm rcp}, \tag{3.31a}$$

$$s(\phi_j) = V_g \int_{\phi_j}^{\phi_{\rm fcc}} \frac{d\phi}{X(\phi)\phi^2}, \qquad \phi_{\rm melt} \le \phi_j \le \phi_{\rm fcc}, \tag{3.31b}$$

where we have used that the entropy of FCC, $s_{\rm fcc}$, is zero in the thermodynamic limit.

Equations (3.29) and (3.31) require three constants of integration: $X_{\rm rlp}, X_{\rm melt}$ and the entropy of RCP: $s_{\rm rcp}$. We now introduce three extra constraints to close the system. First, there are two conditions for equilibrium between two phases in jammed matter [25, 78]: (a) “thermal” equilibrium

$$X_{\rm melt} = X_{\rm rcp} \equiv X_c, \tag{3.32}$$

where X_c is the critical compactivity at the transition. (b) The equality of the chemical potentials of the two phases at the melting and the freezing RCP point: $\mu_{\rm melt} = \mu_{\rm freez}$ due to the conservation of number of particles. This is analogous to the equality of the free energy density at the transition from Eq. (3.24), which allows to calculate the entropy at the freezing point via $f_{\rm melt} = f_{\rm rcp}$:

$$s_{\rm rcp} = s_{\rm melt} + V_g \Big(\frac{\omega_{\rm rcp} - \omega_{\rm melt}}{X_c}\Big), \tag{3.33}$$

and the entropy of fusion is then:

$$\Delta s_{\rm fus} \equiv s_{\rm rcp} - s_{\rm melt} = V_g \Big(\frac{\omega_{\rm rcp} - \omega_{\rm melt}}{X_c}\Big). \tag{3.34}$$

The final constant of integration to be obtained is the compactivity at the RLP point. As a first order approximation, X_{rlp} can be taken as infinite as has been shown in previous experimental and numerical studies [32, 82]. However, when we compare the obtained entropy Eq. (3.31) with an independent measure of the entropy using Shannon information theory (explained in Sec. 3.4.2) we find that there are slightly differences between both values of the entropy. Therefore, we consider X_{rlp} as a fitting parameter to be obtained by fitting the result of Eq. (3.31) with the Shannon entropy which in principle does not require any integration constant to be calculated. We note that using the fitted value of X_{rlp} instead of infinity does not change the final results, specifically the values of X_c and the entropy of fusion, even though the obtained X_{rlp} is "far" from infinite.

We summarize the calculation as follows: (a) We assume a value of X_{rlp} (which is later fitted with Shannon entropy) and integrate Eq. (3.29a) from RLP to ϕ_{rcp} and obtain the compactivity $X_{\text{rcp}} = X(\phi_{\text{rcp}})$. (b) Using Eq. (3.32) we obtain X_{melt} (or X_c). (c) Using X_{melt}, we integrate Eq. (3.29b) to obtain the $X(\phi_j)$ in the ordered branch, thus completing the calculation of the compactivity equation of state. (d) We integrate Eq. (3.31b) up to ϕ_{melt} to obtain the entropy of the melting point: s_{melt}. (e) Using Eq. (3.33) we obtain the entropy at RCP, s_{rcp}. (f) This value is then plugged into Eq. (3.31a) to finish the calculation of $s(\phi_j)$ by a final integration. The above procedure is repeated for different values of X_{rlp} starting from infinite up to a finite value that will match the Shannon entropy (discussed in Sec. 3.4.2).

Figure 3.12 shows that the entropy from the thermodynamic integration Eq. (3.31) and s_{shan} agree well (up to a multiplicative constant) supporting the framework of

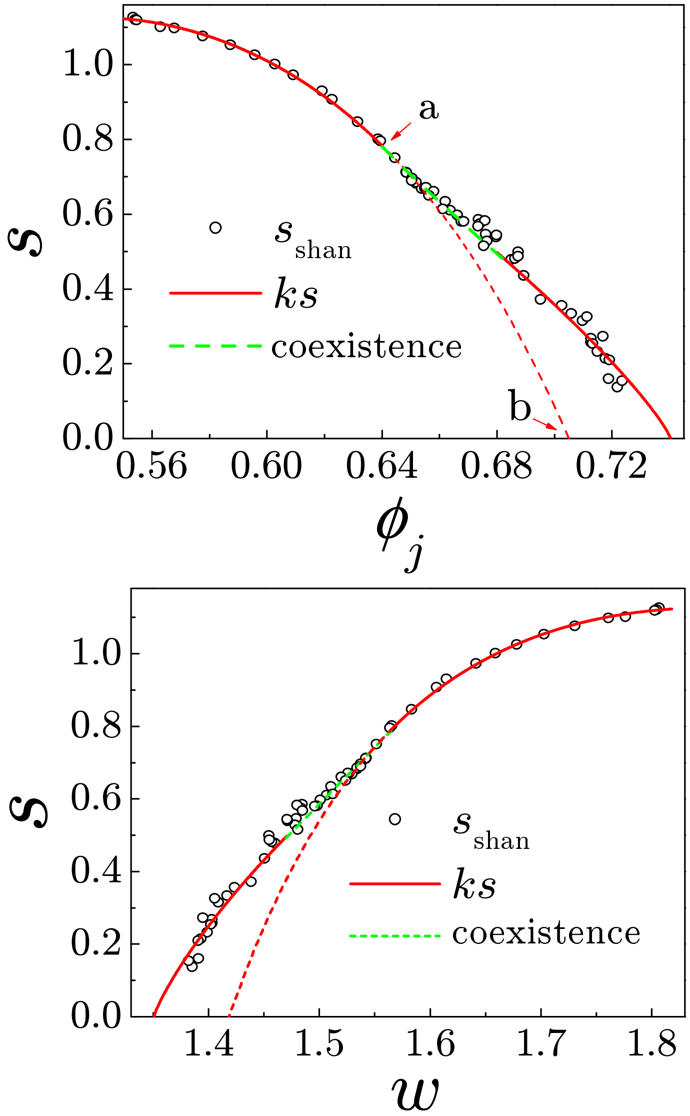

(a)

(b)

Figure 3.12: Equations of state of the RCP transition. (a) Entropy obtained from fluctuation theory in Eq. (3.31), s, and Shannon entropy from information theory, s_{shan}, versus volume fraction ϕ_j. Both entropies agree (up to a multiplicative constant, $k = 0.1$, as indicated) confirming our calculations. The extended branch denotes a metastable state ending at point b at an hypothetical Kauzmann density, ϕ_K, in analogy with the physics of glasses [3] (see Sec. 3.4.3). (b) Entropy versus reduced volume function $\omega = 1/\phi_j$.

Eqs. (3.29)-(3.31). The entropy is composed of two branches plus the coexistence region (green line in Fig. 3.12). Figure 3.12b plots the entropy versus w showing a linear dependence in the coexistence region. The entropy is an interpolation of the form: $s_x = x s_{\rm melt} + (1-x) s_{\rm freez}$ where x is the concentration of crystal clusters in the coexistence. Since $X = \frac{\partial W}{\partial S}$, the linearity of s versus w between 0.64 and 0.68 is a manifestation of the coexistence of two phases at a constant X_c.

Figure 3.13 shows the thermodynamic quantities in the first order phase transition of jammed matter. They are consistent with the general thermodynamic picture. Figure 3.13a displays a discontinuity in $s(X)$ at $X_c = 0.031V_g$ revealing the first-order nature of the transition which is accompanied by an "entropy of fusion"

$$\Delta s_{\rm fus} \equiv s_{\rm rcp} - s_{\rm melt} = 3.0 \tag{3.35}$$

The volume fraction is discontinuous at X_c (Fig. 3.13b) where the system jumps from RCP to the melting point releasing an amount of volume given by the "enthalpy of fusion"

$$\Delta h_{\rm fus} = X_c \Delta s_{\rm fus} = 0.09 V_g, \tag{3.36}$$

while the compactivity stays constant. This process corresponds to the typical latent heat in exothermic first-order transitions.

Systems jammed at RCP need to overcome a volume barrier $\Delta h_{\rm fus}$ for crystal formation or, equivalently, particle displacements $\Delta r_{\rm fus} \approx 0.45R$. From a thermodynamic perspective, the requirement is equivalent to bringing a random packing in contact with a compactivity bath at $X < X_c = 0.031V_g$. The fundamental idea is to surround a random packing above X_c with a crystal lattice below X_c

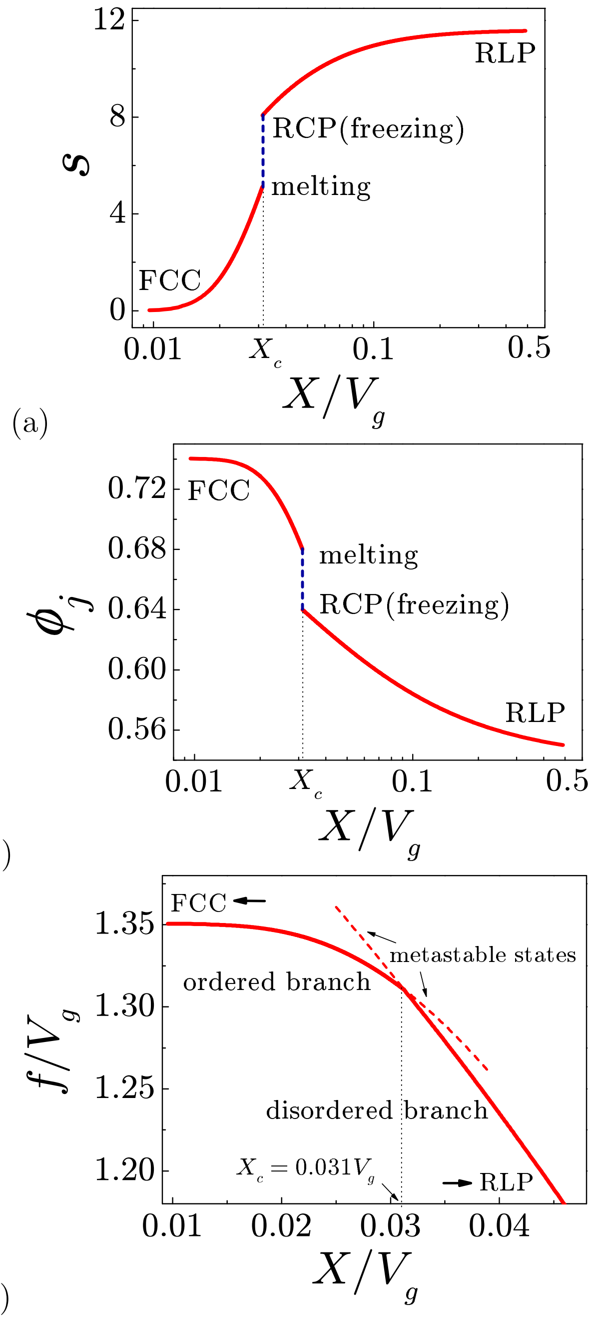

Figure 3.13: Thermodynamic viewpoint of the RCP transition. All the observables obtained from the integration of simulated data are consistent with a transition at $X_c = 0.031V_g$. (a) Entropy s versus X. (b) Volume fraction ϕ_j versus X. (c) Free energy density f versus X. We extend f for both branches to indicate the possible metastable states. At X_c the system follows the minimization of the free energy signaling the transition from RCP to order.

and perturb the system to equilibrate. A shear cycling experiment—which conserves the shape of the box containing the particles—suffices to explore the crystal branch [83, 84]. Shear-induced crystallization has been observed [83, 84] when the maximum angle of horizontal shear is above $\theta \approx 10^\circ$. This value is of the same order as our estimate of the shear amplitude to crystallize at $\phi_j = 68\%$ based on the entropy of fusion, which gives $\theta \equiv \tan^{-1}(\Delta r_{\mathrm{fus}}/2R) \approx 13^\circ$. Furthermore, recent shear cycling experiments [72] appear to be in reasonable agreement with the present results as well as shaking experiments of [85]. We also expect that 2d equal-sized disks may have a near zero entropy of fusion ($\Delta s_{\mathrm{fus}} \sim 0$) owning to their tendency to easily crystallize. On the other hand, the entropy of fusion Δs_{fus} may sharply increase in polydisprese systems and higher dimensional systems due to their difficulty to crystallize [3]. The situation might be even more complicated in these systems due to the possibility of multiple values of ϕ_{rcp} once crystallization is suppressed [3, 47, 86]. However, we note that for 3d monodisperse spheres the value of ϕ_{rcp} is fairly unique and robust and the RCP state is reproducible in various experiments and simulations [71], which therefore deserve a rigorous definition mathematically and physically.

The behavior of the free energy density shown in Figs. 3.13c and 3.14 summarizes the mechanism to achieve RCP. The free energy in Fig. 3.13c increases as X decreases from RLP to freezing at RCP. At X_c, the system transitions to the phase with the lower free energy through an entropy discontinuity given by $s = -\partial f/\partial X$. The system may also enter the metastable branch as indicated in Fig. 3.13c and in Figs. 3.1 and 3.12a from $a \to b$. In the spirit of Landau mean field theory of phase transitions, we relate the distribution of the local order parameter to the

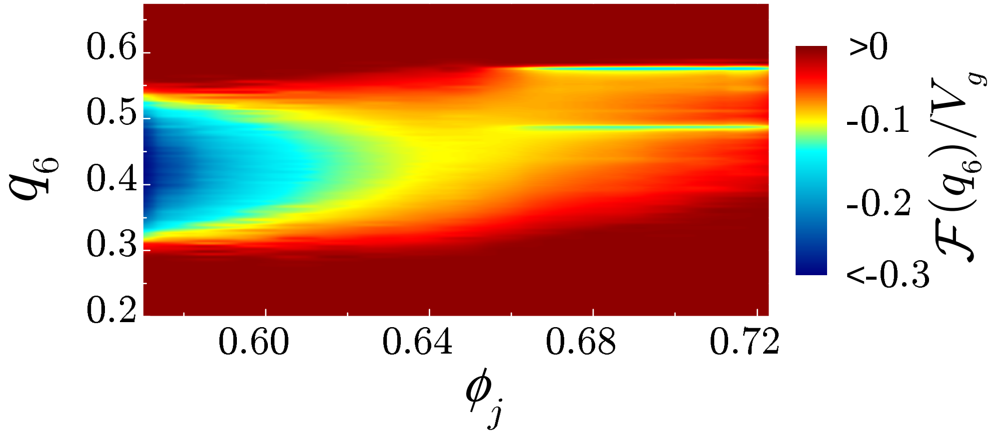

Figure 3.14: Free energy functional $\mathcal{F}(q_6)$ versus q_6 (vertical axis) ϕ_j (horizontal axis). Color bar indicates the values of $\mathcal{F}(q_6)$, which are plotted in the range indicated to focus on the region of coexistence. The minima correspond to the disordered phase and the FCC and HCP phases in the ordered branch.

free energy functional, $\mathcal{F}$, and X as [80, 85]

$$P(q_6) \approx \exp[-\mathcal{F}(q_6)/X]. \tag{3.37}$$

Figure 3.14 shows $\mathcal{F}(q_6)$ displaying the minima of $\mathcal{F}(q_6)$ defining the order and disorder phases at different ϕ_j. We find that the location of the minimum at $q_6^{\text{min}} \approx 0.425$ remains constant from RLP up to the freezing point as expected in the disordered phase. The value of $\mathcal{F}(q_6^{\text{min}})$ is very deep for $\phi_j = 0.55$ and becomes less deep as the freezing point is approached. The value of $\mathcal{F}(q_6^{\text{min}})$ at the freezing and melting points become approximately equally deep indicating the phase coexistence at X_c. Within a statistical mechanics framework of jammed matter, these results are a natural consequence. Although there are still debates upon the assumptions of the Edwards' ensemble descriptions [57], our results give support to such an underlying statistical picture.

3.4.2 Shannon entropy

Entropy of jammed matter can be calculated in two different ways: (i) The entropy from fluctuation theory explained above. (ii) The entropy from information theory [69, 82], so called ”Shannon entropy”, related to configurational disorder since topologically equivalent structures are considered as the same state. Shannon entropy attempts to measure the disorder in a string of information as defined in the seminal work of Shannon. This concept has been adapted to the measurement of the configurational entropy in physical systems defined through a contact network by Vink and Barkema [87]. In that work it was shown that the entropy obtained from the thermodynamic integration of fluctuations (or equivalently the specific heat) and the Shannon entropy are equivalent and accurately describe amorphous silicon and vitreous silica networks. The method has been extended to calculate the entropy of packings of granular materials in [82]. Below we explain the main details.

The advantage of the Shannon entropy calculation over the thermodynamic integration is that it does not require a constant of integration as in Eq. (3.31). For each state of jammed matter, we associate a probability of occurrence p_i to the state, which is calculated as follows.

We use the Voronoi cell and Delaunay triangulation for each particle to define a Voronoi network by considering contacts when a Voronoi side is shared between two particles, and hence are Delaunay contacts. A graph is constructed as a cluster of n particles that are Delaunay contacts, and by means of graph automorphism [88] can be transformed into a standard form or “class” i of topologically equivalent graphs with a probability of occurrence $p(i)$. In practice, we determine $p(i)$ by extracting a large number m of clusters of size n from the system and count the number of times, f_i, a cluster i is observed, such that:

$$p(i) = f_i/m. \tag{3.38}$$

Then the Shannon entropy is defined as:

$$H(n) = -\sum p_i \ln p_i, \tag{3.39}$$

where we have again assumed the "Boltzmann-like" constant in front to be one. The Shannon entropy density is obtained as:

$$s_{\text{shan}} = \lim_{n\to\infty} \left[H(n+1) - H(n)\right], \tag{3.40}$$

by linear fitting of the extensive part of the Shannon entropy.

In general, the fluctuation entropy from Eq. (3.31) is greater than the Shannon entropy from Eq. (3.40) because Shannon entropy only counts configurational disorder and additional entropy could arise from freedom to move grains within the clusters of n particles without disrupting the Delaunay network. However, we discover that the fluctuation entropy obtained from Eq. (3.31) and Shannon entropy from Eq. (3.40) only differ by a scaling constant $k = 0.1$, ie., $ks = s_{\text{shan}}$, see Fig. 3.12. Beyond this multiplicative constant the agreement between both estimations of the entropy is very good. Due to finite size effects the Shannon entropy also gives a nonzero value of the entropy of FCC, $s_{\text{fcc}} = 0.6$. This value is subtracted from the calculations. By fitting s_{shan} with the thermodynamic entropy we obtain the final constant of integration in Eq. (3.29a), $X_{\text{rlp}} = 0.5V_g$. While it is obvious that this constant is far from the infinite value which is expected and used in [32, 82] for the RLP limit, we notice that our final results are not very sensitive to the exact value of X_{rlp}. For instance, by setting $X_{\text{rlp}} \to \infty$ the fitting of the fluctuation entropy is slightly off in comparison with s_{shan} only in the vicinity of RLP but the values of X_c and the entropy of fusion do not have appreciable change. We also note that the finite value of $X_{\text{rcp}} = X_c = 0.031V_g$ is different from the assumptions used in [1, 82], where X_{rcp} is assumed to be zero since only disordered states are considered.

3.4.3 Relation to the liquid-solid phase transition and glass transition of equilibrium hard spheres

It is well known that an equilibrium system of hard spheres exhibits a first-order phase transition between a liquid phase and a crystalline solid phase. This transition has been shown from simulations [77, 89–91], experiments with hard sphere colloids [92, 93], and theories [94, 95]. For an equilibrium system of hard spheres, the freezing point is at $\phi \sim 0.49$ and the melting point is at $\phi \sim 0.54$. Our results show that there is a shift of the coexistence region for jammed granular matter, from $0.49 < \phi < 0.54$ to $0.64 < \phi < 0.68$.

Numerical simulations [96, 97] and experiments [92] have also shown that long-lived metastable hard sphere glasses exist beyond the equilibrium liquid states [3]. Based on this scenario, different conjectures have been proposed to understand the RCP limit. It was conjectured by Torquato et al. [16] that the concept of RCP is mathematically ill-defined and could be replaced by the maximally random jammed

(MRJ) conception. The MRJ state is the divergent point of the metastable branch at infinite pressure, and has minimal values of typical order parameters, such as bond-orientational order or translational order. This point has been generalized by Kamien and Liu in [71]. They proposed that there might be multiple metastable branches and RCP corresponds to the endpoint of a maximally random jammed metastable branch. A similar but more elaborate scenario was proposed by Parisi and Zamponi [3] based on the results of replica theory. Replica theory predicts that a hard sphere system can remain in a liquid state up to a certain dynamical transition density $\phi \in [\phi_d, \phi_K]$, where a dynamical transition to a glass phase happens. Here ϕ_d is the density where many metastable states first appear in the liquid phase, and ϕ_K is the Kauzmann density of the ideal glass transition. These glass states can jam at infinite pressure in a range of densities $\phi_j(\phi) \in [\phi_{\mathrm{th}}, \phi_{\mathrm{GCP}}]$, and RCP can be found everywhere in this range depending on the preparation protocol. Interestingly, the two limits of the volume fraction of amorphous jammed states in replica theory are $\phi_{\mathrm{th}} \approx 0.64$ and $\phi_{\mathrm{GCP}} \approx 0.68$ (see Table I in Ref. [3]), which coincide respectively with the volume fractions of the melting point and freezing point in our first-order phase transition picture. The key point here is to distinguish between a pure amorphous state and a mixture of amorphous state and crystal state in the jammed volume fraction region $0.64 \leq \phi \leq 0.68$. The structure analysis and order parameter measures used in this work are supportive for the existence of glass-crystal mixture.

The thermodynamic character of the RCP transition seemingly contrasts to the non-thermodynamic viewpoint of the glass transition which proposes a dynamical arrest upon supercooling [78]. However, the same phenomenology of vitrification could be applied to the RCP transition by extrapolating the entropy of the disordered branch $s(\phi_j)$ into a metastable region below the freezing point as schematically shown in Figs. 3.1 and 3.12a from $a \rightarrow b$. Two scenarios may emerge: the metastable branch may end in a metastability limit at the spinodal $\partial X/\partial S = 0$ [78] or it may continue until the entropy of the metastable liquid is zero as shown in Fig. 3.12a. Such a scenario would predict a Kauzmann density ϕ_K at which the entropy of the disordered branch vanishes, signaling the existence of an ideal jammed glass analogous to the Kauzmann temperature in glasses [3].

Chapter 4

Jammed packings of high dimensional spheres

The sphere packing problem in large spatial dimension d is related to several important mathematical problems in the context of signal digitalization and of error correcting codes, in particular. It has been investigated in detail by the information theory community [18, 19], but in spite of such strong interest, the known rigorous bounds on packing fractions ϕ are not very restrictive. For the lower bound, the classical Minkowsky result $\phi \sim 2^{-d}$ [18, Chap. 1, Sec. 1.5] can be improved for lattice packings $\phi \geq 2d\,2^{-d}$ [98], and Ref. [99] discusses a procedure to actually construct packings that achieve this bound. For the upper bound, Kabatiansky and Levensthein have obtained an asymptotic scaling $\phi \sim 2^{-0.5990\ldots d}$ [100]. Though the ϕ values of laminated lattices up to $d = 50$ seem to suggest that there exist lattices where $2^d\phi$ grows exponentially with d [18, Chap. 6], it is quite possible for this observation to result from pre-asymptotic effects. The gap between the known upper and lower bounds thus grow exponentially with d. This broad uncertainty leaves open the possibility that the densest packings for $d \to \infty$ may be amorphous. It has indeed been proposed in Ref. [17] that it could be possible to construct amorphous packings that have a density not only exponentially higher than the Minkowsky lower bound, but actually very close to the Kabatiansky-Levensthein upper bound. A better understanding of high-dimensional amorphous and lattice packings would help clarify this intriguing issue.

Dense amorphous packings of hard spheres are produced according to a specific dynamical protocol. Typically, one starts from an initial random configuration of spheres obtained, e.g., by throwing them into a container, then shaking, tapping, or agitating them until a jammed structure is obtained [12,32,92,101–108]. In numerical simulations, amorphous packings are produced by inflating hard particles while avoiding superposition via molecular dynamics [46,47,74], by compressing deformable particles [20,38], or by minimizing the interaction energy of soft particles [21,37,109–111]. It is an observational fact that these procedures, when crystallization is avoided, lead to a final packing fraction close to 0.64 in $d = 3$. This "random close packing density", which is approximately 10% smaller than the density of the best lattice packing in the same dimension, is conjectured to be the densest possible packing that does not display local crystalline order. An important remark for the following discussion is that the random close packings are found to be "isostatic", that is, their average coordination number z is at the limit of mechanical stability $z = 2d$ [21,37,47,74]. A completely satisfactory characterization of the amorphous states of a system of identical hard spheres is, however, not yet available. The definition of amorphous close packed states is still matter of debate [16, 37, 71, 72, 112], in part because the metastability of the jammed amorphous state with respect to the crystal order leads to a thermodynamic ambiguity [3].

Classical statistical mechanics provide useful insights into the problem of sphere packing in large d, for both lattice (see Ref. [113] for an attempt in this direction) and amorphous packings [3]. In the limit of large spatial dimension mean-field theory becomes exact because each degree of freedom interacts with a large number of neighbors [114]. Additionally, because surfaces and volumes scale the same way for large d and geometrical frustration between the liquid and the crystal persists [115, 116], nucleation is strongly suppressed. Metastability effects become less important, which reduces the definitional ambiguity. It is thus likely for statistical mechanics to provide precise information on the behavior of amorphous packings in this limit.

Edwards proposed a volume ensemble statistical approach to study the "out-of-equilibrium" nature of jammed states [24, 27, 70, 117–119]. A simple mean-field theory based on this approach is developed [1, 116, 120, 121], and discussed in Chapter 2. At the theory's core is the distribution of Voronoi volumes associated with particles. Information about the packings can be extracted from the probability distribution of this "volume function". The self-consistent integral equation for the free volume that results can then be solved analytically or numerically to derive a relation between the packing fraction and the average coordination number. This approach has been used in low dimensions to predict the density and other properties of jammed packings.

In this chapter, we provide an alternative derivation of the probability distribution of the volume function that is based on a large d approach. From the theory, we derive a general relation between the density of jammed packings and their average coordination number $\phi \sim z/2^d$, that holds at exponential order in d and is consistent with the one found in Ref. [17] using a different approach. For isostatic random close packings we then obtain $\phi \sim (4/3)\, d\, 2^{-d}$, which is denser than the Minkowsky lower bound. Comparing the theoretical predictions with computer-generated amorphous packings shows that, though generally poor, the agreement nonetheless increases with dimension.

4.1 Notation and Simulation details

Following standard mathematical notation, we define the $(d-1)$-dimensional volume, i.e., the surface, of the $(d-1)$-dimensional unit sphere at the boundary of the d-dimensional unit ball

$$S_{d-1} = \frac{2\pi^{d/2}}{\Gamma(d/2)} \tag{4.1}$$

which is related to the volume of the unit ball $V_d = S_{d-1}/d$. The discussion that follows will consider hard spherical particles of radius $a = 1/2$ and volume $V_g = V_d/2^d$, using the particle diameter as unit of length. We denote by $\rho = N/V$ the number density of particles and by $\phi = \rho V_g$ the packing fraction.

Isostatic random packings in $d = 3$–6 are generated using the simulation code of Skoge *et al.* [47] for $N = 500$ particles. The event-driven molecular dynamics simulations use a modified Lubachevsky-Stillinger algorithm to generate jammed hard-sphere packings. The system dynamically evolves according to Newtonian mechanics until a diverging pressure is obtained. For sufficiently large compression rates γ the compressed fluid falls out of equilibrium, which results in a jammed configuration. Structural analysis reveals that these jammed configurations are isostatic and disordered without any sign of crystallization [47]. We find that compressing the system with $\gamma = 10^{-3}$ in reduced units, until the reduced pressure $p = 10^{12}$, is sufficient to reproduce the results reported in the original work [47]. Finite size analysis conducted for packings in $d = 6$ further indicates that no significant changes are observed for N up to 3000.

Simulations are also employed for testing the theoretically predicted distribution functions of contact spheres (Sec. 4.4.1). For this task, we randomly generate positions for z contact balls on the surface of a d-dimensional central ball, and keep only the configurations that present no overlap. This approach guarantees that the resulting configurations do not depend on the dynamical sequence of sphere addition.

4.2 Method

Before obtaining a high-dimensional form for the mean-field theory, we briefly review the volume function approach and generalize it to arbitrary d. Note that a more complete discussion of the case $d = 3$ can be found in Ref. [1, 59].

4.2.1 Calculation of the volume function

Recall that a Voronoi cell is defined as a convex polygon whose interior consists of the points that are closer to a given particle than to any other. We refer to a particle j as the Voronoi particle of particle i if i and j share a common Voronoi boundary B_{ij}, defined as the $(d-1)$-dimensional surface that bisects the separation r_{ij} between the two particles (Fig. 4.1). For a given direction $\hat{s}$, the distance $l_i(\hat{s})$ from particle i to the boundary B_{ij} is

$$l_i(\hat{s}) = \min_{\hat{s}\cdot\hat{r}_{ij'}} \frac{r_{ij'}}{2\hat{s}\cdot\hat{r}_{ij'}} = \frac{r_{ij}}{2\hat{s}\cdot\hat{r}_{ij}} = \frac{r_{ij}}{2\cos\theta_{ij}} = \frac{c}{2}, \tag{4.2}$$

where $c \equiv r_{ij}/\cos\theta_{ij}$. Operationally, a Voronoi particle j is thus one that minimizes $r_{ij'}/(2\hat{s}\cdot\hat{r}_{ij'})$. Note that c is the diameter of a spherical region

$$\Omega\,(c) \equiv \{(r, \theta_1, \theta_2, \ldots \theta_{d-1}) \;\;|\;\; r/\cos\theta_1 \leq c\}, \tag{4.3}$$

where $(r, \theta_1, \theta_2, \ldots \theta_{d-1})$ are d-dimensional spherical coordinates and θ_1 is the angle between $\hat{r}$ and $\hat{s}$ (see Fig. 4.1). If particle j is truly a Voronoi particle, $\Omega(c)$ should be empty given that the central particle i is at the origin. The Voronoi volume of particle i can thus be expressed as the angular integral

$$W_i = \int d\hat{s}\,\frac{l_i(\hat{s})^d}{d}. \tag{4.4}$$

It follows that the ensemble average $\langle\cdots\rangle$ of the total volume V of a packing

$$\begin{aligned}\langle V\rangle = \left\langle \sum_{i=1}^{N} W_i \right\rangle &= \left\langle \sum_{i=1}^{N} \int d\hat{s}\frac{l_i(\hat{s})^d}{d} \right\rangle \\ &= NV_d\langle l_i(\hat{s})^d\rangle = N\langle W_i\rangle,\end{aligned} \tag{4.5}$$

where the last line results from assuming that the system is isotropic and homogenous, such that the ensemble average of particle i and direction $\hat{s}$ is equivalent to

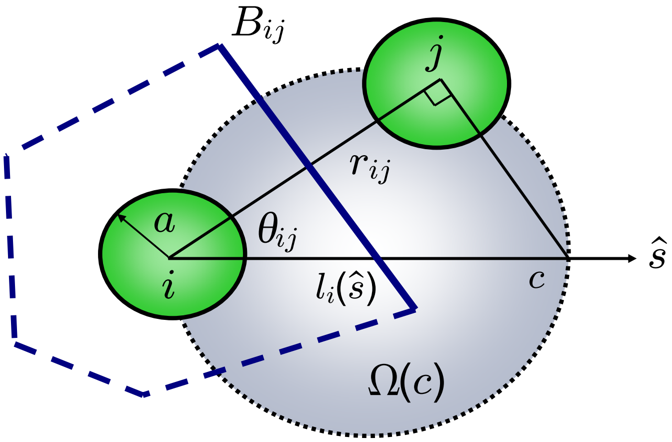

Figure 4.1: Voronoi construction. The boundaries of the Voronoi cell of particle i are illustrated by the thicker lines. The Voronoi boundary B_{ij} between the central particle i and a Voronoi particle j is a $(d-1)$-dimensional face bisecting the separation r_{ij}. The Voronoi boundary along the direction $\hat{s}$ is given by $l_i(\hat{s}) = r_{ij}/(2\cos\theta_{ij})$, where θ_{ij} is the angle between $\hat{s}$ and $\hat{r}_{ij}$. The short-dashed (blue) sphere is the region $\Omega(c)$, where $c = 2l_i(\hat{s}) = r_{ij}/\cos\theta_{ij}$.

the overall ensemble average of the packing. The reduced free volume per particle then simplifies to

$$w = \frac{\langle W_i \rangle - V_g}{V_g} = \frac{V_d \langle l_i(\hat{s})^d \rangle - V_g}{V_g} = \langle c^d \rangle - 1 \ . \tag{4.6}$$

The key quantity missing in the analysis of the Voronoi volumes is the probability distribution for c. We define $f(c)dc$ as the probability that $l_i(\hat{s}) \in [c/2, (c+dc)/2]$ for i at the origin. Note that because for hard spheres $c \in [1, \infty)$, by definition, $f(c)$ can only be non-zero over this same interval. We also define the inverse cumulative distribution function $P_>(c)$ that $\Omega(c)$ is empty of particle centers for i at the origin

$$P_>(c) \equiv 1 - \int_1^c f(c')dc' \ , \tag{4.7}$$

and thus

$$f(c) = -\frac{dP_>(c)}{dc} \ . \tag{4.8}$$

We then obtain that

$$\begin{aligned} w = \frac{1}{\phi} - 1 &= \int_1^\infty \left(c^d - 1\right) f(c)dc \\ &= -\int_1^\infty \left(c^d - 1\right) \frac{dP_>(c)}{dc} dc \\ &= d\int_1^\infty c^{d-1} P_>(c)dc, \end{aligned} \tag{4.9}$$

where the last line is obtained after integrating by parts and noting that the boundary terms vanish. Tests of this identity on amorphous hard spheres packings from simulations, where $P_>(c)$ is obtained directly from each packing (see Fig. 4.7 below), confirm the validity of the underlying isotropy assumption.

4.2.2 Liquid state derivation of $P_>(c)$

From Eq. (4.9), the problem of identifying the packing fraction at jamming is transformed into that of identifying the form of $P_>(c)$ from the structure of jammed configurations. The language of liquid state theory is particularly well-suited for this task because the jammed packings have structural features similar to that of high-density liquids.

Consider the N-particle probability density $P_N(\mathbf{R}^N)$ of finding the particles $1, 2, \ldots, N$ with configuration $\mathbf{R}^N \equiv \mathbf{R}_1, \mathbf{R}_2, \ldots, \mathbf{R}_N$. Unit normalization is set by integrating the particle positions over space

$$\int P_N(\mathbf{R}^N)d\mathbf{R}^N = 1. \tag{4.10}$$

The configurational average (or ensemble average) of a many-body observable $F(\mathbf{R}^N)$ is then

$$\langle F(\mathbf{R}^N)\rangle \equiv \int F(\mathbf{R}^N) P_N(\mathbf{R}^N) d\mathbf{R}^N. \tag{4.11}$$

The associated reduced n-particle probability density (or n-point correlation function)

$$\begin{aligned} \rho_n(\mathbf{R}^n) &\equiv \sum_{i_1 \neq i_2 \neq \cdots \neq i_n}^{\infty} \langle \delta(\mathbf{R}_1 - \mathbf{R}_{i_1})\delta(\mathbf{R}_2 - \mathbf{R}_{i_2}) \cdots \delta(\mathbf{R}_n - \mathbf{R}_{i_n})\rangle \\ &= \frac{N!}{(N-n)!} \int P_N(\mathbf{R}^n, \mathbf{R}^{N-n}) d\mathbf{R}^{N-n} \end{aligned} \tag{4.12}$$

is itself normalized to

$$\int \rho_n(\mathbf{R}^n) d\mathbf{R}^n = \frac{N!}{(N-n)!}. \tag{4.13}$$

For a system with translational invariance we can also define the n-particle correlation function

$$g_n(\mathbf{R}_{12}, \mathbf{R}_{13} \ldots \mathbf{R}_{1n}) \equiv \rho_n(\mathbf{R}^n)/\rho^n, \tag{4.14}$$

with normalization

$$\rho^{n-1} \int g_n(\mathbf{R}_{12}, \mathbf{R}_{13} \ldots \mathbf{R}_{1n}) d\mathbf{R}_{12} \cdots \mathbf{R}_{1n} = \frac{(N-1)!}{(N-n)!}. \tag{4.15}$$

The n-particle correlation function reduces to the pair correlation function (or radial distribution function) for the case $n = 2$.

Following the strategy of Refs. [122] and [123] for expressing $P_>$ in terms of n-

particle correlation functions, we define

$$m(\mathbf{R};\Omega) \equiv \begin{cases} 1, \mathbf{R} \in \Omega \\ \\ 0, \text{otherwise}, \end{cases} \tag{4.16}$$

as a characteristic function of space point $\mathbf{R}$ inside an arbitrary region Ω. Here, we will specialize to the region $\Omega(c)$ defined by Eq. (4.3). We also define the characteristic function

$$J(\mathbf{R}_1;\Omega) \equiv \prod_{i=2}^{N} [1 - m(\mathbf{R}_i - \mathbf{R}_1;\Omega)] \tag{4.17}$$

of all $N-1$ particles outside region Ω centered at $\mathbf{R}_1$, with $\mathbf{R}_1$ the center of particle 1. Considering the cumulative probability function $P_>(\mathbf{R}_1;\Omega)$ as the probability that all $N-1$ particles are outside of Ω gives

$$\begin{aligned} P_>(\mathbf{R}_1;\Omega) &= \frac{N}{\rho_1(\mathbf{R}_1)} \int J(\mathbf{R_1};\Omega) P_N(\mathbf{R}^N) d\mathbf{R}^{N-1} \\ &= 1 - \frac{1}{\rho_1(\mathbf{R}_1)} \int m(\mathbf{R}_2 - \mathbf{R}_1;\Omega) \rho_2(\mathbf{R}_1,\mathbf{R}_2) d\mathbf{R}_2 \\ &+ \frac{1}{2\rho_1(\mathbf{R}_1)} \int m(\mathbf{R}_2 - \mathbf{R}_1;\Omega) m(\mathbf{R}_3 - \mathbf{R}_1;\Omega) \rho_3(\mathbf{R}_1,\mathbf{R}_2,\mathbf{R}_3) d\mathbf{R}_2 \mathbf{R}_3 - \cdots \\ &\equiv \sum_{k=0}^{N-1} (-1)^k F_k(\mathbf{R}_1;\Omega), \end{aligned} \tag{4.18}$$

where the last expression implicitly defines

$$F_k(\mathbf{R}_1;\Omega) \equiv \begin{cases} 1 \ , & k=0 \ , \\ \frac{1}{\rho_1(\mathbf{R}_1)k!}\int \rho_{k+1}(\mathbf{R}^{k+1})\prod_{i=2}^{k+1} m(\mathbf{R}_{1i};\Omega)d\mathbf{R}_i \ , & k \geq 1 \ . \end{cases} \tag{4.19}$$

If the system has translational invariance, then for $k \geq 1$

$$\begin{aligned} F_k(\Omega) &= \frac{\rho^k}{k!}\int g_{k+1}(\mathbf{R}_{12},\ldots,\mathbf{R}_{1(k+1)})\prod_{i=2}^{k+1} m(\mathbf{R}_{1i};\Omega)d\mathbf{R}_{1i} \\ &= \frac{\rho^k}{k!}\int_\Omega g_{k+1}(\mathbf{R}_{12},\ldots,\mathbf{R}_{1(k+1)})d\mathbf{R}_{1i}\cdots d\mathbf{R}_{1(k+1)}. \end{aligned} \tag{4.20}$$

$F_2(\Omega)$, $F_3(\Omega)$, …, are respectively the probabilities of finding a pair, triplet, etc., within Ω. Equations (4.18) and (4.20) show that the problem can be solved exactly only if a complete knowledge of the n-particle correlation function $g_n(\mathbf{R}_{12},\mathbf{R}_{13}\ldots\mathbf{R}_{1n})$ is available to all orders. But an accurate theoretical prediction of g_n for jammed states is still lacking, even for the lowest order pair correlation function g_2. In the following, we use the generalized Kirkwood superposition approximation [124] and a theoretically conjectured form for the pair correlation function in high dimensions to simplify Eq. (4.18). These approximations result in a simple factorized form of $P_>(c)$ that only depends on the packing density ρ and coordination number z.

For dimensions greater than one, the generalized Kirkwood superposition approximation offers a way to reexpress these higher-order correlations in terms of pair correlations

$$g_n(\mathbf{R}_{12},\mathbf{R}_{13},\ldots,\mathbf{R}_{1n}) \simeq \prod_{1\leq i<j\leq n} g_2(\mathbf{R}_{ij}). \tag{4.21}$$

In order to proceed any further with this analysis, we need to approximate $g_2(\mathbf{r})$. Following Torquato and Stillinger's suggestion [17] and the results of replica theory [3], we postulate that the pair correlation for a jammed configuration with z average contacts per particle is angularly independent and decomposable into contact and bulk contributions as

$$g_2(r) \simeq \frac{z}{\rho S_{d-1}} \delta(r-1) + \Theta(r-1), \tag{4.22}$$

where $\Theta(x)$ is the Heaviside step function.

The superposition approximation then becomes

$$\begin{aligned} g_n(\mathbf{R}_{12}, \mathbf{R}_{13}, \ldots, \mathbf{R}_{1n}) &\simeq \prod_{i=2}^{n} g_2(\mathbf{R}_{1i}) \prod_{2 \leq j < k \leq n} g_2(\mathbf{R}_{jk}) \\ &\approx \prod_{i=2}^{n} g_2(\mathbf{R}_{1i}) \prod_{2 \leq j < k \leq n} [1 + \frac{z}{\rho S_{d-1}} \delta(R_{jk}-1) - \Theta(1-R_{jk})] \\ &= \prod_{i=2}^{n} g_2(\mathbf{R}_{1i}) \left[1 + \sum_{2 \leq j < k \leq n} \frac{z}{\rho S_{d-1}} \delta(R_{jk}-1) - \sum_{2 \leq j < k \leq n} \Theta(1-R_{jk}) + \cdots \right]. \end{aligned} \tag{4.23}$$

The relative importance of the various terms in the bracket comes from the scaling of their integral over the volume V of the spherical region Ω with diameter c and noting that $V_g/V \sim c^{-d}$

$$\begin{aligned}
&\int_\Omega \left[1 + \sum_{2\leq j<k\leq n} \frac{z}{\rho S_{d-1}}\delta(R_{jk}-1) - \sum_{2\leq j<k\leq n} \Theta(1-R_{jk}) + \cdots \right] d\mathbf{R}_{12}\ldots d\mathbf{R}_{1n} \\
&= V^{n-1} + V^{n-2}\frac{(n-1)(n-2)}{2}\frac{z}{\rho} - V^{n-2}\frac{(n-1)(n-2)}{2}V_g + \ldots \\
&= V^{n-1}\left[1 + \mathcal{O}\left(\frac{z}{\rho V}\right) + \mathcal{O}\left(\frac{1}{c^d}\right)\right].
\end{aligned} \tag{4.24}$$

To first-order we can then make the approximation

$$g_n(\mathbf{R}_{12}, \mathbf{R}_{13}, \ldots, \mathbf{R}_{1n}) \simeq \prod_{i=2}^{n} g_2(\mathbf{R}_{1i}), \tag{4.25}$$

which amounts to saying that spheres 2...n are correlated with the central sphere 1 but not with each other. Though crude, this treatment is reasonable in large d, because the sphere surface is very large compared to the occupied surface and the packing is increasingly inefficient. Plugging this result into Eq. (4.20) gives

$$F_k(\Omega) = \frac{\rho^k}{k!}\left(\int_\Omega g_2(\mathbf{R}_{12})d\mathbf{R}_{12}\right)^k \tag{4.26}$$

and in the limit $N \to \infty$

$$\begin{aligned}
P_>(\Omega) &= \sum_{k=0}^{N-1}(-1)^k\frac{\rho^k}{k!}\left(\int_\Omega g_2(\mathbf{r})d\mathbf{r}\right)^k \\
&\approx \exp\left[-\rho\int_\Omega g_2(\mathbf{r})d\mathbf{r}\right].
\end{aligned} \tag{4.27}$$

Approximating the pair correlation with Eq. (4.22) finally gives a factorized form whose validity should improve with increasing dimension

$$\begin{aligned} P_{>}(c) &= \exp\left[-\rho V^*(c) - \frac{zS^*(c)}{S_{d-1}}\right] \\ &= P_B(c)P_C(c), \end{aligned} \tag{4.28}$$

where

$$P_B(c) = \exp\left[-\rho V^*(c)\right] \tag{4.29}$$

and

$$P_C(c) = \exp\left[-\frac{zS^*(c)}{S_{d-1}}\right] \tag{4.30}$$

represent the contributions from bulk and contact particles respectively, and

$$\begin{aligned} S^*(c) &= \int \delta(r-1)\Theta(c - r/\cos\theta)d\mathbf{r} \\ &= S_{d-2}\int_0^{\arccos(1/c)} d\theta(\sin\theta)^{d-2} \end{aligned} \tag{4.31}$$

and

$$\begin{aligned} V^*(c) &= \int \Theta(c - r/\cos\theta)d\mathbf{r} \\ &= \frac{S_{d-2}}{d}\int_0^{\arccos(1/c)} d\theta(\sin\theta)^{d-2}[(c\cos\theta)^d - 1]. \end{aligned} \tag{4.32}$$

are empty of particle centers (see Fig. 4.2). Fig. 4.2 (b) also shows that $V^*(c)$ is smaller than the volume of $\Omega(c)$, because of the volume exclusion by the central particle.

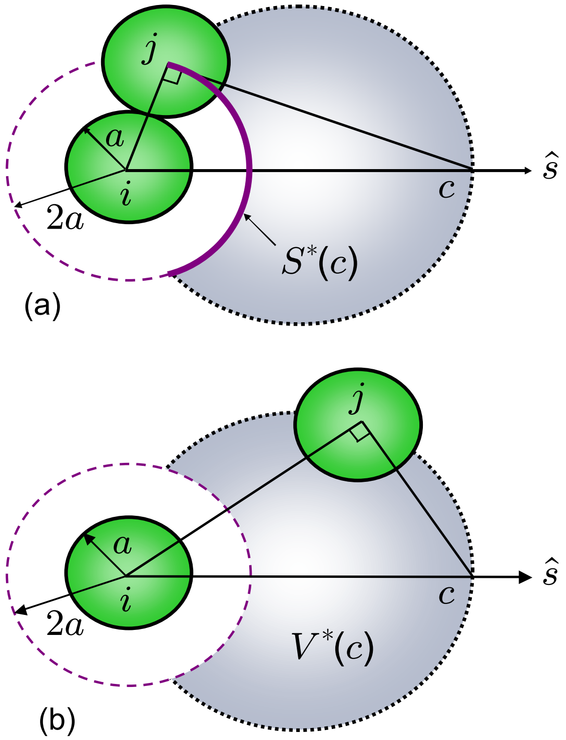

Figure 4.2: Schematic illustration of (a) $S^*(c)$ and (b) $V^*(c)$. The white sphere is the excluded zone of the central particle.

4.3 Large d analytical solution

Substituting the factorized form Eq. (4.28) for $P_>(c)$ into Eq. (4.9), one obtains a self-consistency relation for w that is amenable to further analytical and numerical treatment in the high-dimensional limit

$$w = d\int_1^\infty dc\, c^{d-1} \exp\left[-\frac{2^d V^*(c)}{(w+1)V_d} - \frac{zS^*(c)}{S_{d-1}}\right]. \tag{4.33}$$

4.3.1 Change of variable

For notational convenience, we define

$$\begin{aligned} s^*(1/c) &\equiv \int_0^{\arccos(1/c)} d\theta (\sin\theta)^{d-2} \\ &= \int_{1/c}^1 d\xi (1-\xi^2)^{(d-3)/2} \end{aligned} \tag{4.34}$$

and

$$\begin{aligned} v^*(1/c) \equiv& \int_0^{\arccos(1/c)} d\theta (\sin\theta)^{d-2}[(c\cos\theta)^d - 1] \\ =&\frac{c^d}{2^d}\left[s^*(-1) - s^*(1-2/c^2)\right] + \frac{c}{2d-2}\left(1-\frac{1}{c^2}\right)^{\frac{d-1}{2}} - s^*(1/c), \end{aligned} \tag{4.35}$$

and note that $s^*(-x) = s^*(-1) - s^*(x)$. We reexpress

$$\begin{aligned} \frac{V^*(c)}{V_d} &= \frac{S_{d-2}}{S_{d-1}} v^*(1/c) = \frac{v^*(1/c)}{s^*(-1)} \\ \frac{S^*(c)}{S_{d-1}} &= \frac{S_{d-2}}{S_{d-1}} s^*(1/c) = \frac{s^*(1/c)}{s^*(-1)}. \end{aligned} \tag{4.36}$$

For large d and $x > 0$ we can evaluate $s^*(x)$ by saddle-point approximation. Developing the exponential around $\xi = x$ and using the fact that the integrand decays rapidly in large d allows to extend the upper boundary of integration to $\xi = \infty$ and leaves corrections of order $\mathcal{O}(1/d)$, i.e.,

$$\begin{aligned} s^*(x) &= \int_x^1 d\xi (1-\xi^2)^{(d-3)/2} \\ &= \int_x^1 d\xi \, e^{\frac{d-3}{2}\log(1-\xi^2)} \\ &\approx \int_x^\infty d\xi \, e^{\frac{d-3}{2}\{\log(1-x^2) - \frac{2x}{1-x^2}(\xi - x) - \frac{1+x^2}{(1-x^2)^2}(\xi-x)^2\}} \\ &= \frac{e^{\frac{(d-3)x^2}{2(1+x^2)}}(1-x^2)^{d/2}}{\sqrt{\frac{2}{\pi}(d-3)(1-x^4)}} \left[1 - \mathrm{Erf}\left(\sqrt{\frac{(d-3)x^2}{2(1+x^2)}}\right)\right] \\ &\simeq \frac{1}{dx}(1-x^2)^{(d-1)/2}, \end{aligned} \tag{4.37}$$

where Erf(x) is the error function. Note that the last expression is only reasonable for x away from zero.

By using the relations above and noting that $w \sim w + 1$ in the high-dimensional limit, Eq. (4.33) becomes

$$w = d \int_1^\infty dc \, c^{d-1} \exp\left[-\frac{c^d}{w} + H_d(c; w, z)\right] \tag{4.38}$$

with

$$\begin{aligned} H_d(c; w, z) &= \frac{1}{s^*(-1)} \left\{ \frac{c^d}{w} s^*(1-2/c^2) - \frac{2^d c (1-1/c^2)^{(d-1)/2}}{w(2d-2)} + \left(\frac{2^d}{w} - z\right) s^*(1/c) \right\} \\ &\simeq \frac{2^d}{w s^*(-1)} \left(1 - \frac{1}{c^2}\right)^{(d-1)/2} \left\{ \frac{c}{2d(1-2/c^2)} - \frac{c}{2d-2} + \frac{c}{d}\left(1 - \frac{zw}{2^d}\right) \right\}, \end{aligned} \tag{4.39}$$

where the last result is obtained by using the simplified expression for $s^*(x)$ in Eq. (4.37). A change of variable $y = c^d/w$ further reduces the expression to

$$1 = \int_{1/w}^{\infty} dy \, e^{-y+H_d[(wy)^{1/d};w,z]}. \tag{4.40}$$

Because we expect w to exponentially diverge for large d, the lower integration limit should rapidly go to zero. For any finite y, $y^{1/d} \to 1$ in high dimension. The equation above then becomes

$$1 \sim \int_0^{\infty} dy \, e^{-y} e^{H_d(w^{1/d};w,z)} = e^{H_d(w^{1/d};w,z)} \, . \tag{4.41}$$

Assuming H_d is well behaved at the boundaries, the problem reduces to finding a solution for the condition

$$H_d(w^{1/d}; w, z) = 0. \tag{4.42}$$

4.3.2 Asymptotic solution

For analytical convenience we pose that z and the solution $w(z)$ have a form

$$\begin{aligned} w &= f_w w_0^d \\ z &= f_z z_0^d, \end{aligned} \tag{4.43}$$

where f_w and f_z are polynomial functions of d. Equation (4.42) then becomes

$$\frac{w_0}{2d(1-2/w_0^2)} - \frac{w_0}{2d-2} + \frac{w_0}{d}\left[1 - f_z f_w \left(\frac{z_0 w_0}{2}\right)^d\right] = 0. \tag{4.44}$$

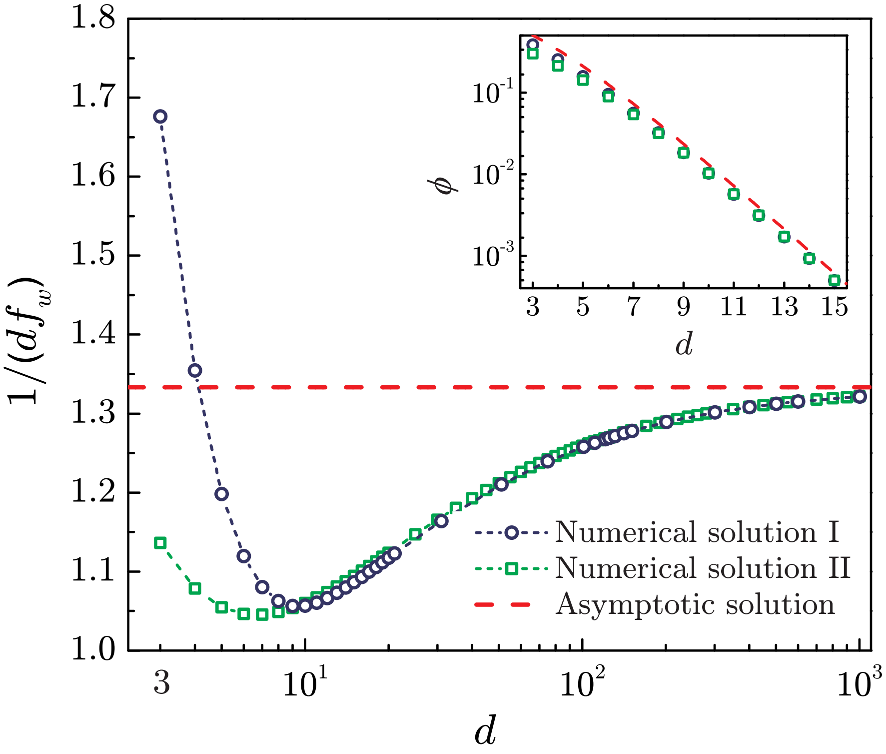

Figure 4.3: The values of $1/(d\,f_w)$ obtained from (i) the exact numerical solution of Eq. (4.33) (numerical solution I), (ii) the correction to the asymptotic analysis in large d obtained by numerically solving Eq. (4.48) (numerical solution II), and (iii) the leading term Eq. (4.46) in the asymptotic analysis (asymptotic solution). The insert shows the dimensional scaling of the corresponding volume fraction ϕ from Eq. (4.47). The numerical values for $d = 3-6$ are also listed in Table 4.1.

The necessity to avoid an exponential divergence of the last term imposes

$$w_0 = 2/z_0, \tag{4.45}$$

and allows to express f_w as a function of f_z. In the isostatic case $z = 2d$, i.e., when $z_0 = 1$ and $f_z(d) = 2d$, simple algebraic manipulations give $f_w = \frac{3}{4d}$, or equivalently,

$$w = \frac{3}{4d}2^d, \tag{4.46}$$

and

$$\phi \sim \frac{4d}{3} 2^{-d}. \tag{4.47}$$

The scaling form of w provides a way to critically examine the simplifications done to $s^*(x)$. Using the rigorous bounds on packing volume fraction for large d, $2^{-d} \leq \phi \leq 2^{-0.5990d}$ [18, Chap 1. Sec. 1.5], and $w \sim 1/\phi$, we get $2 \geq w_0 \geq 2^{0.5990} \approx 1.5146$. Because $w^{1/d} \to w_0$, we use the bound on w_0 to directly check that $1/w_0 \in [0.5, 0.66]$ and $1 - 2/w_0^2 \in [0.128, 0.5]$. We conclude that the use of Eq. (4.37) to approximate $s^*(x)$ in H_d is justified, because its arguments are always positive and bounded away from zero. The validity of the simplified expression for H_d in Eq. (4.41) is also verified.

4.3.3 Finite d corrections

Assuming that Eq. (4.42) has only corrections that are subdominant, the above analysis also provides the leading finite d corrections to w. These corrections can be obtained by numerically solving the condition $H_d(c; w, z)$ with the exact expression Eq. (4.37) for s^* in the case $z = 2d$ and $w = f_w 2^d$, then computing f_w from the condition

$$H_d(2f_w^{1/d}; f_w 2^d, 2d) = 0. \tag{4.48}$$

The results are compared with the self-consistent solution of Eq. (4.33) obtained by direct numerical evaluation of the expressions with the exact form for s^* in Fig. 4.3. The quality of the match at high d provides a further verification of the simplifying approximations made in deriving Eq. (4.42).

Both treatments agree rather well down to $d \approx 10$. The change in behavior of the packing fraction then observed corresponds to where the decay of $P_>(c)$ becomes slower than the growth of c^{d-1} as the dimension increases. This inversion results in $c \sim 2$ maximizing the integrand in high dimensions instead of $c \sim 1$, as in low dimensions. Eq. (4.42) is derived under the assumption that the integral is dominated by $c \sim 2$, which may explain why the two curves deviate from each other in that dimensional regime. Physically, this change corresponds to the jammed packings becoming relatively less efficient with dimension. In high dimensions, nearby spheres do not provide sufficient cover of the sphere surface, which results in the inclusion of farther neighbors within the Voronoi cell. In low dimensions, the screening is efficient, so the integral is dominated by low c values. Because an open structure is less prone to particle-particle correlations, this interpretation is at least consistent with the assumptions made in developing the theory.

4.4 Low d analysis

The analysis in the previous section is based on the approximate high-dimensional expression for $P_>(c)$ from Eq. (4.28) . Errors resulting from the superposition approximation and the postulated form for $g_2(r)$ should be taken into account, in order to improve ϕ results in finite dimensions. Though a systematic expression for these corrections is not trivial to obtain, it is nonetheless possible to guess some of their forms by inspection. And by comparing their predictions with the properties of packings obtained from simulation, we can assess their success. Our low-dimensional analysis expands and generalizes the approach of Ref. [1] for the case $d = 3$ [1, 59].

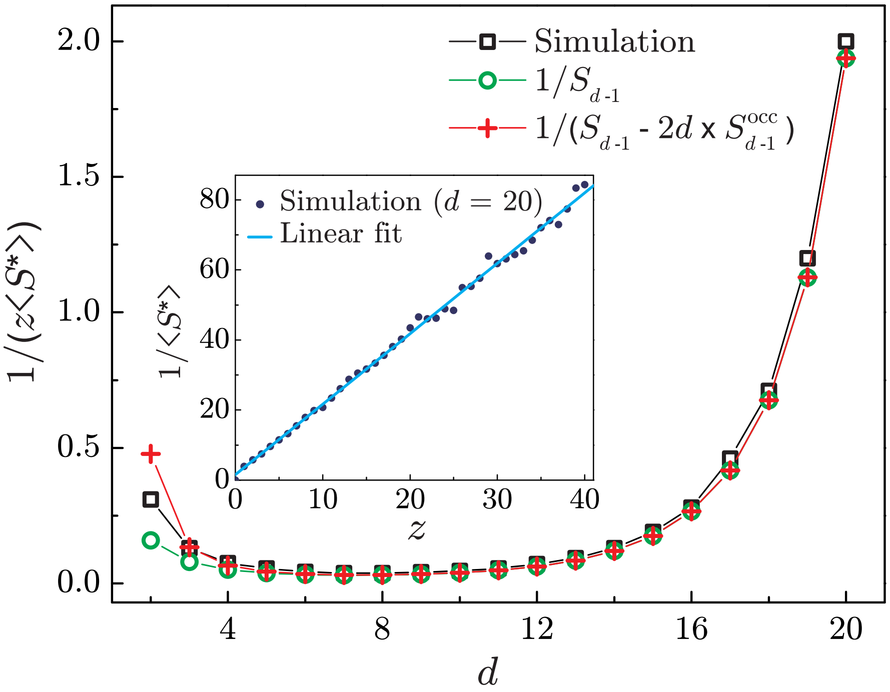

Figure 4.4: Comparison of the approximations for $\langle S^*\rangle$ from Eq. (4.52) and Eq. (4.54) with the simulated results. The results show that $1/\langle S^*\rangle$ is proportional to z when z is not too large ($z \leq 2d$). (inset) The simulation results in $d = 20$ illustrate the linear behavior of $1/\langle S^*\rangle$ with z.

4.4.1 Low d corrections of $P_>(c)$

We first assume that $P_>(c)$ can be factorized in bulk $P_B(c)$ and contact $P_C(c)$ contributions as in Eq. (4.28), and examine the correlations between the different types of particles separately. The contact term has the general form

$$P_C(c) = e^{-S^*(c)/\langle S^*\rangle}, \tag{4.49}$$

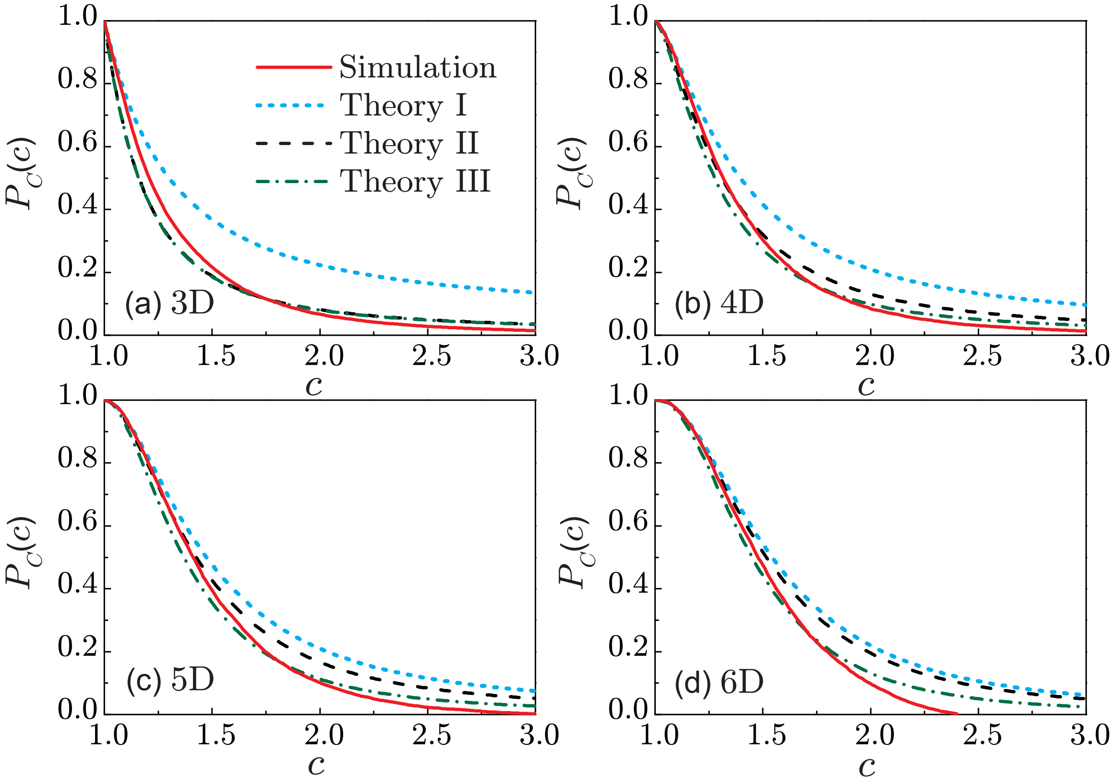

Figure 4.5: Comparison of the simulation and theoretical forms of $P_C(c)$ from Eq. (4.49) using different $\langle S^* \rangle$: (i) Eq. (4.52) for a low-density (high-dimensional) limit (theory I), (ii) Eq. (4.54) for a van der Waals-like correction (theory II), and (iii) direct surface simulations of $\langle S^* \rangle$ (theory III).

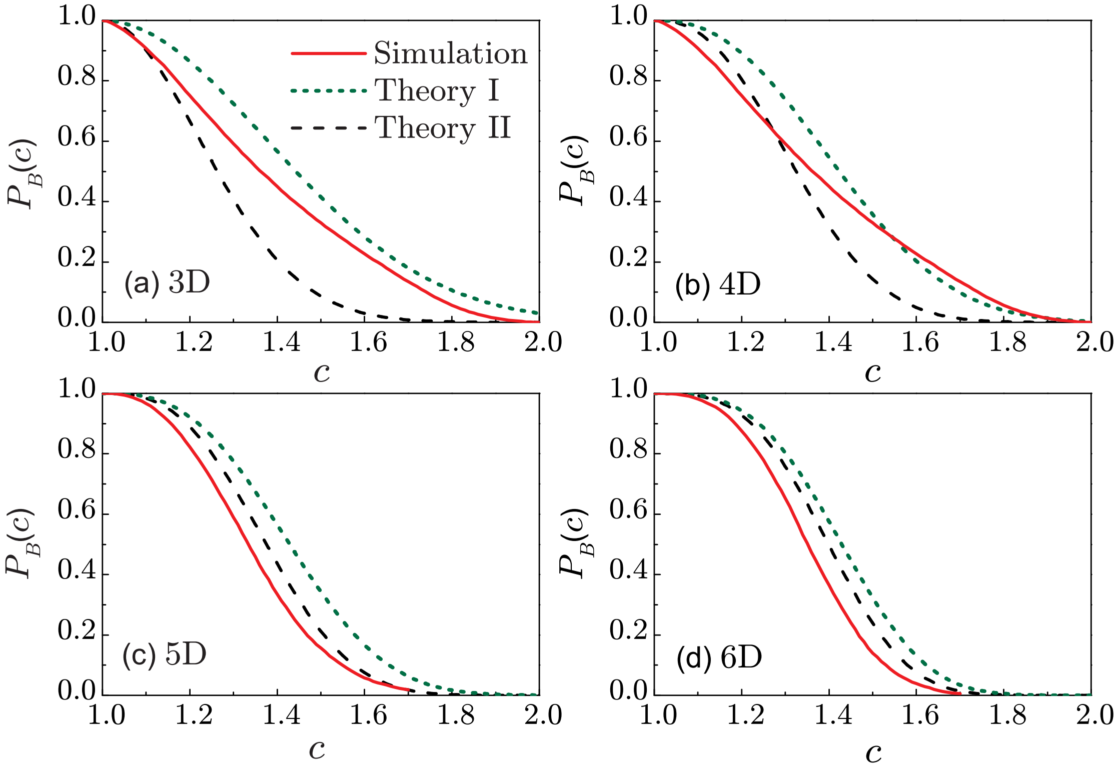

Figure 4.6: Comparison of the simulation and theoretical forms of $P_B(c)$ from Eq. (4.55) using the packing fraction from simulation and different $\langle V^* \rangle$: (i) Eq. (4.56) for the low density limit (theory I) and (ii) Eq. (4.57) for a van der Waals-like correction (theory II).

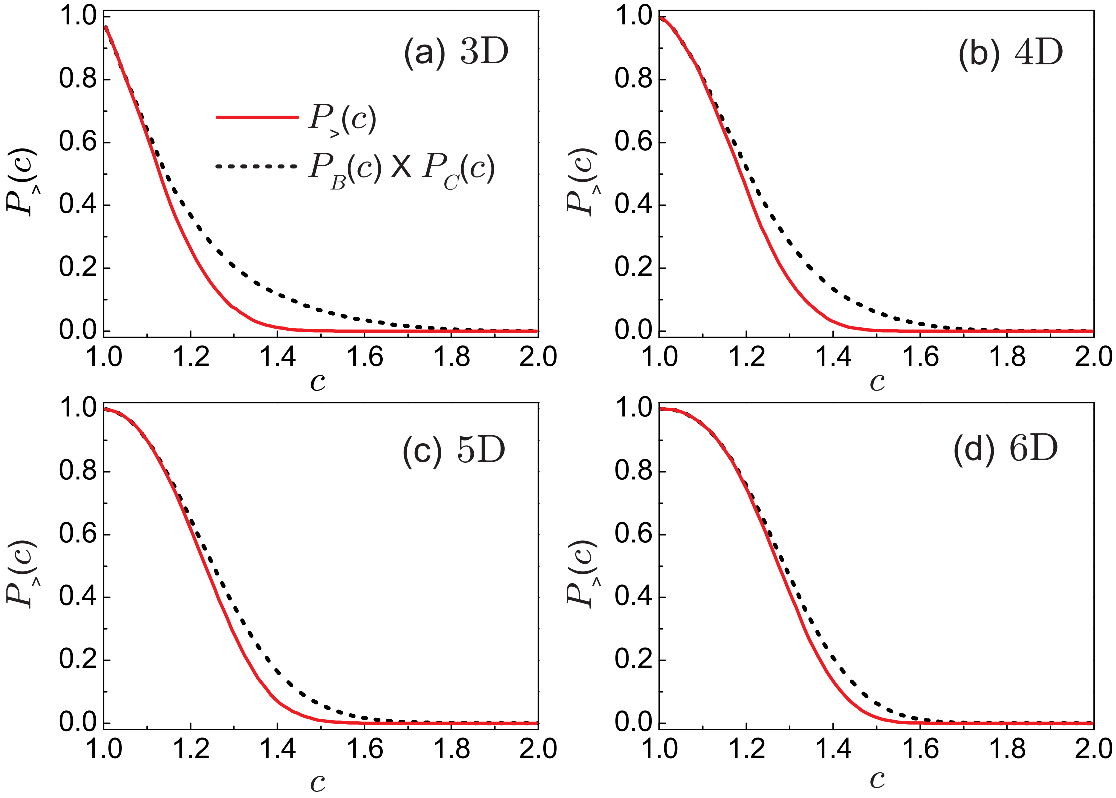

Figure 4.7: Evaluation of the factorization approximation by comparing simulation results for $P_>$ in jammed systems with the product of the bulk and contact contributions also from simulations.

because

$$\begin{aligned}\langle S^*\rangle &= \int_1^\infty S^*(c)f(c)dc = \int_0^1 S^*\,dP_C \\ &\approx \int_0^\infty P_C\,dS^*,\end{aligned} \tag{4.50}$$

where the last step is obtained after integrating by parts and assuming that the upper limit of the integration (the maximum of S^*) goes to infinity. The average of the available solid angle $\langle S^*\rangle$ can also be calculated directly from simulations of surface sphere configurations. In the limit of low occupancy, where the particle volume is negligible and correlations are absent, the probability that z contact particles lie outside $S^*(c)$ is

$$P_C(c) \approx \left[1 - \frac{S^*(c)}{S_{d-1}}\right]^z \approx \exp\left[-\frac{zS^*(c)}{S_{d-1}}\right] \tag{4.51}$$

or

$$\langle S^*\rangle \approx \frac{S_{d-1}}{z}. \tag{4.52}$$

This result is the same as Eq. (4.30) from the previous analysis, because an equivalent approximation to the low-density approximation was taken in the high-dimensional treatment [17]. Surface correlations are, however, particularly significant in low d even for low occupancy, and therefore the S_{d-1} volume (sphere surface) should be corrected for the non-negligible volume occupied by the particles. We define the surface occupied by a sphere at contact

$$S_{d-1}^{\mathrm{occ}} \equiv S_{d-2}\int_0^{\pi/6} (\sin\theta)^{d-2} d\theta, \tag{4.53}$$

to include a van der Waals-like correction for the occupied volume

$$\langle S^* \rangle \approx \frac{S_{d-1} - z S_{d-1}^{\mathrm{occ}}}{z}. \tag{4.54}$$

This expression reduces to the decorrelated form in high dimensions, because $S_{d-1}^{\mathrm{occ}}/S_{d-1}$ vanishes faster than $z \sim d$ grows. Figure 4.4 shows that the latter is slightly better at low d and that both approximations rapidly converge to the $\langle S^* \rangle$ numerically obtained from random distributions of surface sphere configurations. A similar treatment can be applied to the bulk term, which has the form

$$P_B(c) = e^{-V^*(c)/\langle V^* \rangle} \tag{4.55}$$

with $\langle V^* \rangle$ the average volume available to particles beyond the contact rim. Without taking into account the volume excluded by the central sphere, and assuming that there are no angular correlation, the large d limit is recovered

$$\langle V^* \rangle = V/N = 1/\rho. \tag{4.56}$$

A correction *à la* van der Waals for the correlations that arise from the excluded volume by the central particle gives a form similar to that of the surface term

$$\langle V^* \rangle = \frac{V - N V_g}{N} = V_g w. \tag{4.57}$$

The expression reduces to the uncorrelated form in high dimensions, because the volume of a unit-diameter ball grows much slower than the volume per particle at jamming.

The contact and bulk corrections above are equivalent to those obtained in the original derivation of the theory in $d = 3$ [1]. Comparing the different expressions with the simulation results should inform us on the reasonableness of the approximations made in the derivation. As can be seen in Fig. 4.5, even a crude treatment of volume exclusion improves the quality of the scaling form of the contact contribution [1]. Using the simulated value of $\langle S^* \rangle$ does even better. Moreover, the agreement with the scaling form steadily improves from three to six dimensions. Figure 4.6 shows that the bulk contribution is also better captured when correlations are included. We note however that though the agreement of the bulk scaling form improves with dimension, convergence is slower than for the contact contribution. Higher-dimensional comparisons would be useful to confirm the trend, but are unfortunately beyond current computational reach.

Even assuming that we could obtain separate perfect bulk and contact scaling forms, the factorization of the two contributions itself remains an approximation. The corrections to this approximation are not easily directly tractable, but the rapidity at which it vanishes can be indirectly evaluated by analyzing the structure of jammed configurations. Figure 4.7 indicates that corrections to the factorization vanish fairly rapidly with dimension, which supports the validity of the high-dimensional treatment.

d	ϕ_{sim}	ϕ_{fact}	ϕ_{lowD}	ϕ_{highD}
3	0.64(1)	0.54	0.64	0.39
4	0.46(1)	0.39	0.38	0.25
5	0.31(1)	0.27	0.22	0.16
6	0.20(1)	0.18	0.13	0.10

Table 4.1: Jamming packing fraction of frictionless spheres at $z = 2d$. Compression results from various simulation approaches ϕ_{sim} (see text) are compared with the integration of the surface and bulk decomposition of $P_>(c)$ (ϕ_{fact}), the low-dimensional approximation (ϕ_{lowD}), and the high-dimensional approximation (ϕ_{highD}), as introduced in the text.

4.4.2 Low d jammed packing fraction

Comparing the numerical jamming packing fraction obtained under different approximation schemes with the direct compression of the system for various dimensions provides a final evaluation of the theoretical treatment (see Table 4.1). From a simulation perspective, it is reassuring to note that the packing fraction obtained from compression simulations agree not only with the previously reported 4-6d values [47], but also with the free volume estimates from the metastable liquid state [116], the zero-shear limit in 4d [125], and the canonical 3d results [7,12,14]. From the theoretical point of view, three different levels of approximation for $P_>$ are selected to solve Eq. (4.9).

- ϕ_{highD}: the high-dimensional approximation is the numerical solution to Eq. (4.33) plotted in Fig. 4.3 (numerical solution I). This approximation is only valid in the high-dimensional or low-density limit. Therefore, ϕ_{highD} is expected to have significant deviations from the simulation values in low

---

[1] Note that the agreement with the theoretical tail of $P_c(c)$ improves with increasing simulated system size in $d = 6$ (not shown), but does not significantly affect the agreement with $P_>(c)$.

d.

- ϕ_{lowD}: the low-dimensional corrections Eqs. (4.49), (4.55) and (4.57) to $P_>(c)$ give

  $$P_>(c) \approx \exp\left[-\frac{2^d V^*(c)}{wV_d} - \frac{S^*(c)}{\langle S^*\rangle}\right], \tag{4.58}$$

  where $\langle S^*\rangle$ is obtained from analyzing simulations of surface sphere configurations [2]. This is exactly the same approach as what was used in Ref. [1] for the 3d case.

- ϕ_{fact}: the factorized approximation of $P_>(c) = P_B(c)P_C(c)$ is obtained by computing $P_B(c)$ and $P_C(c)$ directly from simulations of jammed configurations.

The first approximation is the crudest, while the last one only assumes $P_>$ to be factorizable. The latter should therefore be the most accurate and become more so with increasing dimension. The factorized version ϕ_{fact} indeed steadily approaches the simulation results ϕ_{sim} with increasing dimension. The agreement of ϕ with ϕ_{sim} with theoretical sophistication from ϕ_{highD} to ϕ_{fact} also generally improves for a given dimension. Note that the 3d result for frictionless spheres of Song *et al.* [1] (ϕ_{lowD} in Table 4.1), which agrees very well with the simulation value, defies however this last trend.

Deviations between theory and simulation confirm that correlations are not negligible in low dimensions. The assumption of the factorizability of $P_>$ as well as

---

[2] The ϕ_{lowD} results in Table 4.1 are different from the $\phi_{\text{MRJ}}^{\text{stat}}$ of van Meel *et al.* [116], where $\langle S^*\rangle = (S_{d-1}/2 + S_{\text{occ}})/z$ was used as ansatz for $P_C(c)$ as suggested in [1, 59].

the theoretical forms of P_B and P_C should thus be refined by including the contributions from these correlations, in order to obtain a systematic quantitative agreement in low dimensions.

4.5 Discussion and relation with other approaches

In this section, we discuss the relation of the results obtained above with other approaches to the problem of sphere packing in large dimension. The present theory predicts that amorphous isostatic, i.e., random close packed, configurations have a *unique* packing fraction $\phi \sim (4/3)\, d\, 2^{-d}$. This scaling lies within the known rigorous upper and lower bounds for packings. But because these constraints are not so difficult to satisfy, it is more instructive to contrast the scaling form with that of approaches developed specifically to deal with amorphous packings.

A first set of results for amorphous packings has been obtained by analyzing the behavior of a class of simple algorithms, such as Ghost Random Sequential Addition (GRSA). GRSA is actually able to *construct* packings up to density $\phi = 2^{-d}$, which provides a nice way of generating amorphous configurations up to the Minkowski lower density bound [126]. Random Sequential Addition (RSA), where one attempts to add a sphere randomly and accepts the move only if there are no overlaps, produces more efficient packings. But RSA is already too complex to be analyzed analytically, so one has to resort to numerical investigations [127, 128]. The results of RSA are consistent with $\phi = d\, 2^{-d}$, which is closer to but still lower than our scaling form. It is well known that RSA algorithms are not very efficient in low dimensions. A much more efficient approach is the Lubachevsky-Stillinger

(LS) algorithm, which is able to construct isostatic packings with a density close to random close packing in low dimensions (see Sec. 4.1) [47]. Unfortunately, investigating the LS algorithm in the large d limit is not possible. The extrapolation of the scaling form to low dimensions $\phi \sim 2.56\, d\, 2^{-d}$ [47] is probably not reliable due to the change in the nature of packings around $d \approx 10$, as discussed above.

In the absence of a direct way to analyze the packing algorithms, we resort to an alternate approach that provides an estimate of the random close packing density in large d. The mean field approach to the glass transition known as Random First Order Transition (RFOT) theory [129] assumes that amorphous packings correspond to the infinite pressure limit of long-lived metastable hard sphere glasses [3]. The problem of random close packing is then reduced to the study of a simpler equilibrium problem, that of computing the equation of state of the glass. This approach predicts that the system remains a liquid [130,131] up to a certain packing fraction ϕ_{dyn}, where a dynamical transition to a finite pressure glass occurs [129]. Inside the glass phase, a huge number of glassy states coexist. Applying an infinite pressure on these glassy states results in isostatic jammed configurations with a *range* of packing fractions, as has been numerically verified in low dimensions [47,86]. In general, the range extends from a threshold (th) packing fraction to the glass close packed (GCP) packing fraction, i.e., $\phi \in [\phi_{\mathrm{th}}, \phi_{\mathrm{GCP}}]$ [3]. One of the key qualitative results of the RFOT treatment therefore differs from the present theory's uniqueness prediction.

Comparing the detailed high-dimensional behavior of the various approaches sheds some light on this disagreement. Several different implementations of the general RFOT approach provide scaling forms for its constitutive densities.

- Density Functional Theory (DFT) predicts $\phi_{\rm dyn} = \sqrt{2\pi e}\, d\, 2^{-d} \sim 4.13 d\, 2^{-d}$ [129].

- Mode-Coupling Theory (MCT) predicts $\phi_{\rm dyn} \sim d^2\, 2^{-d}$ in its full version [132,133] and $\phi_{\rm dyn} = 2\sqrt{2\pi e}\, d\, 2^{-d} \sim 8.26 d\, 2^{-d}$ when using a Gaussian approximation for the non-ergodic parameter [129, 132]. It was shown in Ref. [132], however, that MCT leads to inconsistencies above $\phi \sim d\, 2^{-d}$. The scaling $\phi_{\rm dyn} \sim d^2\, 2^{-d}$ predicted by the full MCT thus seems unreliable.

- Replica Theory (RT) predicts $\phi_{\rm dyn} \sim 4.8\, d\, 2^{-d}$ for the dynamical transition, and $\phi_{\rm th} \sim 6.26\, d\, 2^{-d}$ and $\phi_{\rm GCP} \sim d \ln(d)\, 2^{-d}$ as boundaries for jamming.

Interestingly, DFT, RT, the corrected MCT, and the present theory all predict $\phi \sim d\, 2^{-d}$ for the glassy/jamming density. It remains a problem of RFOT to reconcile the $\phi_{\rm dyn}$ predictions coming from the different approaches (DFT and MCT cannot make any prediction for the jamming densities). But, for now, all RFOT theories give $\phi_{\rm dyn}$ bigger than $(4/3)\, d\, 2^{-d}$, which suggest that the system should still be a liquid at the density where the current theory predicts it to be jammed. If one believes the RFOT results, this discrepancy suggests that the present theory might still be missing some correlations that, although irrelevant to determine the overall scaling of the density, are important for the precise determination of the prefactor. The replica theory prediction that jammed packings exist in an interval $\phi \in [6.26\, d\, 2^{-d}, d \ln(d)\, 2^{-d}]$, whose width grows with dimension might be also encoded in some missing correlations. Understanding the nature of these correlations, or disproving the replica results, could be considerable advances in the microscopic comprehension of amorphous high- and low-dimensional jammed packings.

Finally, an interesting byproduct of the current analysis is a relation between the volume fraction ϕ and the average coordination number z in high dimensions from Eq. (4.45)

$$\phi \sim \frac{z}{2^d}. \tag{4.59}$$

This scaling is consistent with the results obtained in Refs. [17, 134], which use a rather different approach. The relation thus seems well verified (possibly with sub-exponential corrections) for amorphous packings and a range of known lattice (see [18, 135] for the volume fraction and the kissing number of a list of all known densest packings up to $d = 128$).

Chapter 5

Jammed packings of different size spheres

In parallel with the large literature dealing with monodisperse sphere packings, a large body of experimental, theoretical and numerical work has been devoted to the analysis of polydisperse systems; the interest arising due to the simple fact that polydispersivity is omnipresent in most realistic systems and industrial applications [73, 136–138]. While previous approaches have focused on frictionless packings, an integrated analytical approach that brings together different observations for all packings from RLP to RCP and for any friction or coordination number is still lacking. Based on our previous statistical mechanics approach [1] (Chapter. 2), here we build such a framework.

We show that the key aspect to solve this problem is the dependence of the various coordination numbers between the different species and the concentration of the species. This is calculated here and shown to agree well with computer simulations.

This result is then incorporated into a statistical theory of volume fluctuations as in [1] which calculates the free volume of a particle in terms of the coordination number. The main result is the prediction of the RLP and RCP limiting densities for a given distribution of sphere sizes as well as the prediction of densities for any packing in between those limits. The formalism allows for a determination of the best packing fraction in terms of different distributions of sphere sizes with specified constraints, as we show with a simple example. We discuss possible generalization of the method to solve more difficult problems like the phase behavior of systems of non-spherical particles like rods or spherocylinders in any dimensions; problems of long-standing history in condensed matter [139].

The theory developed in Ref. [1] (Chapter 2) allow for the prediction of the density of RCP and RLP for equal-size sphere packings using a relation between the average volume and the geometrical coordination number. Following this approach, we here describe long-range spatial correlations through a mean-field background term. This approximation makes the problem amenable to analytic calculations, and is shown to describe well our simulation results. An explicit inclusion of such correlations is possible in our framework, but severely complicates any solution attempts.

The above theoretical framework will guide the present formalism for polydisperse systems. We first treat the case of binary mixtures of hard spheres of radius R_1 and R_2 ($R_2 > R_1$) in 3d and then generalize the problem to any distribution.

5.1 Binary packings

5.1.1 Coordination number

The key quantity to calculate is z_{ij}, denoting the mean number of contacts of a sphere of radius R_i with a sphere of radius R_j, versus the concentration of one of the species. We need a formula for z_{ij} as a function of $(z, x, \frac{R_2}{R_1})$, the later being the size ratio, x is the fraction of small spheres in the packing $x \equiv N_1/(N_1 + N_2)$ with N_i the number of i spheres and z is the global geometrical coordination number averaged over all the particles: $z \equiv xz_1 + (1-x)z_2$ where z_i is the average coordination of each species. The coordinations are determined by three equations:

$$z_i = z_{i1} + z_{i2}, \ (i = 1, 2), \qquad xz_{12} = (1-x)z_{21}. \tag{5.1}$$

We assume that these coordinations are inversely proportional to the average solid angle extended by contacting spheres R_1 and R_2. The average solid angles are denoted $\langle S_i^{occ} \rangle$ and are calculated in terms of the solid angle that a sphere R_j occupy on a sphere R_i according to

$$\langle S_i^{occ} \rangle = xS_{i1}^{occ} + (1-x)S_{i2}^{occ} \tag{5.2}$$

with (see Fig. 5.1a)

$$S_{ij}^{occ}/2\pi \equiv \int_0^{\arcsin(\frac{R_j}{R_i+R_j})} \sin\theta \, d\theta = 1 - \sqrt{1 - (\frac{R_j}{R_i + R_j})^2}. \tag{5.3}$$

Thus, $\langle S_i^{occ} \rangle$ represents the mean occupied surface on a i sphere weighted by the

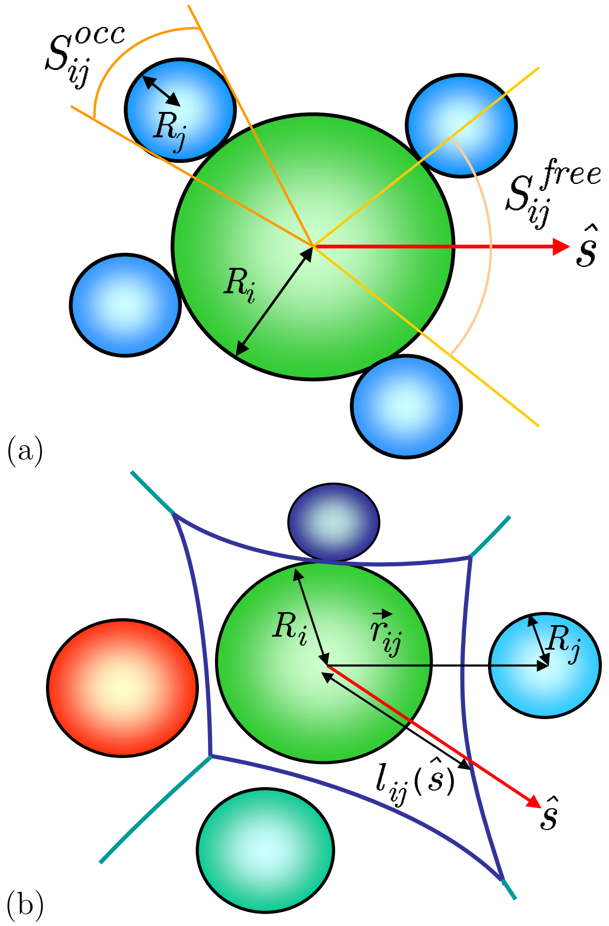

Figure 5.1: (a) Occupied surface and free surface. (b) Voronoi cell for polydisperse spheres. Plots are in 2d for easier visualization.

concentrations x and $(1-x)$. This represents an approximation since the real weights are z_{i1}/z_i and z_{i2}/z_i, respectively. Then, $z_i \propto 1/\langle S_i^{occ}\rangle$ leading to the following normalizations:

$$z_1 = \frac{z}{x + (1-x)\frac{\langle S_1^{occ}\rangle}{\langle S_2^{occ}\rangle}}, \qquad z_2 = \frac{z}{x\frac{\langle S_2^{occ}\rangle}{\langle S_1^{occ}\rangle} + (1-x)}. \tag{5.4}$$

Thus, the system of Eqs. (5.1) is reduced to a system of three equations for four unknowns z_{ij}. To close the system we assume proportional laws and deduce z_{ij}

from z_i by considering that z_{ij} is proportional to the number of contacts of the i spheres times the number of contacts of the j spheres:

$$\begin{aligned} z_{11} &= A(z_1x)(z_1x), & z_{12} &= A(z_1x)z_2(1-x), \\ z_{21} &= Bz_2(1-x)(z_1x), & z_{22} &= Bz_2(1-x)z_2(1-x). \end{aligned} \tag{5.5}$$

Using the first equation in (5.1) we find the constants A and B, leading to the solution:

$$\begin{aligned} z_{11} &= \frac{z_1^2 x}{z}, & z_{12} &= \frac{z_1 z_2(1-x)}{z}, \\ z_{21} &= \frac{z_1 z_2 x}{z}, & z_{22} &= \frac{z_2^2(1-x)}{z}. \end{aligned} \tag{5.6}$$

Figure 5.2a, compares this solution to numerical simulations of Hertz packings jammed at RCP [1] for $R_1/R_2 = 1.4$ and $z = 6$. We find that the formulae are very accurate for size ratios below 1.5 and present small deviations up to size ratio 2. The results are also in agreement with [73, 136–138].

5.1.2 Voronoi cell

The common way to divide a system into volumes associated with each particle is the Voronoi tessellation. The Voronoi cell for monodisperse particles [1] is composed by all the points nearest to the center of the sphere than to any other sphere. This definition has been extended in [140] to the case of polydisperse systems and non-spherical particles: instead of considering the classical Voronoi polyhedron defined by the center of the particle, one should consider all the points which are

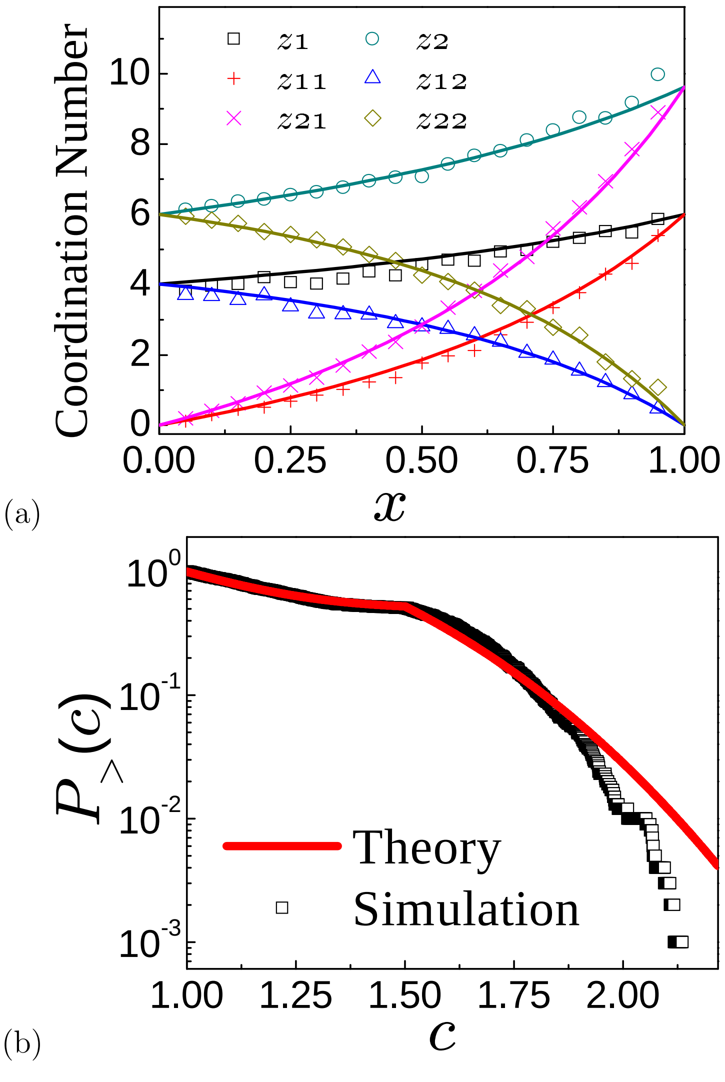

Figure 5.2: Comparison between theory and numerical simulations for (a) z_{ij}, Eq. (5.6), and (b) $P_>(c)$, Eq. (5.13).

closer to the surface of a given particle. Such a construction is called the *Voronoi S region* and tiles a system of nonspherical convex particles and polydisperse systems as can be seen in Fig. 5.1b. Following this approach we calculate the average volume of a polydisperse Voronoi cell, denoted W. The volume fraction is given by $\phi = \frac{V_g}{W}$, where $V_g = \frac{4\pi}{3}(xR_1^3 + (1-x)R_2^3)$ is the mean volume of a sphere. We first find the analytical formula of the Voronoi S region. The boundary of the Voronoi cell in the direction $\hat{s}$ of a i sphere next to a j sphere at position r_{ij} is (Fig. 5.1b):

$$l_{ij}(\hat{s}) = \frac{1}{2}\frac{r_{ij}^2 - (R_i - R_j)^2}{r_{ij}(\hat{r}_{ij} \cdot \hat{s}) - (R_i - R_j)}, \tag{5.7}$$

where $\hat{s}$ and $\hat{r}_{ij}$ are unitary. Thus, the boundary of a Voronoi cell of a sphere i in the direction $\hat{s}$ is the minimum of $l_{ij}(\hat{s})$ over all the particles j for any $l_{ij}(\hat{s}) > 0$. This leads to

$$l_i(\hat{s}) = \frac{1}{2} \min_{\hat{s}.\hat{r}_{ij} > \frac{R_i - R_j}{r_{ij}}} \frac{r_{ij}^2 - (R_i - R_j)^2}{r_{ij}(\hat{r}_{ij} \cdot \hat{s}) - (R_i - R_j)}. \tag{5.8}$$

The volume of the cell of the sphere i is then given by $W_i = \frac{1}{3}\oint l_i(\hat{s})^3 ds$. We define the orientational Voronoi volume, W_i^s, along the direction $\hat{s}$ by $W_i \equiv \frac{1}{4\pi}\oint W_i^s ds = \langle W_i^s \rangle_s$. This leads to

$$W_i^s = \frac{\pi}{6} \min_{\hat{r_{ij}}.\hat{s} > \frac{R_i - R_j}{r_{ij}}} \left(\frac{r_{ij}^2 - (R_i - R_j)^2}{r_{ij}(\hat{r_{ij}}.\hat{s}) - (R_i - R_j)}\right)^3. \tag{5.9}$$

This definition leads to the results of [1] when $R_1 = R_2$. Since the system is isotropic, the mean Voronoi volume can be calculated as:

$$W \equiv \langle\langle W_i^s \rangle_s\rangle_i = \langle\langle W_i^s \rangle_i\rangle_s = \langle W_i^s \rangle_i. \tag{5.10}$$

5.1.3 Mean Voronoi volume

Having calculated the Voronoi cell exactly in Eq. (5.9), we now proceed to develop a probability theory of volume fluctuations in the spirit of the quasiparticle approximation used in [1] to obtain the mean Voronoi volume. For a given sphere i, the calculation of W_i^s reduces to finding the sphere j^* that minimizes $l_{ij}(\hat{s})$. We call j^* the Voronoi sphere for the sphere i. We consider $r \equiv r_{ij^*}$, $\cos\theta \equiv \hat{s} \cdot \hat{r}_{ij^*}$ and $c \equiv 2l_{ij^*}$. We have $c = \frac{r^2-(R_i-R_j)^2}{r\cos\theta-(R_i-R_j)}$. Therefore, we just need to compute the inverse cumulative distribution function, denoted $P_>(c)$, to find all the spheres j with $l_{ij} > \frac{c}{2}$, and thus not contributing to the Voronoi volume of the sphere i. The average Voronoi volume is then given by the expression

$$W = \frac{\pi}{6}\langle c^3 \rangle = -\frac{\pi}{6}\int_0^\infty c^3 \frac{dP_>(c)}{dc} dc = \frac{\pi}{2}\int_0^\infty c^2 P_>(c) dc. \tag{5.11}$$

We calculate the mean Voronoi volume for the spheres of radius R_1 and R_2 separately and then average them. We denote $P_>^1(c)$ and $P_>^2(c)$ the inverse cumulative distributions respectively, and $W = x\frac{\pi}{2}\int_0^\infty c^2 P_>^1(c)dc + (1-x)\frac{\pi}{2}\int_0^\infty c^2 P_>^2(c)dc$, and therefore,

$$P_>(c) = xP_>^1(c) + (1-x)P_>^2(c). \tag{5.12}$$

5.1.4 Inverse cumulative distribution function $P_>(c)$

There are three salient steps in the calculation of $P_>(c)$: (i) The separation of $P_>(c)$ following Eq. (5.12). (ii) The separation of each term $P_>^i(c)$, $i = 1, 2$, into two contributions: a term taking into account the contact spheres, $P_>^{iC}(c)$, and a bulk term, $P_>^{iB}(c)$. The contact term clearly depends on z_{ij}. The bulk term averages over all spatial correlations of non-contact particles and, without significant loss of accuracy as shown below, we assume that it only depends on the average value of W. In principle, it is possible to use a more realistic form for this term, but this would render the problem practically unsolvable. (iii) The separation of $P_>^{iC}(c)$ and $P_>^{iB}(c)$ into two terms $P_>^{ijC}(c)$ and $P_>^{ijB}(c)$, $j = 1, 2$, for each species.

An assumption of the theory (to be tested a posteriori with computer simulations) is that all of these terms are independent. Thus

$$\begin{aligned} P_>(c) &= xP_>^{11C}(c)P_>^{12C}(c)P_>^{11B}(c)P_>^{12B}(c) \\ &+ (1-x)P_>^{21C}(c)P_>^{22C}(c)P_>^{21B}(c)P_>^{22B}(c). \end{aligned} \tag{5.13}$$

Also, we work in the limit of large number of particles leading to Boltzmann-like exponential distributions for each $P_>^{ijC}$ and $P_>^{ijB}$ [1]. Four important quantities are then defined: (i) $V_{ij}^*(c)$ and (ii) $S_{ij}^*(c)$: the excluded volume and surface on the sphere, respectively, where no center of a sphere j can be located for a given sphere i and for a given c. (iii) ρ_j: the mean number of spheres j by the left free volume. (iv) ρ_{ij}^s: the mean number of spheres j by the left free surface on a sphere

i. These considerations lead to:

$$\begin{aligned} P_{>}^{ijB}(c) &= \exp\Big(-\rho_j V_{ij}^*(c)\Big), \\ P_{>}^{ijC}(c) &= \exp\Big(-\rho_{ij}^s S_{ij}^*(c)\Big). \end{aligned} \tag{5.14}$$

Next, we calculate these four quantities. To simplify we denote $l \equiv R_i + R_j$, $k \equiv R_i - R_j$ and Θ the step-function. We obtain:

$$\begin{aligned} S_{ij}^*(c) &= \int \Theta(c - \frac{l^2 - k^2}{l\cos\theta - k}) ds = 2\pi(1 - \frac{l^2 - k^2 - kc}{lc}), \\ V_{ij}^*(c) &= \int \Theta(c - \frac{r^2 - k^2}{r\cos\theta - k}) dr^3 = 2\pi(-\frac{1}{4c}((c+k)^4 - l^4) \\ &\quad + \frac{1}{3}((c+k)^3 - l^3) + (\frac{k^2}{2c} + \frac{k}{2})((c+k)^2 - l^2)), \\ \rho_j(W) &= \frac{x_j}{W - V_g}, \end{aligned} \tag{5.15}$$

where $x_1 = x$ and $x_2 = (1-x)$. The fourth quantity, ρ_{ij}^s, is the most difficult to calculate. In terms of the occupied areas Eqs. (5.3) we have $\rho_{ij}^s = \frac{z_{ij}}{4\pi - z_{i1}S_{i1}^{occ} - z_{i2}S_{i2}^{occ}}$. However, for the contact terms, the analogy with the Boltzmann-like exponential distribution of volumes is far from being exact. This is because this form is based on the large number limit which in the case of contacting spheres is no more than around 6. Therefore, the exponential distribution is used as an Ansatz with ρ_{ij}^s a variational parameter as in [1]. We denote $\langle S_{ij}^{\text{free}} \rangle$ the mean solid angle of the gaps left between the j contacting neighbors of a i sphere (Fig. 5.1a). We obtain:

$$\begin{aligned}\langle S_{ij}^{\text{free}}\rangle &= \int_0^\infty S_{ij}^*(c)\frac{d(1-P_>(c))}{dc}dc \\ &\approx \rho_{ij}^s\int_0^{2\pi} S_{ij}^*\exp(-\rho_{ij}^s S_{ij}^*)dS_{ij}^* = \frac{1}{\rho_{ij}^s}.\end{aligned} \tag{5.16}$$

Then, we perform numerical simulations to find $\langle S_{ij}^{free}\rangle$. We randomly generate spheres of radius R_i and R_j with the proportion z_{i1}/z_i and z_{i2}/z_i respectively around a sphere of radius R_i and then evaluate the mean free surface $\langle S_{ij}^{free}\rangle$ and its inverse to obtain ρ_{ij}^s. We find

$$\begin{aligned}\rho_{ij}^s(z_{ij}) &= \frac{z_{ij}}{2\pi}(1-\frac{z_{i1}}{z_i}\frac{S_{i1}^{occ}}{2\pi}-\frac{z_{i2}}{z_i}\frac{S_{i2}^{occ}}{2\pi}) \\ &= \frac{z_{ij}}{2\pi}(\frac{z_{i1}}{z_i}\sqrt{1-(\frac{R_1}{R_i+R_1})^2}+\frac{z_{i2}}{z_i}\sqrt{1-(\frac{R_2}{R_i+R_2})^2})),\end{aligned} \tag{5.17}$$

which is a generalization of the results of [1] to polydisperse systems.

Using Eqs. (5.14), (5.15) and (5.17) into (5.13), $P_>(c)$ can be calculated by solving the equations numerically. Figure 5.2b depicts the comparison of the theoretical results of the probability of Voronoi volumes $P_>(c)$ with computer generated Hertzian packings with $z = 6$ for $x = 0.5$ at RCP. The calculated distribution is quite accurate for most of the range except for small deviations at high values of c, which however, do not affect much the value of the average $\langle c^3\rangle$ in Eq. (5.11). This shows that our mean-field approximation already captures the main contribution of the probability distribution function $P_>(c)$.

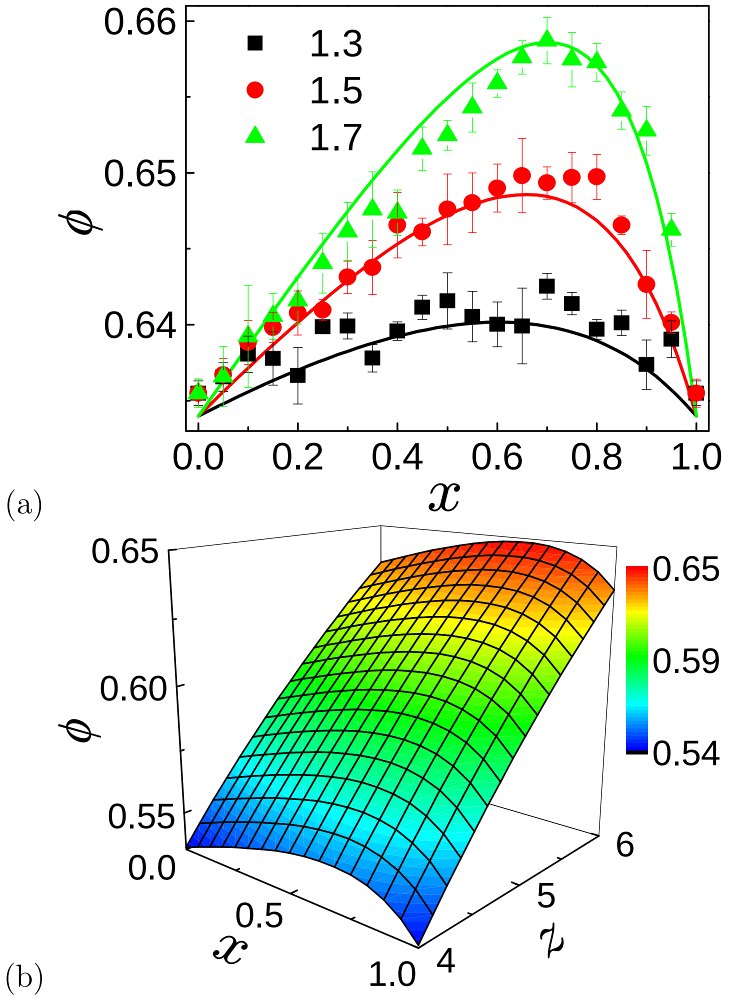

Figure 5.3: (a) Comparison between theory and numerical simulations of Hertzian packings at RCP, i.e. $z = 6$ versus x for different values of R_1/R_2 as indicated. Error bars are std over 10 realizations of the packings with 10,000 spheres. (b) Three dimensional surface plot of ϕ as a function of z and x for $R_1/R_2 = 1.5$.

5.1.5 Volume fraction

The above considerations lead to a final form to calculate W using Eq. (5.13) into (5.11):

$$W = \frac{\pi}{2} \sum_i x_i \int_0^\infty c^2 \exp\Big(\sum_j (-\rho^s_{ij} S^*_{ij}(c) - \rho_j(W) V^*_{ij}(c))\Big) dc. \tag{5.18}$$

Notice that $\rho_j(W)$ depends on W, Eq. (5.15), and $\rho^s_{ij}(z_{ij})$ depends on the z_{ij}, Eq. (5.17), which in turn depends on the concentration x and z through Eq. (5.6). Therefore Eq. (5.18) is a self-consistent equation to obtain $W(z, x)$, for a given R_1/R_2. A numerical integration of Eq. (5.18) is performed versus x for a given value of z. By considering the isostatic limits of $z = 6$ and $z = 4$ we predict the limits of RCP and RLP at zero friction and infinite friction between the spheres, respectively [1]. The results for the volume fraction at RCP versus x are depicted in Fig. 5.3a which also compares the results to numerically generated packings of Hertz spheres [1]. We see a very good agreement indicating that the theory captures well the behavior of polydisperse packings and that the approximations used are reasonable. For size ratios larger than 2 deviations are found indicating the limit of validity of the approach. For any other value of interparticle friction between 0 and ∞, the density is obtained by setting z between the limiting isostatic values of 6 and 4, respectively. The resulting volume fraction is shown in Fig. 5.3b. The result for RLP for a given x is a new prediction as this problem has not been investigated before. Our results promote new experiments to test the RLP limit of polydisperse systems shown in Fig. 5.3b. The numerical results at RCP and RLP are provided in Table 5.1 and 5.2.

x	0	0.1	0.2	0.3	0.4	0.5	0.6	0.7	0.8	0.9
$\frac{R_2}{R_1}$										
1.3	0.535	0.538	0.539	0.541	0.542	0.542	0.543	0.542	0.541	0.539
1.5	0.535	0.539	0.543	0.546	0.548	0.550	0.552	0.552	0.550	0.545
1.7	0.535	0.541	0.546	0.551	0.555	0.559	0.562	0.563	0.561	0.536

Table 5.1: Volume fraction of binary packings for $z = 4$, RLP.

x	0	0.1	0.2	0.3	0.4	0.5	0.6	0.7	0.8	0.9
$\frac{R_2}{R_1}$										
1.3	0.634	0.636	0.637	0.638	0.639	0.640	0.640	0.640	0.639	0.634
1.5	0.634	0.637	0.640	0.642	0.645	0.647	0.648	0.648	0.647	0.643
1.7	0.634	0.639	0.643	0.648	0.652	0.655	0.658	0.659	0.657	0.651

Table 5.2: Volume fraction of binary packings for $z = 6$, RCP.

5.2 Polydisperse packings

The formalism can be extended to consider any distribution of sphere radius. The main modification is that all the sums over the radius are replaced by integrations over the desired distribution of radius $P(R)$ (the binary case corresponds to two delta-functions at R_1 and R_2). And all the quantities are calculated for spheres of internal radius r and external R and x and $(1-x)$ are replaced by $P(r)dr$ and $P(R)dR$, respectively, including the coordinations:

$$W = \frac{\pi}{2} \int dr P(r) \int_0^\infty c^2 \exp\Big(\int dR(-\rho^s_{rR} S^*_{rR}(c) - \rho_R(W) V^*_{rR}(c)) \Big) dc, \tag{5.19}$$

where

$$S^*_{rR}(c) = \int \Theta(c - \frac{l^2 - k^2}{l\cos\theta - k}) ds = 2\pi(1 - \frac{l^2 - k^2 + kc}{lc}),$$

$$
\begin{aligned}
V^*_{rR}(c) &= \int \Theta(c - \frac{r^2 - k^2}{r\cos\theta - k}) dr^3 \\
&= 2\pi(-\frac{1}{4c}((c-k)^4 - l^4) + \frac{1}{3}((c-k)^3 - l^3) + (\frac{k^2}{2c} - \frac{k}{2})((c-k)^2 - l^2)),
\end{aligned}
$$

$$
\rho_R(W) = \frac{P(R)}{W - V_g},
$$

$$
\rho^s_{rR} = \frac{z_{rR}}{2\pi} \int_0^\infty \frac{z_{rr'}}{z_r} \sqrt{1 - (\frac{r'}{r+r'})^2)} dr',
$$

$$
z_r = z \frac{A}{\langle S^{occ}_r \rangle},
$$

$$
\langle S^{occ}_r \rangle = \int_0^\infty 2\pi(1 - \sqrt{1 - (\frac{r'}{r+r'})^2)} P(r') dr',
$$

$$
A^{-1} = \int_0^\infty \frac{P(r')}{\langle S^{occ}_{r'} \rangle} dr',
$$

and

$$
z_{rr'} = \frac{z_r z_{r'} P(r')}{z}.
$$

To simplify the expressions, we have used $l = r + R$, $k = r - R$.

This result allows to explore the space of radius distributions in search of the optimal packings for a given polydispersivity. This analysis could be of industrial interest if one wishes to optimize the packing fraction by introducing different species in the mixture.

We calculate the volume fraction for several distributions $P(R)$ constraint by sphere radius in the range [1,2], in search of the optimal packing. We calculate the volume fraction for various $P(R)$ ranging from uniform to two-peaked Gaussian distributions of varied widths. We find that the more small spheres we add the better the packing until a certain point where the volume fraction starts to decrease.

This maximum can be rationalized assuming that the small spheres always fill the gaps between the large ones as long as there are enough large spheres. Further extensions of the theory to any dimension can be performed by replacing 3 by d in Eq. (5.9). We notice that many of the approximations employed in 3d may become exact for large d, thus we expect improved results in the mean field limit of infinite dimensions.

The method allows to treat more difficult problems. For instance, the prediction of the volume fraction of a jammed system of non-spherical particles is a long-standing problem. Theoretical predictions of Onsager [139] are valid for large aspect ratios, like elongated rods. Experiments however, find interesting new physics for small aspect ratios. In this respect, the present polydisperse theory could be mapped to the problem of ellipsoids, spherocylinders or rods. A Voronoi cell needs to be calculated as a function of the angles defining the orientation of the non-spherical particles in analogy of the calculation between two particles of different radii. The integration over $P(r)dr$ in Eq. (5.18) is then replaced by integration over weighted orientational angles.

Chapter 6

Conclusions and outlook

In conclusion, treating granular packings from the perspective of theoretical physics developed by Boltzmann and Gibbs has the potential to answer basic questions in the field of disordered media. State variables like the compactivity can be introduced with the potential of identifying transition points between different phases, a fact that defines RCP as the freezing point in a discontinuous transition. This formalism may be useful in analyzing other related transitions in complex systems ranging from optimization problems in computer science [48] to the physics of glasses [3].

The present theory provides a general method for relating the local surface constraint in a jammed packing to its global properties. A simple relation between the volume fraction and the average coordination number is obtained by constraining the contact value of the pair distribution function. We note, however, that the current approach is a mean-field theory that neglects unconstrained spatial correlations and coordination number fluctuations. The long-range or quasi-long-range spatial correlations may not be neglected in an amorphous packing of monodisperse spheres, even though the system appears mescoscopically homogeneous. The low-dimensional results suggest indeed that the role of spatial correlations can be particularly significant. Higher level coarse-graining, such as explicitly treating the second-layer neighbors, the contributions from coordination number fluctuations and spatial correlations might thus improve the theory's predictions.

This study identifies many open questions and suggests numerous directions for future research. In the following, we point to several interesting problems.

(a) Reconcile the prediction of RCP density with other theories at the mean-field level. As discussed in Sec. 4.5, the high dimensional RCP density obtained from this theory has a scaling $\phi \sim (4/3)d2^{-d}$, while the replica theory predicts an interval $\phi \in [6.26\, d\, 2^{-d}, d\, \ln(d)\, 2^{-d}]$. The discrepancy suggests that the present theory might still be missing some correlations even in infinite dimensions. This problem is especially important because a unified picture at the mean-field level would build a solid foundation for the overall packing problem.

(b) Application to packings of non-spherical objects. The theory provides a route to study the phases of jammed packings of non-spherical particles under the umbrella of Edwards ensemble. It is still an unsolved problem finding the densest arrangement of rods, ellipsoids [141], spherocylinders, tetrahedrons [142], etc. The Edwards ensemble approach might be useful in search of novel phases of jammed matter, such as the jammed nematic phase analogy to that of the equilibrium suspension of thin hard rods.

(c) Towards the exact solution using a layer expansion method. The mean field approach is promising since it is simple enough to have analytical solutions. However, it is necessary to go beyond mean-field to answer more profound questions regarding the nature of the jammed state. The idea of layer expansion is to first consider the contribution from the contact neighbors, then include the contributions from the spheres at the second layer, the third layer, etc. Thus, the theory is exact up to a certain truncated layer. Since the Voronoi volume is determined most probably by a few layers, the solution may converge very quickly.

(d) Geometry-force ensemble. Finally, a complete ensemble would include both the geometric constrains and force balance conditions. Such an ensemble would characterize full information of jammed packings. For a fixed contact network (which is determined by the geometric configuration), the fundamental question of the force ensemble is to find the number of solutions satisfying the force balance conditions. This problem may be mapped to a constrain satisfaction problem and addressed by the standard cavity method [143, 144].

Bibliography

[1] C. Song, P. Wang, and H. Makse, Nature **453**, 629 (2008).

[2] P. J. Steinhardt, D. R. Nelson, and M. Ronchetti, Phy. Rev. B **28**, 784 (1983).

[3] G. Parisi and F. Zamponi, Rev. Mod. Phys. **82**, 789 (2010).

[4] T. C. Hales, Ann. of Math. **162**, 1065 (2005).

[5] A. Thue, Forand. de Skand. Natur. **14**, 352 (1892).

[6] A. Thue, Christinia Vid. Selsk. Skr. **1**, 1 (1910).

[7] J. D. Bernal and J. Mason, Nature **188**, 910 (1960).

[8] J. D. Bernal, Nature **185**, (1960).

[9] J. D. Bernal, Proc. Roy. Soc. London, Ser. A **280**, (1964).

[10] Anonymous, Nature **239**, 488 (1972).

[11] G. D. Scott, Nature **188**, 908 (1960).

[12] G. D. Scott and D. M. Kilgour, Brit. J. Appl Phys (J. Phys. D) **2**, 863 (1969).

[13] J. L. Finney, Proc. Roy. Soc. London, Ser. A **319**, 479 (1970).

[14] J. D. Berryman, Phys. Rev. A **27**, 1053 (1983).

[15] G. Y. Onoda and E. G. Liniger, Phys. Rev. Lett. **64**, 2727 (1990).

[16] S. Torquato, T. M. Truskett, and P. G. Debenedetti, Phys. Rev. Lett. **84**, 2064 (2000).

[17] S. Torquato and F. H. Stillinger, Exp. Math. **15**, 307 (2006).

[18] J. H. Conway and N. J. A. Sloane, *Sphere Packings, Lattices and Groups*, Vol. 290 of *A Series of Comprehensive Mathematics*, 3rd ed. (Springer-Verlag, New York, 1999).

[19] C. A. Rogers, *Packing and Covering* (Cambridge University Press, Cambridge, 1964).

[20] H. A. Makse, D. L. Johnson, and L. M. Schwartz, Phys. Rev. Lett. **84**, 4160 (2000).

[21] C. S. O'Hern, L. E. Silbert, A. J. Liu, and S. R. Nagel, Phys. Rev. E **68**, 011306 (2003).

[22] A. Liu and S. R. Nagel, Nature **396**, 21 (1998).

[23] *Unifying concepts in granular media and glasses*, edited by A. Coniglio, A. Fierro, H. H., and M. Nicodemi (Elsevier, Amsterdam, YEAR).

[24] S. F. Edwards and R. B. S. Oakeshott, Physica A **157**, (1989).

[25] S. F. Edwards, in *Granular matter: an interdisciplinary approach*, edited by A. Mehta (Springer-Verlag, New York, 1994), pp. 121–140.

[26] S. F. Edwards, Physica A **353**, 114 (2005).

[27] R. Blumenfeld and S. F. Edwards, Phys. Rev. Lett. **90**, 114303 (2003).

[28] E. Bertin, O. Dauchot, and M. Droz, Phys. Rev. Lett. **96**, 120601 (2006).

[29] M. P. Ciamarra, A. Coniglio, and M. Nicodemi, Phys. Rev. Lett. **97**, 158001 (2006).

[30] E. R. Nowak *et al.*, Phys. Rev. E **57**, 1971 (1998).

[31] J. Brujić *et al.*, Phys. Rev. Lett. **95**, 128001 (2005).

[32] M. Schröter, D. I. Goldman, and H. L. Swinney, Phys. Rev. E **71**, 030301(R) (2005).

[33] L. F. Cugliandolo, J. Kurchan, and L. Peliti, Phys. Rev. E **55**, 3898 (1997).

[34] A. Barrat, J. Kurchan, V. Loreto, and M. Sellitto, Phys. Rev. Lett. **85**, 5034 (2000).

[35] H. A. Makse and J. Kurchan, Nature **415**, 614 (2002).

[36] A. Fierro *et al.*, Phys. Rev. E **71**, 061305 (2005).

[37] C. S. O'Hern, S. A. Langer, A. J. Liu, and S. R. Nagel, Phys Rev. Lett. **88**, 075507 (2002).

[38] H. P. Zhang and H. A. Makse, Phys. Rev. E **72**, 011301 (2005).

[39] L. E. Silbert *et al.*, Phys. Rev. E **65**, 031304 (2002).

[40] V. Trappe *et al.*, Nature **411**, 772 (2001).

[41] T. Under, J. Kertesz, and D. E. Wolf, Phys. Rev. Lett. **94**, 178001 (2005).

[42] K. Shundyak, M. van Hecke, and W. van Saarloos, Phys. Rev. E **75**, 010301 (2007).

[43] L. D. Landau and E. M. Lifshitz, *Theory of Elasticity* (Pergamon, New York, 1970).

[44] R. D. Mindlin, Trans. ASME J. Appl. Mech. **71**, (1949).

[45] J. Brujić *et al.*, Faraday Discuss. **123**, 207 (2003).

[46] B. D. Lubachevsky and F. H. Stillinger, J. Stat. Phys. **60**, 561 (1990).

[47] M. Skoge, A. Donev, F. H. Stillinger, and S. Torquato, Phys. Rev. E **74**, 041127 (2006).

[48] F. Krzakala and J. Kurchan, Phys. Rev. E **76**, 021122 (2007).

[49] S. Torquato and F. H. Stillinger, Rev. Mod. Phys. **82**, 2633 (2010).

[50] P. Philippe and D. Bideau, Europhys. Lett. **60**, 677 (2002).

[51] S. Henkes and B. Chakraborty, Phys. Rev. Lett. **95**, 198002 (2005).

[52] R. Blumenfeld, in *Lecture Notes in Complex Systems Vol. 8: Granular and Complex Materials*, edited by T. Aste, T. Di Matteo, and A. Tordesillas (World Scientific, Singapore, 2007), pp. 43–53.

[53] T. Aste, M. Saadatfar, and T. J. Senden, J. Stat. Mech. P07010 (2006).

[54] F. Lechenault, F. da Cruz, O. Dauchot, and E. Bertin, J. Stat. Mech. P07009 (2006).

[55] H. A. Makse, J. Brujić, and S. F. Edwards, in *The Physics of Granular Media*, edited by H. Hinrichsen and D. E. Wolf (Wiley-VCH, Berlin, 2004), pp. 45–85.

[56] G.-J. Gao, J. Blawzdziewicz, and C. S. O'Hern, Phys. Rev. E **74**, 061304 (2006).

[57] G.-J. Gao, J. Blawzdziewicz, C. S. O'Hern, and M. Shattuck, Phys. Rev. E **80**, 061304 (2009).

[58] L. D. Landau and E. M. Lifshitz, *Statistical Physics* (Pergamon, New York, 1970).

[59] C. Song, P. Wang, Y. Jin, and H. A. Makse, Physica A (2010).

[60] R. C. Ball and R. Blumenfeld, Phys. Rev. Lett. **88**, 115505 (2002).

[61] R. Blumenfeld, Eur. Phys. J. B **29**, 261 (2005).

[62] J. Zhou, S. Long, Q. Wang, and A. D. Dinsmore, Science **312**, 1631 (2006).

[63] S. Alexander, Phys. Rep. **296**, 65 (1998).

[64] C. F. Moukarzel, Phys. Rev. Lett. **81**, 1634 (1998).

[65] S. F. Edwards and D. V. Grinev, Phys. Rev. Lett. **82**, 5397 (1999).

[66] S. Torquato and F. H. Stillinger, J. Phys. Chem. B **105**, 11849 (2001).

[67] C. Briscoe, C. Song, P. Wang, and H. A. Makse, Physica A **389**, 3978 (2010).

[68] P. Wang, C. Song, Y. Jin, and H. A. Makse, Physica A **390**, 427 (2011).

[69] J. Brujić *et al.*, Phys. Rev. Lett. **98**, 248001 (2007).

[70] T. Aste and T. di Matteo, Phys. Rev. E **77**, 021309 (2008).

[71] R. Kamien and L. A. J., Phys. Rev. Lett. **99**, 155501 (2007).

[72] C. Radin, J. Stat. Phys. **131**, 567 (2008).

[73] M. Clusel, E. I. Corwin, A. O. N. Siemens, and J. Brujić, Nature **460**, 611 (2009).

[74] A. Donev, S. Torquato, and F. H. Stillinger, Phys. Rev. E **71**, 011105 (2005).

[75] J. Moscinski, M. Bargiel, Z. A. Rycerz, and P. W. M. Jacobs, Mol. Sim. **3**, 201 (1989).

[76] W. S. Jodrey and E. M. Tory, Phys. Rev. A **32**, 2347 (1985).

[77] B. Alder and T. Wainwright, J. Chem. Phys. **27**, 1208 (1957).

[78] P. G. Debenedetti, *Metastable liquids: Concepts and Principles* (Princeton University Press, Princeton, 1996).

[79] T. M. Truskett, S. Torquato, and P. G. Debenedetti, Phys. Rev. E **62**, 993 (2000).

[80] K. Binder, Rep. Prog. Phys. **50**, 783 (1987).

[81] M. Bargiel and E. M. Tory, Adv. Powder Technol. **12**, 533 (2001).

[82] C. Briscoe, C. Song, P. Wang, and H. A. Makse, Phys. Rev. Lett. **101**, 188001 (2008).

[83] G. D. Scott, A. M. Charlesworth, and M. K. Mak, J. Chem. Phys. **40**, 611 (1964).

[84] M. Nicolas, P. Duru, and O. Pouliquen, Eur. Phys. J. E **3**, 309 (2000).

[85] M. D. Shattuck, eprint arXiv:cond-mat/0610839 (2006).

[86] P. Chaudhuri, L. Berthier, and S. Sastry, Phys. Rev. Lett. **104**, 165701 (2010).

[87] R. L. Vink and G. T. Barkema, Phys. Rev. Lett. **89**, 076405 (2002).

[88] B. D. McKay, Nauty user's guide (version 1.5), Tech. Rep. TR-CS-90-02 (1990).

[89] W. W. Wood and J. D. Jacobson, J. Chem. Phys. **27**, 1207 (1957).

[90] W. G. Hoover and R. F. H., J. Chem. Phys. **49**, 3609 (1968).

[91] D. Frenkel and A. J. C. Ladd, J. Chem. Phys. **81**, 3188 (1984).

[92] P. N. Pusey and W. van Megen, Nature **320**, 340 (1986).

[93] J. Zhu *et al.*, Nature **387**, 883 (1997).

[94] A. D. J. Haymet, Ann. Rev. Phys. Chem. **38**, 89 (1987).

[95] A. Daanoun, C. F. Tejero, and M. Baus, Phys. Rev. E **50**, 2913 (1994).

[96] M. D. Rintoul and S. Torquato, Phys. Rev. Lett. **77**, 4198 (1996).

[97] R. J. Speedy, J. Phys. Cond. Mat. **9**, 8591 (1997).

[98] K. Ball, Int. Math. Res. Not. 217 (1992).

[99] M. Krivelevich, S. Litsyn, and A. Vardy, Int. Math. Res. Not. 2271 (2004).

[100] G. A. Kabatiansky and V. I. Levensthein, Probl. Inf. Transm. **14**, 1 (1978).

[101] C. H. Bennett, J. Appl. Phys. **43**, 2727 (1972).

[102] S. Torquato, *Random Heterogeneous Materials: Microstructure and Macroscopic Properties* (Springer-Verlag, New York, 2002).

[103] K. E. Daniels and R. P. Behringer, J. Stat. Mech.: Theory Exp. 07018 (2006).

[104] O. Dauchot, G. Marty, and G. Biroli, Phys. Rev. Lett. **95**, (2005).

[105] A. Abate and D. Durian, Phys. Rev. E **74**, 031308 (2006).

[106] M. Pica Ciamarra, M. Nicodemi, and A. Coniglio, Phys. Rev. E **75**, (2007).

[107] M. Jerkins *et al.*, Phy. Rev. Lett. **101**, (2008).

[108] T. S. Majmudar, M. Sperl, S. Luding, and R. P. Behringer, Phys. Rev. Lett. **98**, (2007).

[109] A. S. Clarke and H. Jónsson, Phys. Rev. E **47**, 3975 (1993).

[110] L. E. Silbert, A. J. Liu, and S. R. Nagel, Phys. Rev. E **73**, (2006).

[111] E. Somfai *et al.*, Phys. Rev. E **75**, (2007).

[112] Y. Jin and H. A. Makse, Physica A **389**, 5362 (2010).

[113] G. Parisi, J. Stat. Phys. **132**, 207 (2008).

[114] G. Parisi, *Statistical field theory* (Addison-Wesley, Redwood City, 1988).

[115] J. A. van Meel, D. Frenkel, and P. Charbonneau, Phys. Rev. E **79**, 030201(R) (2009).

[116] J. A. van Meel, B. Charbonneau, A. Fortini, and P. Charbonneau, Phys. Rev. E **80**, 061110 (2009).

[117] Y. Srebro and D. Levine, Phys. Rev. E **68**, 061301 (2003).

[118] R. Blumenfeld and S. F. Edwards, Eur. Phys. J. E **19**, 23 (2006).

[119] G. Frenkel, R. Blumenfeld, Z. Grof, and P. R. King, Phys. Rev. E **77**, 041304 (2008).

[120] M. Danisch, Y. Jin, and H. A. Makse, Phys. Rev. E **81**, 051303 (2010).

[121] S. Meyer *et al.*, Physica A **389**, 5137 (2010).

[122] H. Reiss, H. L. Frisch, and J. L. Lebowitz, J. Chem. Phys. **31**, 369 (1959).

[123] S. Torquato, B. Lu, and J. Rubinstein, Phys. Rev. A **41**, 2059 (1990).

[124] J. G. Kirkwood, J. Chem. Phys. **3**, 300 (1935).

[125] M. Otsuki and H. Hayakawa, Prog. Theor. Phys. **121**, 647 (2009).

[126] S. Torquato and F. H. Stillinger, Phys. Rev. E **73**, 031106 (2006).

[127] J. Talbot, G. Tarjus, P. R. V. Tassel, and P. Viot, Colloids Surf., A **165**, 287 (2000).

[128] S. Torquato, O. U. Uche, and F. H. Stillinger, Phys. Rev. E **74**, 061308 (2006).

[129] T. R. Kirkpatrick and P. G. Wolynes, Phys. Rev. B **36**, 8552 (1987).

[130] H. L. Frisch and J. K. Percus, Phys. Rev. E **60**, 2942 (1999).

[131] G. Parisi and F. Slanina, Phys. Rev. E **62**, 6554 (2000).

[132] A. Ikeda and K. Miyazaki, Phys. Rev. Lett. **104**, 255704 (2010).

[133] B. Schmid and R. Schilling, Phys. Rev. E **81**, 041502 (2010).

[134] A. Scardicchio, F. H. Stillinger, and S. Torquato, J. Math. Phys. **49**, 043301 (2008).

[135] N. J. A. Sloane, http://www.research.att.com/ njas/ (2004).

[136] J. Dodds, Nature **256**, 187 (1975).

[137] K. de Lange Kristiansen, A. Wouterse, and A. Philipse, Physica A **358**, 249 (2005).

[138] I. Biazzo, F. Caltagirone, G. Parisi, and F. Zamponi, Phys. Rev. Lett. **102**, 195701 (2009).

[139] L. Onsager, Ann. N. Y. Acad. Sci. **51**, 627 (1949).

[140] V. A. Luchnikov, N. N. Medvedev, L. Oger, and J.-P. Troadec, Phys. Rev. E **59**, 7205 (1999).

[141] A. Donev *et al.*, Science **303**, 990 (2004).

[142] S. Torquato and Y. Jiao, Nature **460**, 876 (2009).

[143] M. Mézard and G. Parisi, Eur. Phys. J. B **20**, 217 (2001).

[144] M. Mézard and A. Montanari, *Information, Physics and Computation* (Oxford University Press, Oxford, 2009).